Icarus 205 (2010) 2–37

Contents lists available at ScienceDirect

Icarus

journal homepage: www.elsevier.com/locate/icarus

The High Resolution Imaging Science Experiment (HiRISE) during MRO's Primary Science Phase (PSP)

Alfred S. McEwen [a,*], Maria E. Banks [a], Nicole Baugh [a], Kris Becker [b], Aaron Boyd [a], James W. Bergstrom [c], Ross A. Beyer [d], Edward Bortolini [c], Nathan T. Bridges [e], Shane Byrne [a], Bradford Castalia [a], Frank C. Chuang [f], Larry S. Crumpler [g], Ingrid Daubar [a], Alix K. Davatzes [h], Donald G. Deardorff [d], Alaina DeJong [a], W. Alan Delamere [i], Eldar Noe Dobrea [e], Colin M. Dundas [a], Eric M. Eliason [a], Yisrael Espinoza [a], Audrie Fennema [a], Kathryn E. Fishbaugh [j], Terry Forrester [a], Paul E. Geissler [b], John A. Grant [j], Jennifer L. Griffes [k], John P. Grotzinger [k], Virginia C. Gulick [d], Candice J. Hansen [e], Kenneth E. Herkenhoff [b], Rodney Heyd [a], Windy L. Jaeger [b], Dean Jones [a], Bob Kanefsky [d], Laszlo Keszthelyi [b], Robert King [a], Randolph L. Kirk [b], Kelly J. Kolb [a], Jeffrey Lasco [c], Alexandra Lefort [l], Richard Leis [a], Kevin W. Lewis [k], Sara Martinez-Alonso [m], Sarah Mattson [a], Guy McArthur [a], Michael T. Mellon [m], Joannah M. Metz [k], Moses P. Milazzo [b], Ralph E. Milliken [e], Tahirih Motazedian [a], Chris H. Okubo [b], Albert Ortiz [a], Andrea J. Philippoff [a], Joseph Plassmann [a], Anjani Polit [a], Patrick S. Russell [l], Christian Schaller [a], Mindi L. Searls [m], Timothy Spriggs [a], Steven W. Squyres [n], Steven Tarr [c], Nicolas Thomas [l], Bradley J. Thomson [e,o], Livio L. Tornabene [a], Charlie Van Houten [c], Circe Verba [b], Catherine M. Weitz [f], James J. Wray [n]

[a] *Lunar and Planetary Lab, University of Arizona, Tucson, AZ 85721, USA*
[b] *U.S. Geological Survey, 2255 N. Gemini Drive, Flagstaff, AZ 86001, USA*
[c] *Ball Aerospace & Technologies Corp., 1600 Commerce St., Boulder, CO 80301, USA*
[d] *NASA Ames Research Center and SETI Institute, Moffett Field, CA 94035, USA*
[e] *Jet Propulsion Laboratory, California Institute of Technology, 4800 Oak Grove Dr., Pasadena, CA 91109, USA*
[f] *Planetary Science Institute, 1700 E. Ft. Lowell, Tucson, AZ 85719, USA*
[g] *New Mexico Museum of Natural History and Science, 1901 Mountain Road NW, Albuquerque, NM 87104, USA*
[h] *Department of Earth and Environmental Science, Temple University, 1901 N. 13th St. Philadelphia, PA 19122, USA*
[i] *Delamere Support Systems, 525 Mapleton Ave., Boulder, CO 80304, USA*
[j] *Smithsonian Institution, National Air and Space Museum, 6th at Independence SW, Washington, DC 20560, USA*
[k] *Division of Geological and Planetary Sciences, California Institute of Technology, Pasadena, CA 91125, USA*
[l] *University of Bern, Sidlerstr. 5, CH-3012 Bern, Switzerland*
[m] *University of Colorado, 392 UCB, Boulder, CO 80309, USA*
[n] *Cornell University, 428 Space Sciences Building, Ithaca, NY 14853, USA*
[o] *Applied Physics Laboratory, Laurel, MD 20723, USA*

ARTICLE INFO

Article history:
Received 4 November 2008
Revised 8 April 2009
Accepted 17 April 2009
Available online 18 May 2009

Keywords:
Mars
surface
Mars
climate
Mars
polar geology
Image processing

ABSTRACT

The High Resolution Imaging Science Experiment (HiRISE) on the Mars Reconnaissance Orbiter (MRO) acquired 8 terapixels of data in 9137 images of Mars between October 2006 and December 2008, covering ~0.55% of the surface. Images are typically 5–6 km wide with 3-color coverage over the central 20% of the swath, and their scales usually range from 25 to 60 cm/pixel. Nine hundred and sixty stereo pairs were acquired and more than 50 digital terrain models (DTMs) completed; these data have led to some of the most significant science results. New methods to measure and correct distortions due to pointing jitter facilitate topographic and change-detection studies at sub-meter scales. Recent results address Noachian bedrock stratigraphy, fluvially deposited fans in craters and in or near Valles Marineris, groundwater flow in fractures and porous media, quasi-periodic layering in polar and non-polar deposits, tectonic history of west Candor Chasma, geometry of clay-rich deposits near and within Mawrth Vallis, dynamics of flood lavas in the Cerberus Palus region, evidence for pyroclastic deposits, columnar jointing in lava flows, recent collapse pits, evidence for water in well-preserved impact craters, newly discovered large rayed craters, and glacial and periglacial processes. Of particular interest are ongoing processes such as those

* Corresponding author. Address: Lunar and Planetary Lab, University of Arizona, Sonett Space Sciences, 1541 E. University Blvd., Tucson, AZ 85721, USA.
E-mail address: mcewen@lpl.arizona.edu (A.S. McEwen).

0019-1035/$ - see front matter
doi:10.1016/j.icarus.2009.04.023

driven by the wind, impact cratering, avalanches of dust and/or frost, relatively bright deposits on steep gullied slopes, and the dynamic seasonal processes over polar regions. HiRISE has acquired hundreds of large images of past, present and potential future landing sites and has contributed to scientific and engineering studies of those sites. Warming the focal-plane electronics prior to imaging has mitigated an instrument anomaly that produces bad data under cold operating conditions.

1. Introduction

The Mars Reconnaissance Orbiter (MRO) was launched on August 12, 2005, carrying six scientific instruments (Zurek and Smrekar, 2007). In addition to the HiRISE camera, MRO carries the Compact Reconnaissance Imaging Spectrometer for Mars (CRISM; Murchie et al., 2007), the Shallow Radar (SHARAD; Seu et al., 2007), the Context Camera (CTX; Malin et al., 2007), the Mars Color Imager (MARCI; Malin et al., 2001a), and the Mars Climate Sounder (MCS; McCleese et al., 2007). The Primary Science Phase (PSP) covered a bit more than one Mars year, from November 2006 until December 2008, with MRO in its 255 × 320 km mapping orbit, and is followed by the Extended Science Phase (ESP). Expectations for HiRISE were described by McEwen et al. (2007a); this paper updates that information, summarizes results from the PSP (including results not yet published elsewhere), and describes expectations for the ESP (January 2009 to December 2010).

The HiRISE camera features a 0.5 m diameter primary mirror, 12 m effective focal length, and a focal-plane subsystem (FPS) that can acquire images containing up to 28 Gb (giga-bits) of data in as little as 6 s. HiRISE images are acquired via 14 charge-coupled device (CCD) detectors, each with two output channels, and with multiple choices for pixel binning and number of Time Delay and Integration (TDI) lines. The 10 CCDs that cover the full swath width (1.14°) are covered by broadband red filters (RED) and four extra CCDs in the middle are covered by blue-green (BG) and near-infrared (IR) filters to provide 3-color coverage in the center 20% of the image swath. Fig. 1 shows the layout of the HiRISE FPS.

2. Data acquisition during the PSP

As of December 2008 (end of PSP) HiRISE had acquired 9137 images of Mars consisting of 8 terapixels of data. The images would cover 0.65% of the planet if there were no overlapping data for stereo or change detection. However, ~21% of the images are stereo pairs, ~6% are repeats to monitor seasonal processes (with an average ~5× repetition), and ~1% are re-imaged following excessive gaps or poor seeing, thus ~85% of our images provide unique

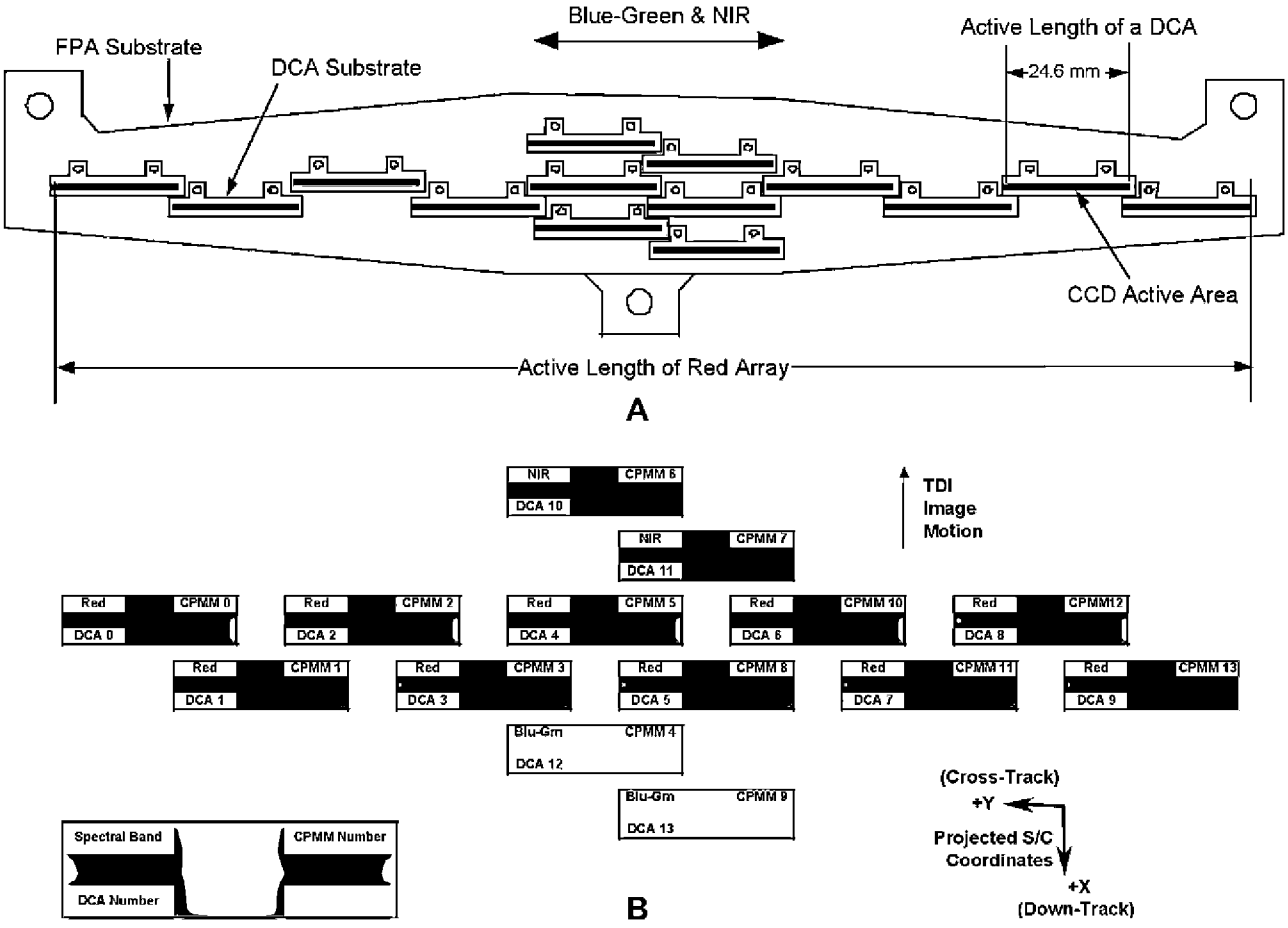

Fig. 1. Top (labeled "A"): Layout of CCDs on the base plate, approximately to actual scale. Bottom (B): Reference data on each Detector Chip Assembly (DCA), which consists of the CCD and CPMM. Spacecraft motion would be down as shown here, although HiRISE will typically image on the ascending side of the orbit.

coverage. If the repeat images are of typical size, this would mean we uniquely covered ~0.55% of Mars during the PSP. The global density of HiRISE images is shown in Fig. 2 and the distribution with latitude is shown in Fig. 3. Images are especially concentrated in areas such as the Phoenix and *Spirit* (Gusev crater) landing sites, Meridiani Planum (including *Opportunity* rover), Valles Marineris, Olympus Mons, Gorgonum Chaos, Hale–Holden–Eberswalde craters, Mawrth Vallis, Nili Fossae, Athabasca Valles, and polar regions.

Our nominal plan was to acquire ~12,000 images of Mars from 12 Tb of telemetry (McEwen et al., 2007a). We actually acquired 9137 images (Table 1), but from 2 to 3 times as much downlink data volume as expected, so the average image sizes are larger than previously expected. We chose to acquire larger images rather than more images because it was operationally easier and because of a lifetime concern related to the number of on–off cycles to the FPS. The lifetime concern has since been lessened by testing on the FPS engineering model (EM) at Ball Aerospace and Technologies Corporation (BATC).

HiRISE image suggestions are placed into one of 18 science themes (Table 2). There is significant overlap among some of these themes and the choice can be somewhat arbitrary. For example, suggestions with gullies or ravines as the feature of interest may be assigned to the fluvial, periglacial, mass wasting, seasonal processes, or other themes, and additional gullies are captured in suggestions to the impact processes, landscape evolution, and other themes. Nevertheless, this system serves to divide the task of prioritizing suggestions among the different science theme leads and has proven satisfactory. The number of retired suggestions exceeds the number of images received because some images retire more than one suggestion. The "other" category includes both random samples and images taken to support other instruments onboard MRO. The global distributions of acquired images in each theme are shown in Fig. 4. At the HiRISE web site (http://hirise.lpl.arizona.edu) users may sort released images by science theme or by searching for keywords (such as "gullies"). Additional search tools are available via the Planetary Data System (PDS) (http://pds-imaging.jpl.nasa.gov/search/search.html).

A total of 960 stereo pairs were completed during the PSP, along with 144 half-completed stereo pairs. We try to complete stereo pairs within a month or two to minimize differences in illumination and potential changes in surface albedo patterns due to redistribution of dust or frost. However, we often cannot complete the stereo pair quickly for a variety of reasons, but can try again at a later time when the sub-solar latitude and illumination angles return to about the same position as in the first image (and take our

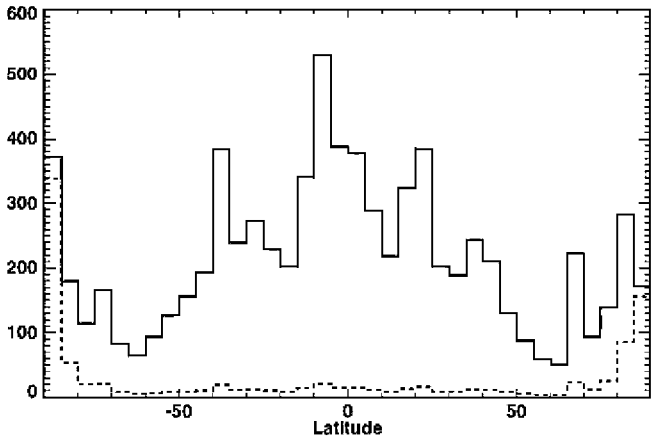

Fig. 3. Histogram of number of images in bins of 5° of latitude; the dashed red curve shows the same histogram normalized for area (images per quarter million km^2 as a function of latitude). Same dataset as that used for Fig. 2.

Table 1
Image types acquired in the PSP.

	Number acquired in PSP	% of total images
Total images	9137	100
Standalone images	3465	38
Coordinated and ride-along images with other teams	5672	62
Stereo images	2064	23
Off-nadir observations	6839	75
Nadir observations	2298	25

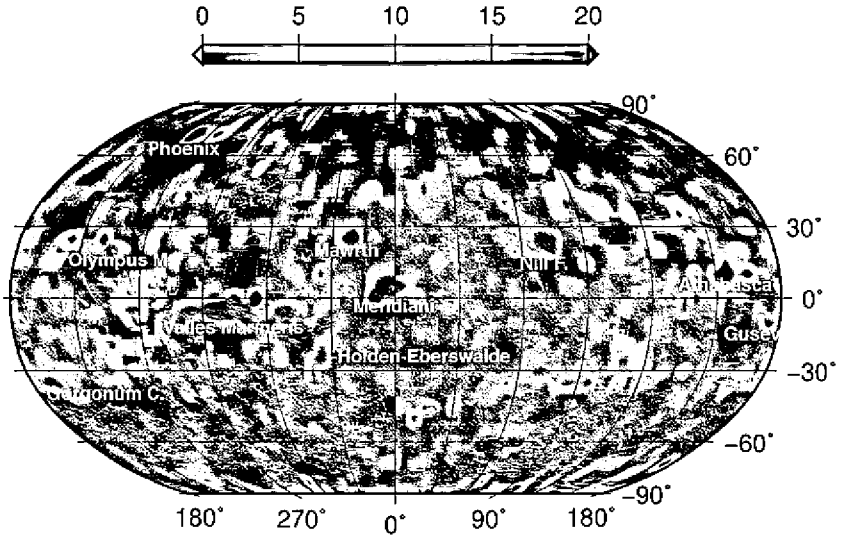

Fig. 2. Map of HiRISE imaging coverage density near end of PSP: number of images in 5 × 5 latitude/longitude bins (not normalized for area). This scale saturates at 20 images, but the most populous bins have >100 images in them. Frequently imaged locations include the Phoenix landing ellipse, Olympus Mons, Gorgonum Chaos, and other mid-latitude regions, Valles Marineris and surrounding plains, Mawrth Vallis region, Meridiani Planum, Holden and Eberswalde craters, the Nili Fossae region, Athabasca Valles, and Gusev crater. Both polar regions are also densely covered by HiRISE images, but that is disguised by the map projection.

Table 2
HiRISE target suggestions and images in the PSP.

Science theme	Science theme lead	Total suggestions	# Retired	Percent retired	# Images	# Stereo pairs	Notes
Composition and photometry	N. Thomas	693	523	75	466	19	Includes many CRISM riders
Impact processes	A. McEwen	1990	1094	55	978	128	
Volcanic processes	L. Keszthelyi	1102	698	63	622	84	
Tectonic processes	C. Okubo	675	375	56	333	58	
Fluvial processes	V. Gulick	1611	921	57	777	107	Includes QUEST challenge suggestions
Hydrothermal processes	V. Gulick	94	75	80	60	7	
Geologic contacts/stratigraphy	C. Weitz	1480	579	39	502	66	
Sedimentary/layering processes	C. Weitz	999	667	67	551	98	
Landscape evolution	J. Grant	546	370	68	337	27	
Aeolian processes	N. Bridges	2478	391	16	309	18	Includes USGS dune database (Hayward et al., 2007)
Glacial/periglacial processes	M. Mellon, M. Searls	1828	1002	55	873	93	
Rocks and regolith	M. Mellon	599	286	48	259	17	
Mass wasting processes	F. Chuang, B. Thomson	411	207	50	186	24	
Polar geology	K. Herkenhoff	1528	984	64	883	130	
Seasonal processes	C. Hansen	1437	688	48	570	31	Usually includes multiple images over each location
Climate Change	P. Russell	279	152	54	146	11	Expect more of these in future Mars years
Future exploration/landing sites	A. McEwen, J. Grant, M. Mellon	845	491	58	400	41	Includes MRO-project requested images
Other (or undefined)	None	1666	1221	73	945	1	Includes small sample images and many of the riders with CTX and CRISM
Totals		20,251	10,724[a]	53	9137[a]	960	

[a] An acquired image can retire more than one suggestion.

chances on albedo changes). We try to achieve a stereo convergence angle of at least 15° to enable a vertical precision of at least 20 cm (Kirk et al., 2008), but during a period of time in which the spacecraft off-nadir roll angles were restricted to small angles for thermal reasons we lowered the convergence angle requirement to at least 10°. All completed and PDS-released stereo pairs are listed at http://hirise.lpl.arizona.edu/stereo_pairs.php.

3. Science and sequence planning

3.1. Science planning

The science team has been actively involved in both time-independent targeting (by building up a database of suggestions and refining and prioritizing those suggestions within their science themes), and also with time-dependent targeting in the role of the "Co-I of the Pay Period" (CIPP) for a specific 2-week planning cycle. Because we have a different CIPP working on each cycle, there have been widely varying approaches to the planning details. The CIPP chooses the scientific emphasis of the cycle, as well as numbers, sizes, and modes of images. This variation in strategy has allowed for more complete coverage of different scientific themes, sub-topics, and types of features, allowing us to address a wide spectrum of Martian surface science.

HiRISE has covered less than 1% of the surface of Mars, so it is very important that the images acquired have high science value. HiRISE team members are responsible for science themes, as listed in Table 2. As science theme leads they have the tasks of being cognizant of ongoing research in their area of expertise, identifying sites with high science potential, entering those locations into the HiRISE target data base (via a tool called HiWeb), prioritizing all the suggestions in their theme, and identifying how the camera should be configured and what lighting conditions are needed to get the desired results. HiWeb allows the user to specify ranges of acceptable incidence, emission, and phase angles, and ranges of areocentric longitude of the Sun (L_s) within which an image should be acquired. Stereo pair requests are treated as two linked requests in the HiRISE catalog (HiCat). Seasonal monitoring series with multiple images can be requested and in this case a series of linked and time-constrained requests are generated. After the images in their theme are acquired, the science theme leads make sure that the image has successfully met the scientific objective; if not, they may choose to repeat the target request (by "unretiring" the suggestion).

The MRO project plans uplink sequences in 2-week cycles. During this time all requests from MRO's science teams and from the Mars Exploration Program are integrated into a conflict-free timeline. Off-nadir pointing of the spacecraft is a resource shared by HiRISE, CRISM, CTX, SHARAD, and the Electra UHF relay, with constraints imposed by the instruments preferring to stay nadir pointed.

The CIPP prioritizes a list of targets to be submitted to the project for that cycle and chooses image parameters based on the scientific objectives. Every planning cycle has a unique set of challenges. There may be regional dust storms, changes in the north polar hood, haze in Hellas basin, or special planning restrictions such as nadir-only zones. There may also be seasonal campaigns. Available data volume is a key factor for planning – when the data rate to Earth is (relatively) low, the CIPP agonizes over which targets to select and how large to make each image. When the data rate is high, the objective is to fill the downlink pipeline with the best possible images without overheating the FPS.

The HiRISE Targeting Specialists (HiTS) are cognizant of all the sequence delivery requirements, run specialized software at HiROC to optimize each observation, and make sure that the sequences ultimately radiated to the spacecraft meet all flight constraints. During each 2-week planning cycle the HiTS and the CIPP work closely together. Once the CIPP has generated a prioritized list of targets, the HiTS transforms the list into a commanding sequence that meets all operating constraints before delivery to the project. The project runs software known as TOS (the Target Opportunity Scheduler) that schedules targets requested from all three imaging teams (and tosses out others) and returns that list to the instrument teams. The CIPP selects targets from CRISM and CTX on

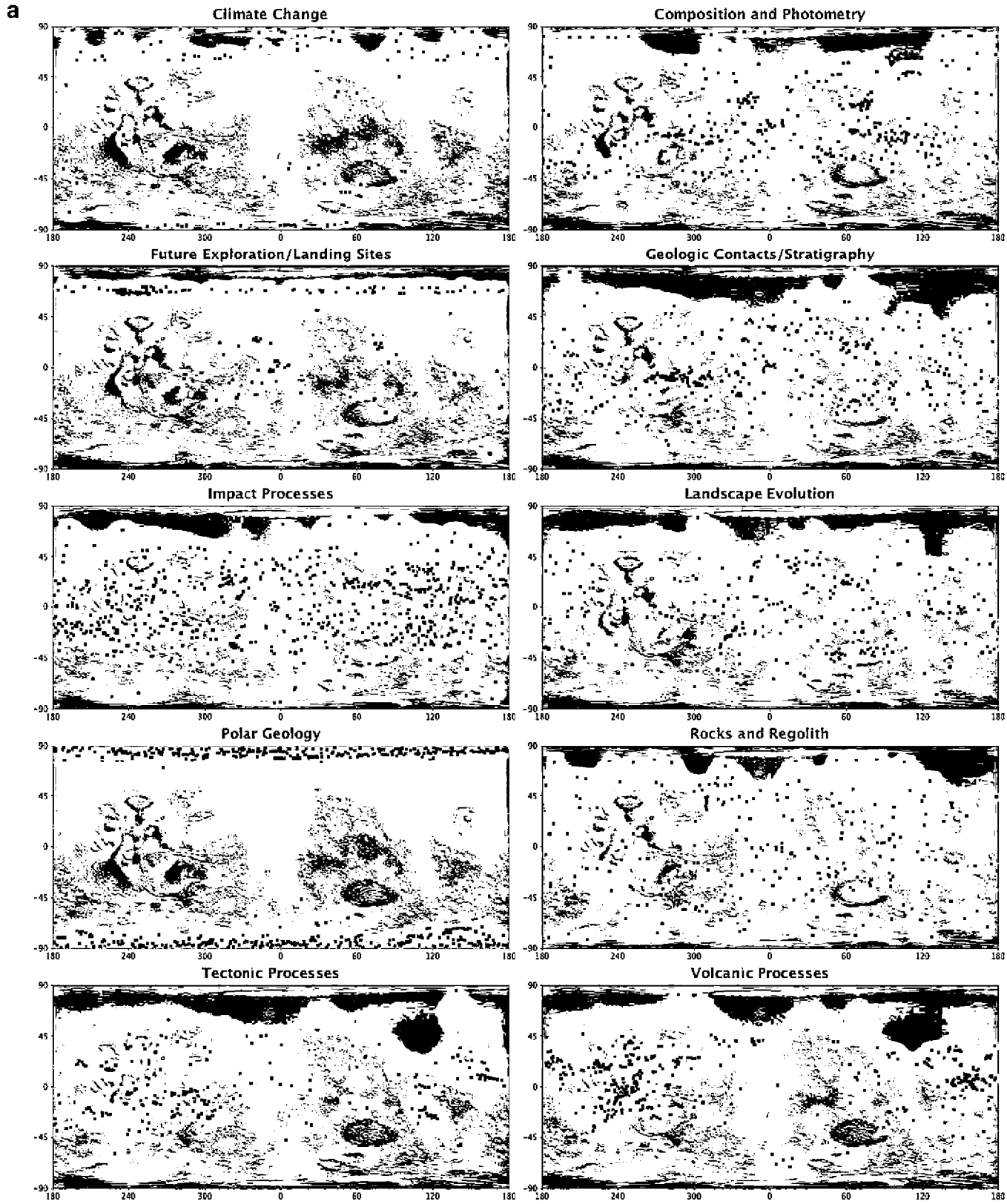

Fig. 4. Maps of all HiRISE images from the PSP assigned to each of the 18 science themes: (a) 10 of the themes, (b) eight additional themes. Base map is MOLA altimetry and shaded relief (Smith et al., 2001) in simple cylindrical map projection. Each dot is a single image or multiple images with nearly the same center coordinates.

which to ride along, and then determines the length of the images and the binning required, staying within available data volume. The CIPP also identifies targets of opportunity along the ground track for nadir imaging.

At this point in the tactical process the HiTS runs the HiRISE photometry program (HIPHOP) to determine, for each CCD, how to select the TDI and look-up table (LUT; used onboard to convert the image from 14 to 8 bits per pixel). This step is highly

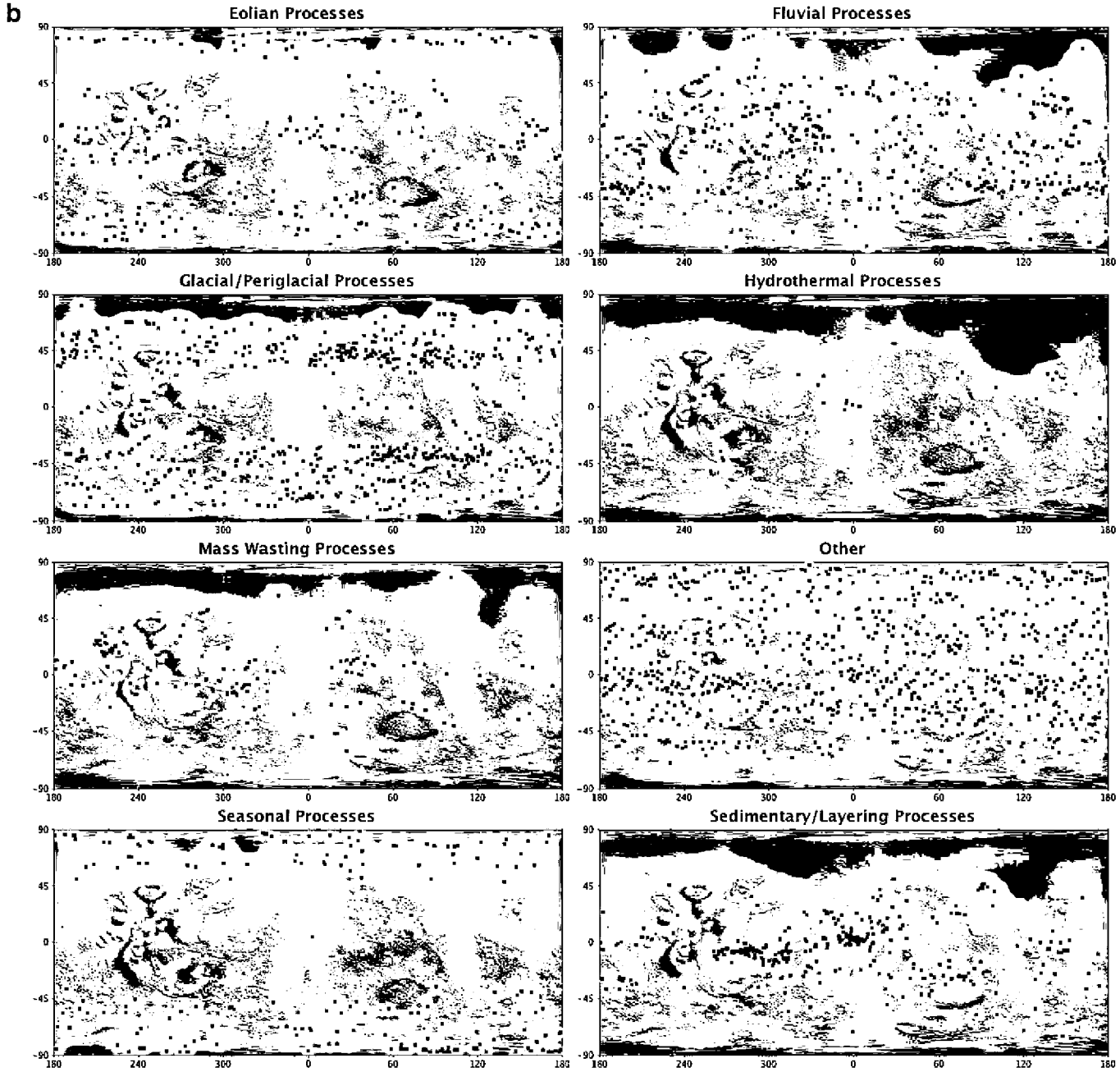

Fig. 4 *(continued)*

scene-dependent and relies on both models of the surface and the judgment of the HiTS. Every image requires six internal parameters to be set: LUT selection, TDI, binning, CCDs to be used, line time, and number of lines. Spacecraft-controlled parameters such as stability mode and targeted center coordinates are planned in concert with the other instruments. The commands are executed by the spacecraft in a sequence engine assigned to HiRISE, at a time calculated by the spacecraft software using the latest ephemeris. Ephemeris uncertainty typically corresponds too less than 1 km distance along the ground track.

3.2. Sequence planning complexities

One of the major ways in which sequence planning has deviated from expectations is in the time and amount of work required. Each image is carefully placed, prioritized, and planned. Given the complex and indeterminate nature of the MRO project planning procedures (which involve round-robin scheduling between the imaging instruments, subject to many and varied constraints), our initial list of observations for a given cycle must be oversubscribed by a factor of three to five.

HiRISE has acquired more data than originally expected. This is partially a result of additional coverage from the Deep Space Network requested by MRO and other Mars missions (Odyssey and Phoenix), better-than-expected FELICS (Fast and Efficient Lossless Image Compression System; Howard and Vitter, 1993) compression ratios, and other instrument teams' occasional underutilization of their downlink allocations (which we try to use). The result is that the number of pixels of data acquired has exceeded our original estimate by more than a factor of three. The planning workload,

however, is largely proportional to the number of images planned, not data volume. For this reason, we limited the number of images early in the PSP, but made them larger on average.

An extensive amount of time is required to plan each 2-week cycle: up to 2 weeks to plan the Interactive Observations (IOs – requiring interaction with operations of the spacecraft or another science instrument and usually equivalent to off-nadir observations), 2 weeks in which to plan Non-Interactive Observations (NIOs), 2 weeks of sequence execution, and up to 2 weeks to validate science objectives and help with daily captioned image releases. With overlapping activities, the whole sequence lasts about 5 1/2 weeks. The long cycle has had technical repercussions on planning – when a cycle's planning begins, the previous cycle has not been finalized, and the previous two cycles have not been fully executed.

Contemporaneous, co-located observations taken by multiple MRO instruments are considered to be one of the highest scientific priorities of the mission (Zurek and Smrekar, 2007). Such observations were originally envisioned as cooperatively pre-planned by two or three of the imaging instruments (HiRISE, CTX, and CRISM); the resulting coordinated observations were given a higher priority in the scheduling process than single-instrument observations. The extra deliveries and complication this added was eventually abandoned in favor of coordinating by simply "riding along" with observations of interest planned by a single team. This has been working well since the HiRISE, CTX, and CRISM teams tend to be interested in many of the same targets, as long as the image center is chosen with consideration of the smallest field of view among the instruments (HiRISE's ~6 km monochromatic/1.2-km color cross-track (i.e., perpendicular to the ground track) swath or CRISM's ~10-km along-track view at full resolution). We can adjust the HiRISE image center in the along-track direction by up to a few tens of kilometers with respect to the driving instrument's center when riding along.

In addition to images coordinated between instruments in these ways, support imaging from CTX is also requested for each off-nadir HiRISE-led observation. This includes stereo pairs of the same location, giving context stereo. The CTX team may omit the image if previous high-quality CTX images satisfy the request.

The MRO spacecraft's high stability (HS) mode, to minimize smear of HiRISE images, has undergone changes of definition. HS mode has always included pausing MCS's motion. Solar array (SA) motions were initially paused for all observations as well, but early in the PSP this was eliminated for nadir images, and as of January 2008 (the beginning of cycle 33), the SA pauses were eliminated for off-nadir observations as well. This was the simplest way to incorporate additional modeling checks on spacecraft motion into the planning process (required after a particular incident), and the SA motion is not a significant source of high-frequency pointing jitter that can smear the images. The high-gain antenna continues tracking regardless of stability mode and also does not seem to be a significant source of jitter, except when given an "unpark" command (this smeared our first image of Viking Lander 2 in PSP_001501_2280).

We always attempt to image in the HS mode, but sometimes are required to image in normal stability due to conflicts with other instrument or spacecraft activities. MCS scans only ~7% of the time, so many non-HS images are indistinguishable from HS images. Many observations have some amount of pointing jitter resulting in geometric distortions that are largely correctable (see Section 4.3), and some of the non-HS images are especially distorted. Smear is difficult to correct, but its magnitude is usually less than half of a pixel. One exception occurred when MCS experimented with faster slew rates in the fall of 2008, resulting in obvious smear (up to 10 pixels) of at least 20 non-HS images. Reducing TDI lines and sacrificing signal-to-noise ratio (SNR) in order to minimize smear has not been desirable, except for the highly oblique Phoenix descent image (PSP_008579_9020).

Managing the temperatures of the HiRISE FPS, to avoiding "saf-ing" (powering off) the instrument, has required considerable effort. Much heating takes place during readout of the data to the spacecraft solid-state recorder (SSR), so larger images bring peak temperatures close to the allowable limits. In addition, in order to mitigate bad data in channel IR10_1 and other channels, increasingly long warm-up times have been used for most images (see Section 8.2). Exceptions to this are where the longer time interfered with other onboard activities, and where a previous image on the orbit provided sufficient warming. In situations where we could not extend the warm-up time and therefore expected some bad image channels, we have also resorted to not returning data from the most problematic CCDs (IR10 and RED9). The long warm-up times were especially problematic during the high data rate period, when we were sometimes temperature-limited rather than downlink-limited. Images often had to be shortened, binned, or canceled in order to avoid overheating the FPS. The allowable flight temperatures were raised in February of 2008 to ease this constraint.

3.3. HiRISE image modes

HiRISE has four TDI levels (128, 64, 32, or 8 lines) and six pixel binning choices (none, 2×2, 3×3, 4×4, 8×8, 16×16), each individually selectable for each of the 14 CCDs, resulting in a total of 336 possible image modes. In Table 5 of McEwen et al. (2007a), we described 20 standard image modes defined for use in operations and calibrations. In practice, we have never used some of these modes, and have added a few new modes, as shown in Table 3.

Note that CCDs RED4-5-6 have been used with less binning in the mixed modes, as RED4-5 are in the center where we have 3-color coverage, and RED6 was added to facilitate precision corrections of the pointing jitter. However, we have since determined

Table 3
Standard HiRISE binning combinations and typical TDI settings used in PSP.

Name	RED4-5-6	Other seven REDs	NIR	BG
Bin1-all	bin1 128	bin1 128	bin1 128	bin1 128
Bin1A	bin1 128	bin1 128	bin2 128	bin2 128
Bin1	bin1 128	bin1 128	bin4 32	bin4 64
Bin1-2A	bin1 128	bin2 64	bin2 128	bin2 128
Bin1-2	bin1 128	bin2 64	bin4 32	bin4 64
Mohawk1A	bin1 128	bin4 32	bin2 128	bin2 128
Mohawk1	bin1 128	bin4 32	bin4 32	bin4 64
Bin2A	bin2 64	bin2 64	bin2 128	bin2 128
Bin2	bin2 64	bin2 64	bin4 32	bin4 64
Mohawk2A	bin2 64	bin4 32	bin2 128	bin2 128
Mohawk2	bin2 64	bin4 32	bin4 32	bin4 64
Bin4	bin4 128	bin4 128	bin4 128	bin4 128
Color sample	bin1 128	No data	bin2 128	bin2 128

that using RED3 along with RED4-5 may be most effective (see Section 4.3), so for the ESP we changed these modes to use RED3-4-5-6 rather than RED4-5-6 at higher resolution.

In addition to selecting TDI and bin settings, we must choose a look-up table (LUT) for converting the data from 14 to 8 bits, prior to FELICS compression (which only operates on 8-bit data). Although we can use linear LUTs with any min–max values, we almost always use a set of 28 stored LUTs because they are non-linear (actually piecemeal linear), designed to optimize SNR. However, the LUTs we initially designed (Table 7 and Fig. 18 of McEwen et al., 2007a) were overly optimistic with respect to how well we could predict the image histogram, with the result that we sometimes saturated the bright regions, especially in polar regions where the frost and haze are variable in space and time, or over compressed the data in an effort to avoid saturation. We then derived and loaded new LUTS (stored in volatile memory) that do not ever saturate a valid 14-bit DN value, but were still designed to optimize the SNR over the expected DN range. If the photometric prediction is off, or there is anomalously bright material in small areas of the scene, then the brighter-than-expected pixel values are heavily quantized in conversion to 8 bits, but not saturated. Likewise the darker-than-expected DN values would be quantized more than is ideal, sacrificing SNR. Which LUT to use is defined by offset level of the CCD (or lowest offset level of the two channels) and expected image mean, as shown in Table 4. We began use of these new LUTs in early 2007, and they have served to eliminate LUT saturation and to minimize time spent agonizing over LUT selection. The downside is that the new LUTs quantize the data a little more than the old LUTs (which are still stored in ROM), but this also served to increase FELICS compression ratios by ~5%.

McEwen et al. (2007a) described an expectation of FELICS compression ratios from 1.5 to 2.0, but in practice they have ranged from ~2.0 to ~3.0, with an average near 2.5. The lossless compression ratio is this high because (1) HiRISE images usually have SNR > 100 (random noise tends to foil predictive compression algorithms), and (2) the LUT-compressed histograms typically use less than 100 of the 256 DN values. The histograms are often narrow because Mars is typically a low-contrast target due to the intense diffuse illumination caused by scattering from fine dust in the atmosphere. This scattered light also enables detection of a fair amount of surface detail within shadows.

3.4. Special observations

In addition to observing Mars via normal procedures as IOs or NIOs, we have completed a set of special observations that required unique spacecraft sequences. Those performed during cruise and in the weeks after Mars orbit insertion were described in McEwen et al. (2007a). Those performed during the PSP are listed in Table 5. We have not performed stellar calibrations to check on the focus as often as expected prior to launch, as there has been no indication of any drift in the focus.

The first special sequence in the PSP was the equivalent of a "flat field" calibration for pixel responsivity. MRO was yawed 90° from its usual nadir-down orientation, such that TDI integration occurred in the cross-track direction instead of along track. The combination of TDI integration and spacecraft motion perpendicular to this direction resulted in each pixel being similar to its neighbor but offset vertically, producing an image unaffected by surface variations in each brightness band that crosses all pixels (Fig. 5). The bands were realigned (by shifting each line vertically—Fig. 5, right), the incomplete lines at top and bottom were trimmed, and then the lines were summed and divided by the average of the summed array to produce a calibration matrix. These images were acquired at a variety of TDI, bin, and line time settings appropriate for Mars orbit. The results produced flat field matrices for TDI 128/bin 1, TDI 64/bin 2, TDI 64/bin 4, TDI 32/bin 2, TDI 32/bin 4, and TDI 8/bin 4.

The search for the Mars Global Surveyor (MGS) soon after the spacecraft ceased communication involved a series of aborted plans following failed attempts to first locate MGS in other data. We did acquire one record-setting image (120,000 lines, the longest image attempted up to that point in time) but to no avail. The image of Jupiter and the Galilean satellites (http://hirise.lpl.arizona.edu/jupiter.php) was successful except for an error in the

Table 5
Special observations during the PSP.

Target	Dates	Observation IDs[a]	Notes
Mars radiometric calibration (MRO yawed 90°)	November 9, 2006	PSP_001355_2320	For "flat field" matrices
		PSP_001355_2260	
		PSP_001355_2180	
		PSP_001355_2105	
		PSP_001355_2010	
		PSP_001355_1900	
		PSP_001355_1825	
		PSP_001355_1750	
		PSP_001353_1585	
		PSP_001353_1520	
		PSP_001353_1455	
		PSP_001353_1405	
		PSP_001353_1350	
		PSP_001353_1300	
		PSP_001353_1250	
		PSP_001353_1205	
Deimos ridealong with CRISM	November 13, 2006	PSP_001401_9000	Intended as stray light test; missed Deimos
Search for Mars Global Surveyor (MGS)	November 20, 2006	PSP_001453_9020	MGS spacecraft not captured in image
Theta crateris	January 11, 2007	PSP_002162_9100	Radiometric calibration; intentionally smeared
Jupiter, all four Galilean satellites, and surrounding stars	January 11, 2007	PSP_002162_9030	For radiometric calibration and E/PO; slightly out of focus
Earth/Moon and surrounding stars	October 03, 2007	PSP_005558_9040 PSP_005558_9045	Earth mostly saturated
Phobos	March 23, 2008	PSP_007769_9010 PSP_007769_9015	Color stereo pair
Phoenix on parachute	May 16, 2008	PSP_008579_9020	Spectacular image

[a] Note that these observation IDs follow the convention of using a target code (last four digits) in the 9000 s for off-planet observations.

Table 4
Stored LUT numbers and target average DN range.

Offset	CCDs	Full range	Very bright	Bright	Medium-bright	Medium-dark	Dark	Very dark
900–1000	6, 12, 13	0	1: 6619–10373	2: 5116–6618	3: 3614–5115	4: 2863–3613	5: 2112–2862	6: 900–2111
1000–1100	1, 2, 3, 4, 7, 9, 10, 11	7	8: 6684–10,413	9: 5191–6683	10: 3699–5190	11: 2953–3698	12: 2207–2952	13: 1000–2206
1100–1200	5	14	15: 6749–10,453	16: 5266–6748	17: 3784–5265	18: 3043–3783	19: 2302–3042	20: 1100–2301
>1200	0, 8	21	22: 6814–10,493	23: 5341–6813	24: 3869–5340	25: 3133–3868	26: 2397–3132	27: 1200–2396

LUTs are defined by offset and optimal range for mean 14-bit DN. The LUTs in column "full range" are optimized over the full 14-bit DN range with no weighting towards expected image values. In the ESP CCD IR10 has been moved to the 900–1000DN offset level.

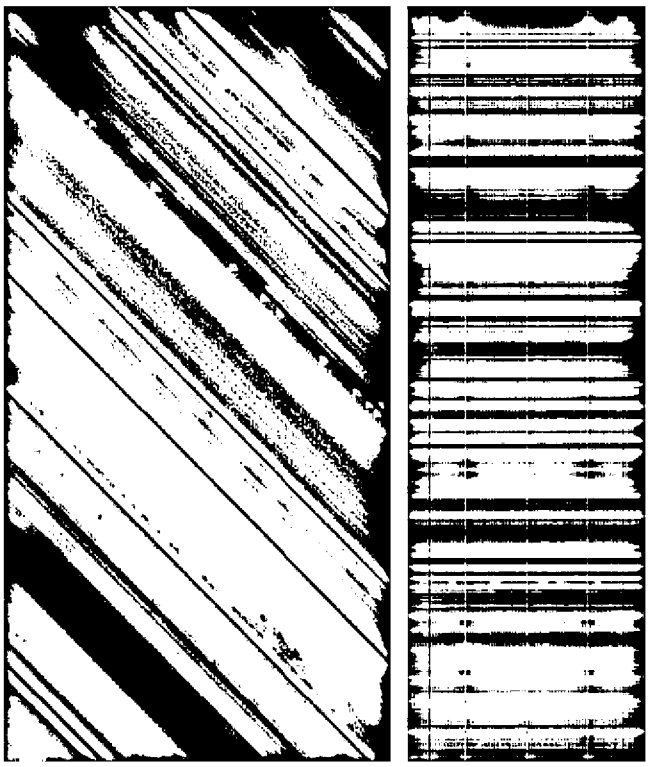

Fig. 5. HiRISE "flat-field" images produced by imaging when MRO was yawed 90° to the ground track. At left is a TDI 64 bin 2 single channel image. The slanted appearance of bright and dark bands is the result of the spacecraft motion during TDI integration, recording brightness variations on Mars that are smeared along each band. At right is a realigned TDI 128 bin 1 single-channel image useful for calibration.

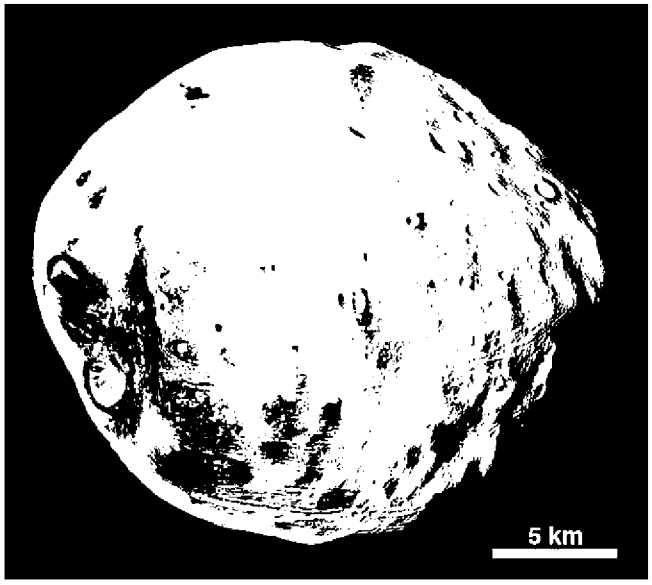

Fig. 6. Phobos image PSP_007769_9010, an enhanced-color product that has been rotated so north is up. The large crater at the lower left is Stickney.

focus setting, so it was not as sharp as it could have been. The image of Earth and the Moon (http://hirise.lpl.arizona.edu/earth-moon.php) was excellent for the Moon, but the illuminated portion of Earth was mostly saturated in all except one IR image.

The Phobos images (Fig. 6 and http://hirise.lpl.arizona.edu/phobos.php) were quite spectacular, providing the highest SNR color images ever acquired of this dark satellite. A relatively blue color

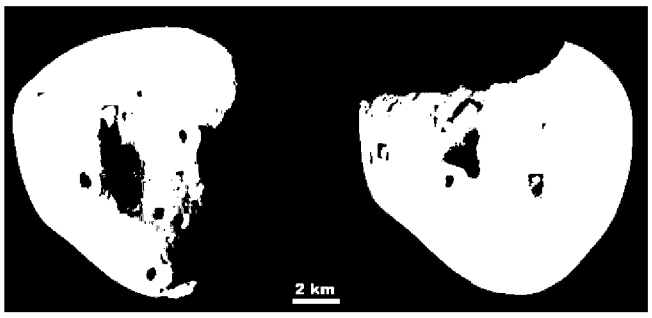

Fig. 7. Enhanced-color images of Deimos from images ESP_012065_9000 (right) and ESP_012068_9000 (left), rotated so north is approximately up.

unit near Stickney crater has been interpreted as Stickney ejecta (Pang et al., 1978), but the streakiness of the "blue" surface materials and its apparent youth suggest that alternate hypotheses should be considered. These images are complementary to observations of Phobos by CRISM (Murchie et al., 2008). We acquired a stereo pair of Phobos, but the HiRISE team has not analyzed the topographic data. Imaging of Deimos (Fig. 7) was completed in February of 2009 (http://hirise.lpl.arizona.edu/deimos.php).

HiRISE imaged the Phoenix lander descending on its parachute (Fig. 8 and http://hirise.lpl.arizona.edu/phoenix-descent.php and http://hirise.lpl.arizona.edu/phoenix-descent-color.php). A few weeks before entry, descent, and landing (EDL), Wayne Sidney of Lockheed–Martin Space Systems in Denver noted that Phoenix would pass nearly vertically through the HiRISE field of view with a slightly curving trajectory, and asked if it would be possible to take a picture. We determined that adequate SNR could be achieved via the use of just eight TDI lines, to minimize smear, given the 792 km range and ~8× longer line time than normally needed. The MRO project at JPL approved this late request because of its potential value to future EDL attempts. The image captured not only the parachuting Phoenix lander, but also captured the heat shield while in free-fall beneath the lander (http://hirise.lpl.arizona.edu/images/2008/details/cut/PSP_008579_9020-B_cut_a.jpg).

4. Ground data system and data products

4.1. Downlink processes

The objectives of the HiRISE downlink processes are to retrieve data from the MRO project database at JPL, then produce and validate the products to be shared with users (the HiRISE science team, other MRO investigators, the Mars Exploration Program, the Mars science community, and the general public), ultimately delivering archived products to the NASA Planetary Data System (PDS). The data processing begins when the downlink organizer (HiDOg) detects and retrieves science data from the project's Raw Science Data Server (RSDS) at JPL and delivers them to HiCat. HiROC uses fully automated processing to create raw and processed HiRISE images based on information in HiCat. HiROC serves as the HiRISE sub node of the PDS Imaging Node, thus simplifying the release of final products. This process is basically as we had originally planned, except for some modifications to special products.

The US Geological Survey's (USGS) Integrated Software for Imagers and Spectrometers (ISIS-3) system is used by the HiROC automated processing procedures for creating standard data products (Anderson et al., 2004; Becker et al., 2007). ISIS-3 (see http://wwwflag.wr.usgs.gov/isis-bin/isis.cgi) has been adapted to handle the instrument specific requirements for radiometric correction

Fig. 8. Phoenix spacecraft descending through the Martian atmosphere suspended from its parachute, PSP_008579_9020. Shown here is a reduced-scale version in the raw geometry (emission angle 59.5°). The crater is Heimdal, ~11.5 km diameter, located at 68.5°N, 235.3°E. Inset is a full-resolution enlargement of Phoenix on the parachute, which is ~20 km in front of the crater.

and geometric processing, and was modified to enable processing of very large images. Table 6 lists the ISIS-3 routines most useful for processing HiRISE images. The ISIS-3 software is freely available to the science community and is supported by USGS and NASA.

4.2. Standard and special data products

The automated processing system (HiProc; Schaller, 2006) produces three basic product types: EDRs (PDS-labeled Experiment Data Records or "raw" images), RDRs (Reduced Data Records or processed images), and "Extras" (additional image types useful to the science community). EDR generation includes (1) image decompression (from FELICS), (2) organizing the image data by CCD channel, (3) extraction of information needed for the PDS labels, and (4) storing additional metadata in PDS label objects within the EDR file.

For RDR production, the processing begins with the EDRs and includes (1) radiometric correction, (2) geometric transformation to standard map projections, (3) formatting data to PDS standards, and (4) preparation of data products with lossless JPEG2000 compression. Generation of the RDRs requires the incorporation of reconstructed SPICE (Spacecraft and Planet ephemerides, Instrument, Camera-matrix, and Event) kernels generated by the MRO navigation team (http://naif.jpl.nasa.gov/naif/pds.html), typically available within one week after data acquisition. The RDRs are reprojected to a scale of 25 cm/pixel if full-resolution data was acquired in at least one RED CCD, 50 cm/pixel if all RED CCDs have at least 2 × 2 binning, and 1 m/pixel if they all used 4 × 4 binning. We have chosen not to use 3 × 3, 8 × 8, or 16 × 16 binning modes to simplify calibration and image processing. Large-scale topography is orthorectified for geometric reprojections via use of a Mars Orbiter Laser Altimeter (MOLA; Smith et al., 2001) DTM at 64 pixels/degree (0.926 km/pixel), to which was applied three 7 × 7 pixel averaging filters to minimize the introduction of artifacts. The orthorectification affects the off-nadir images, and enables better coregistration with other datasets such as CRISM (Murchie et al.,

Table 6
ISIS-3 applications useful for processing HiRISE images.

hi2isis	Ingests HiRISE PDS EDR files into ISIS-3 format
higlob	Combines HiRISE image and calibration data into single image cube. This is useful for quick look assessment of all data acquired for a single image channel
histat	Computes statistics from the many data sections of an individual HiRISE CCD channel image. Statistics are computed from the calibration arrays and the image data
hifurrows	Detects and removes (or hides) *furrowing*, an anomaly found near the center of binned CCDs where the signal is >~7000 DN
hifringe	Gathers statistics on the outskirts of a CCD channel image. These data are useful for analyzing adjacent CCD channels for merging into a single CCD image (see *histitch*)
hical	Applies radiometric calibration correction including dark current, drift, offset, line-dependant gain, gain, flat field and conversion to I/F units
histitch	Combines left and right HiRISE CCD channels into a single image
spiceinit	This general-purpose application determines all NAIF SPICE kernels that apply to geometric observing conditions for HiRISE images. This application is required for any and all geometric processes
hiccdstitch	This application combines images acquired from a single HiRISE observation consisting of multiple CCDs in a color bandpass into a single image
hijitreg	*Hijitreg* determines the overlap of each CCD and coregisters small subsamples to compute the line and sample offsets as a function of time. The results are used in jitter analysis and color registration (see *slither*). The *reduce*, *enlarge* and *editlab* applications are required to process CCD images that have a different summing mode
slither	Computes an image transformation that shifts lines up or down and left or right while preserving the geometry of each individual line. This is sometimes referred to as a *one-dimensional transform*. The results of *hijitreg* are used as input into this transform. Its primary purpose is to apply precise image coregistration for color products
hicubeit	Stacks *slither*'ed HIRISE RED, BG, and IR cubes into a single cube for view and projection purposes. *Cubeit* is the generic counterpart to *hicubeit*
cam2map	Converts a cube in camera space to a map projection. The input requires SPICE data as applied by the *spiceinit* application
himos	Produces a final projected mosaic derived from one filter within a single HiRISE observation. The output is compliant with PDS HiRISE RDR specifications and ready for export to PDS using the *hirdrgen* application (see *hicolormos*, *hirdrgen*)
hicolormos	Produces a final color product compliant with the RDR specification for PDS data products. The input is typically the results of the *slither* processing sequence. This application is required for proper PDS RDR product generation (see *himos*, *hirdrgen*)
hirdrgen	Converts a HiRISE color mosaic product to PDS RDR format. Input must be generated using the *hicolormos* or *himos* applications
Hirdr2isis	Imports a PDS HiRISE RDR product into ISIS-3 format
qview	This is a standard, general purpose, ISIS-3 image display application
cubenorm	This general-purpose application performs characterization and removal of vertical or horizontal image anomalies
isis2std	This general-purpose application exports an image to JPEG, PNG, or other common image formats

2007, submitted for publication) and THEMIS (Christensen et al., 2004). Because of the MOLA orthorectification, these RDRs should not be used for stereo measurements except on small scales, as the large-scale parallax has been removed.

For the color products we had planned two levels of processing resulting in binned color and full-resolution RDR products. The purpose of the binned color products was to minimize geometric distortions and misregistration of the color bandpasses due to pointing jitter. However, we developed ISIS-3 programs (hijitreg and slither) that do an excellent job of correlating images and warping the BG and NIR images to match the RED images, and thus we go directly to full-resolution color RDRs. Note that geometric distortions from jitter are still present in the final products, but can be removed during geometric reprojection via incorporation of the recently developed HiRISE Jitter-Analyzed Camera Kernel (HiJACK), as described in Section 4.3. The color RDRs are merged with the full-resolution RED data, which often has less binning than the BG and IR data, via the following steps: if necessary, enlarge the BG and IR data to match the RED scale; run *hijitreg* to find match points and run *slither* to warp the BG and IR images to match the corresponding RED images; create BG/RED and IR/RED ratios; low-pass filter (smooth) these ratios by 3×3 if the bin level is $2\times$ that of RED, or 5×5 if the binning difference is $4\times$; then multiply the smoothed ratios by the REDs to create the sharpened BG and IR images. This procedure produces beautiful color images (although in some cases high-frequency noise from the RED data is introduced into the BG and IR data), but can also disguise artifacts such as cosmic-ray hits or misregistration. For more information on HiRISE color products, see Delamere et al. (2009).

The standard map projection scheme used by both HiRISE and CRISM is equirectangular or polar stereographic, in planetocentric coordinates tied to MOLA. Equirectangular is the same as simple cylindrical but with a longitudinal compression factor (cosine of the average latitude of the latitude bin). For the standard products we utilize 5° latitude bins (see Fig. 16 of McEwen et al., 2007a). Although we had planned to use this projection everywhere except above ±85° latitude (switching to polar stereographic), both the HiRISE and CRISM teams revised this boundary to ±65° for compatibility with other datasets such as THEMIS and CTX. Although HiRISE and CRISM use the same map projections, this does not insure good registration with the CRISM gimbaled observations over rugged terrains. To produce good registration in such cases requires orthorectification using a DTM with comparable or better resolution than the CRISM data.

Once an RDR has been produced, it is losslessly compressed using JPEG2000 (http://www.jpeg.org/jpeg2000/index.html). This format reduces our data storage needs and greatly facilitates distribution of the data over the web. We had planned to develop a HiRISE image viewer module using JPEG2000 and incorporating simple tools like pan/zoom and image stretching to facilitate efficient exploration of these gigantic images. However, we instead contracted with ITT Visual Information Solutions (ITT-VIS) to modify the Image Access Solutions (IAS) viewer to achieve this function (see http://hirise.lpl.arizona.edu/support/ and http://www.ittvis.com/ProductServices/IAS.aspx for more information.) The IAS viewer is automatically downloaded the first time a user clicks the appropriate link for a PDS-released HiRISE image at http://hirise/lpl.arizona.edu/.

In addition to the EDRs and RDRs, we produce a variety of "Extra" products that are useful to the science community. HiRISE PDS data products are identified in Table 7. The "NOMAP" images consist of calibrated images in their original viewing geometry, roughly north down for ascending-orbit observations. With these products there are no pointing corrections, geometric corrections, or map projections, just CCD images laid side-by-side according to nominal locations. The NOMAP products retain nearly the full spatial resolution of the images because the pixels are not re-sampled (although CCD images with greater binning are enlarged to match less-binned CCD images.) These products do lose a nearly imperceptible amount of resolution due to the use of a lossy JPEG2000 compression factor of 2.0. Resolution loss in the RDRs is minimized via the use of cubic convolution re-sampling and lossless compression. The color images are called IRB for IR, RED, and BG images displayed in red, green, and blue channels, respectively; and RGB for RED, BG, and synthetic blue images displayed in red, green, and blue channels, respectively. The synthetic blue image consists of the BG image DN multiplied by 2 minus 30% of the RED image DN, for each corresponding pixel (Delamere et al., 2009). RGB products are useful when IR10 data were not acquired or have excessive errors, and are often a nicer-looking product for public release. As of 9 March 2009 the PDS HiRISE dataset consists of 931,744 images and 33 TB (terabytes) total data volume. This data volume is about equally divided between EDRs (9 TB in 257,943 files), RDRs (10.5 TB in 18,488 files), and Extras (13.5 TB in 655,313 files).

Table 7
Standard and extra HiRISE PDS products.

Product type	Format/file extension	Description
EDR	.IMG	Raw image data, one per image channel (up to 28 per observation), FELICS decompressed in raster format
RDR	_RED.JP2	Map-projected mosaic of RED-filter CCDs in JPEG2000 format and losslessly compressed with 10-bits per pixel providing a dynamic range 0–1023
RDR	_COLOR.JP2	Three-color map-projected mosaic of IR, RED, and BG bands in JPEG2000 format and losslessly compressed with 10-bits per pixel providing a dynamic range 0–1023
Extras	.JP2	Stereo anaglyphs produced with stereo pairs at 8-bits/pixel with a lossy compression factor of 2.66
Extras	_RED.QLOOK.JP2	Quicklook version of the RDR RED mosaic product stored as 10-bits/pixel with a compression factor of 5.0 (this compression factor is high due to large areas of null pixels in the projected image and because the losslessly compressed version is available)
Extras	_COLOR.QLOOK.JP2	Quicklook version of the RDR COLOR mosaic product stored as 10-bits/pixel with a compression factor of 5.0
Extras	_RED.NOMAP.JP2	Grayscale not-map-projected image stored as 10-bits/pixel providing a dynamic range of 0–1023 with a compression ratio of 2.0
Extras	_RGB.NOMAP.JP2	Color not-map-projected image stored as 10-bits/pixel providing a dynamic range of 0–1023 losslessly compressed. Color data use the RED, BG, and synthetic blue bands displayed as red, green, blue, respectively
Extras	_IRB.NOMAP.JP2	Color not-map-projected image stored as 10-bits/pixel providing a dynamic range of 0–1023 losslessly compressed. Color data use the IR, RED, and BG bands displayed as red, green, blue, respectively
Extras	.browse.jpg	Browse versions (reduced to 2048 pixels width for RED, 512 pixels for color) for the six JP2 Extra products
Extras	.thumb.jpg	Thumbnail versions (reduced to 512 pixels width for RED, 128 pixels for color) for the six JP2 Extra products
Future products		
RDR	_DTM.IMG	Digital terrain models
Extras	TBD	Precision geometric products (see Section 4.3)

Because the HiRISE Operations Center (HiROC) is serving as a PDS data node, we can release image products before the formal delivery deadlines (6–9 months after acquisition for EDRs and end of mission for RDRs and Extras). Typically, we release all products for 5–10 observations per week, with science team written captions, within a few weeks of acquisition. Remaining products are released from 1 to 3 months after acquisition. Users, including the public, are able to access all released HiRISE image products through http://hirise.lpl.arizona.edu or http://www-pdsimage.jpl.nasa.gov/PDS/public/. More than 1.5×10^7 HiRISE PDS products were downloaded as of 6 September 2008, in addition to more than 4×10^5 IAS Viewer sessions.

4.2.1. Stereo anaglyphs

A stereo anaglyph-processing pipeline for latitudes 80°S–80°N was completed in October 2008. MRO rolls off nadir in the direction across the orbit track and thus parallax is revealed in the cross-track direction. With the High Resolution Stereo Color (HRSC) camera on Mars Express (Neukum et al., 2004), parallax is in the along-track direction. The exception to this cross-track parallax is near the poles where the stereo geometry is complex, and different processing is needed to create anaglyphs for stereo viewing. Our eyes are spaced horizontally, thus an anaglyph should be generated so that parallax remains in the horizontal direction. This means that a HiRISE anaglyph should be constructed so that the vertical edge of an image remains vertical. Because observations from stereo pairs differ in roll angle, the overall cross-orbit scaling differences need to be taken into account or the two images will not register in the anaglyph. Our solution to these constraints is to generate products using a map projection that will allow rotation so that the vertical edge of the raw observation remains vertical in the map-projected image. The Polar Stereographic projection was selected because the ISIS-3 routine for this projection makes it easy to rotate the images properly. A standard longitude of projection is selected so that the vertical edge of the image with the larger emission angle remains vertical in the projected image. North is about 7° to the right of up, except near the poles. Products are scaled to 25 cm/pixel if they contain any CCDs acquired at full resolution, or 50 cm/pixel if all CCDs were binned 2×2 or more, and 1 m/pixel for bin 4×4 imaging (rarely used for stereo pairs). These map projections do not use the full MOLA DTM – we do not want to orthorectify (remove terrain distortions) because that is the information anaglyphs are supposed to capture. Instead the planet is considered to be a sphere but we extract the planet radius at the center of the image from the smoothed MOLA DTM. Uncertainties in the spacecraft pointing and ephemerides can cause misregistration in some stereo pairs, so we use the ISIS-3 *coreg* program on greatly reduced-scale images to shift one of the images to a better match. Anaglyphs with high relief and large stereo convergence angles can be difficult or impossible to view at full resolution unless sub-scenes are extracted or displayed and then the red (left eye) image is translated to better match the green and blue images. Note that the anaglyphs have variable degrees of vertical exaggeration, increasing with larger convergence angles. One qualitative calibration is to look for angle-of-repose slopes for dry, cohesionless materials, which should be ~35°. An example of part of a stereo anaglyph is shown in Fig. 9.

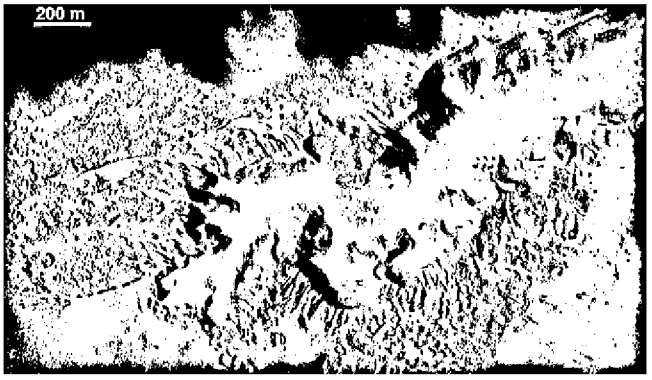

Fig. 9. Stereo anaglyph of a small cataract on the floor of Kasei Valles at 20.85°N, 287.3°E. The cataract is covered by a platy-ridged flow we interpret as flood lava. If the cataract as well as the larger channel were carved by water then floods of lava followed, as seen elsewhere on Mars. Images PSP_002287_2010 and PSP_002788_2010, reduced to 1 m/pixel scale.

4.3. Jitter characterization and corrections

HiRISE is a pushbroom type sensor, so it builds an image line by line as MRO flies over the surface of Mars. The use of CCD charge-transfer TDI greatly improves the SNR via on-chip summing of up to 128 lines, but this summing along with the 1 μrad IFOV make the camera extremely sensitive to any high-frequency spacecraft motions that occur during imaging (Lee et al., 2001). The image line time is typically 80–100 μs depending on the orbital altitude, so with 128 TDI lines the total integration time is ~0.01 s (frequency 100 Hz). Pointing jitter with frequencies below 100 Hz produce geometric distortions whereas all frequencies contribute to image smear. The spacecraft pointing stability requirement was 2.4 μrad in 12 ms (3 sigma) in the high-stability (HS) mode, leading to the worst-case expectation of noticeable (>1 pixel) smear in ~1% of the HS image lines. In practice smear exceeding 1 pixel occurs much less than 1% of the time in any HS image, except in the few cases where mistakes caused the spacecraft to not actually be in HS mode. Nevertheless, jitter does create geometric distortions that limit the accuracy of topographic and temporal change measurements, and we wish to understand and improve the geometric fidelity of the data. Highly accurate DTMs are crucial to the characterization and certification of future landing sites and planning of rover traverses.

The HiRISE camera provides a much more sensitive measure of spacecraft jitter than does the engineering telemetry. The Inertial Measurement Unit (IMU) can sample at 200 Hz but must be filtered to reduce noise and combined with the much lower-frequency star tracker quaternions. These data are captured in the SPICE CK, and serve to remove some of the low-frequency distortions during geometric processing. The layout of overlapping CCDs in the HiRISE FPS was modified from the nominal layout to improve the high-frequency jitter measurements (McEwen et al., 2007a). Analysis of these data was considered a high priority for the early PSP, but the better-than-expected spacecraft performance and the worse-than-expected uplink operations changed our priorities. Correction for jitter has been systematically applied only in a relative sense to register the IR and BG to the RED for color products. Our ultimate goal is to correct geometric distortions in an absolute sense.

Coregistration data from the overlapping parts of the CCDs reveal sinusoidal motions both along- and cross-track with varying periodicity and amplitude. The twist jitter has proven to be insignificant. In order to characterize a phenomenon that is time-variable, unpredictable, and periodic, we approached the solution as a sum of sines and cosines. The algorithm for jitter characterization takes advantage of the fixed time offsets of the CCDs in the focal-plane assembly. Coregistration measurements are gathered for pixels in the overlapping portions of CCD images. The coregistration algorithm measures the pixel offset in the cross-track and down-track directions. The basic concept is that the same part of the surface is imaged at different times, and that the same motion affects all of the CCDs simultaneously. The measured coregistration offset can thus be expressed as

$$F(t) = J(t + \Delta t) - J(t) \quad (1)$$

where $F(t)$ is the coregistration offset in pixels between two overlapping HiRISE CCDs at time t. $J(t)$ is the actual jitter function. $J(t + \Delta t)$ is the same jitter function translated by the offset time Δt.

Three pairs of overlapping CCDs (RED3–RED4, RED4–RED5, and BG12–RED4) have been found (thus far) to give the best results and are used to derive the jitter function. Advantages to using the color CCDs are that they have a larger time offset than do the staggered RED CCDs, and they also provide many columns of registration points. A disadvantage is that the BG and IR images have lower SNRs than the RED images or, more commonly, have more binning than the corresponding RED images in order to achieve high SNRs.

Each set of coregistration data is filtered to remove bad points (false correlations), and then interpolated and smoothed to further reduce noise. A set of evenly spaced points is used from the interpolated data to perform the Fourier analysis. Periods in the Fourier series that are near the time offset of that pair are filtered out and replaced with the average of the other two pairs for that period. This prevents the inclusion of any frequencies of motion that might be aliased to the given time offset of one pair of CCDs. A solution can be derived from any one pair of adjacent CCDs, but it will not be the best solution for all the CCDs in the image (due to noise and aliasing). The solution derived from all three pairs of CCDs is then used to predict what offsets it would produce for each pair of CCDs, transforming it with Eq. (1). The average error of the predicted offsets for all three pairs is minimized to arrive at the final jitter function. The final result is a continuous function that describes the pointing of HiRISE over most of the duration of the image. Motion near the beginning and end of the image are not contained in the same time overlap and cannot be corrected. The motion is described separately in the along-track and the cross-track directions.

The algorithm was tested by transforming all of the CCD images in an observation with the derived jitter function, then repeating the coregistration measurements (Fig. 10). The algorithm was tested on a selection of images with varying jitter conditions; it removed or greatly minimized the jitter in all cases for the RED CCDs. The color (IR and BG) registration data were improved, but not as satisfactorily as the REDs. However, the procedure we use is to warp the BG and IR images to match the corresponding RED images, then correct the coregistered color set with the RED pointing model. Work on merging the jitter function with the spacecraft pointing information has recently been completed and incorporated into the ISIS-3 program *hijitter*. A combination of the high-frequency jitter function and the low-frequency pointing function is made that does not overcorrect motions detected in both datasets. The jitter function, which is expressed in down-track and cross-track pixel offsets must first be converted to rotation angles before being used to improve the camera pointing kernel (CK) and produce the HiRISE Jitter-Analyzed CK (HiJACK). Corrected pointing information will be used to create precision geometry products that will in turn be used to produce the most accurate DTMs, stereo anaglyphs, and change-detection sequences. We are in the process of implementing the complicated processing steps into a pipeline for automated processing, and hope to begin release of precision geometry products sometime in the ESP.

Now that we can model the high-frequency pointing history, we can also measure the image smear in both the along- and cross-track directions. There could be extra smear from jitter that is too high in frequency for us to measure with the image data, although we have seen no evidence for this except when MCS is moving. These jitter models make it possible to more rigorously model the time-varying point-spread function (PSF) and sharpen the images while preserving photometric information. The magnitude of smear is usually well below 0.5 pixel for HS images. Those images acquired during MCS scans tend to have smear of less than 2.5 pixels, except for a period of time in the fall of 2008 when they experimented with faster slew rates, which created smear of up to 10 pixels.

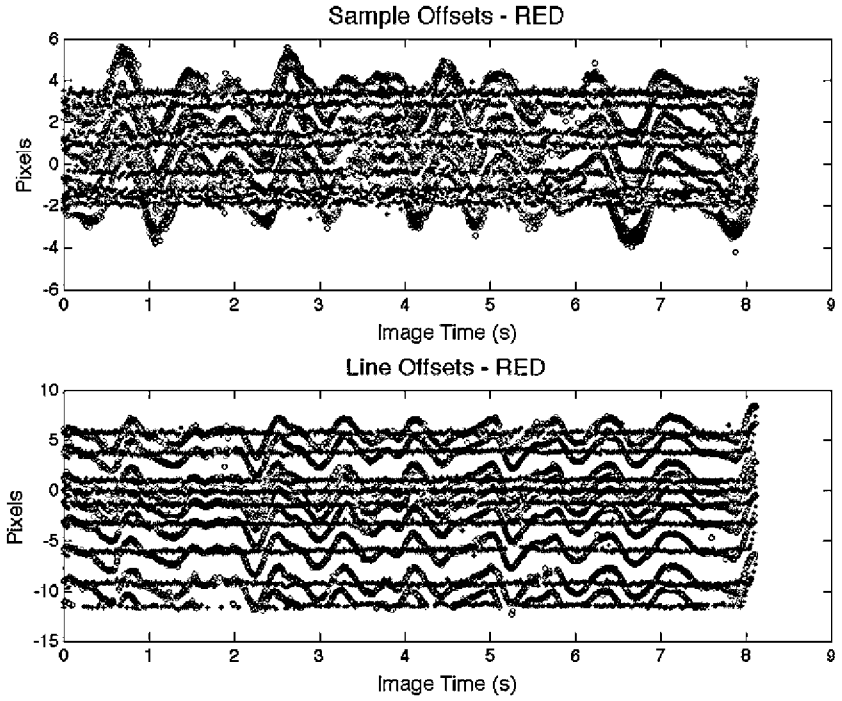

Fig. 10. Coregistration data from all nine of the overlapping RED CCD pairs in PSP_007124_1765 plotted from before jitter removal (red) and after jitter removal (blue). Sample and line offsets are measured in pixels and plotted against the image time in seconds. Data points are extracted every 50 lines. The high-frequency distortions have been removed by the jitter correction algorithm, except near the very ends of the image. The average offset of each CCD pair is preserved, and is a function of the camera geometry. (For interpretation of color mentioned in this figure the reader is referred to the web version of the article.)

4.4. DTM production

Geometric calibration and DTM production steps developed by the Astrogeology Team at USGS and used at the USGS, UA, California Institute of Technology, University of Hawaii at Manoa, and NASA Ames/SETI are described in Kirk et al. (2008). Table 8 lists DTMs that have been completed to date at these five institutions. The level of manual error correction varies in these products. We are working with other institutions to expand the DTM-production effort, since DTMs have been produced to date for only ~5% of the HiRISE stereo pairs. Some of the most significant science results from HiRISE have come from analyses of these DTMs. All of the USGS- and UA-produced DTMs, and perhaps others, will eventually be released as PDS products. Until the format for PDS is finalized, DTMs are being made available at http://webgis.wr.usgs.gov/ftphirise/index.jsp. The landing site DTMs are released as soon as possible whereas those produced for the HiRISE team science are released after initial analysis and publication of results.

For locations where stereo images are not available, the MOLA data provides the best available topographic information. Tools useful for coregistration of MOLA elevations with HiRISE images are described by Kolb and Okubo (in press).

4.5. Radiometric calibration

The radiometric calibration of HiRISE data has been a difficult task. There is great complexity from the number of channels and modes, but also the data are sensitive to FPS thermal state, which varies significantly over time. Fortunately, most HiRISE science objectives do not require highly precise radiometric calibration and we have developed techniques to eliminate artifacts that could complicate interpretations or image correlations for stereo or change detection. Radiometric calibration is most important for analysis of the color data (Delamere et al., 2009). A full description of HiRISE radiometric calibration should be published in the near future. In the meantime, significant progress has been made and we plan to reprocess all images in 2009 to incorporate a number of improvements. The PDS products will be replaced with new versions.

5. Scientific observations and results

5.1. Composition and photometry

One of the novel aspects of HiRISE is the high-resolution color capability (Delamere et al., 2009). The imaging spectrometer, CRISM, is the main tool on MRO for the investigation of the spectrophotometric properties of the surface (Murchie et al., 2007) but the spatial resolution is limited to ~18 m/pixel. In regions where compositional diversity has been found (e.g., Mawrth Vallis; Bishop et al., 2008 and see also Loizeau et al., 2007), HiRISE's color images are being used to map compositional units at scales below that of CRISM. This has proven to be extremely powerful in assessing the spatial relationships between different units and of particular importance for the investigation of potential landing sites for Mars Science Laboratory (MSL) rover mission. Many of the 466 images (Table 2) acquired within the composition and photometry theme are therefore strongly linked to CRISM targets of interest and have either been acquired as joint targets or as "ridealongs" on CRISM high priority targets in the latter phases of the planning cycles.

Although many interesting and scientifically important images have been acquired within this theme, four datasets stand out. First, images acquired in and around Valles Marineris show significant compositional diversity as discussed in, for example, Weitz et al. (2009) and Murchie et al. (submitted for publication).

A second dataset of importance is that relating to mineralogic signatures first recorded by the OMEGA experiment on Mars Express (Poulet et al., 2005; Bibring et al., 2006). Olivine appears frequently in the central peaks of craters or in crater ejecta. HiRISE is being used to survey these sites, often revealing lithologic (color and texture) diversity (e.g., PSP_006860_2370). Using significant signatures in OMEGA, CRISM, THEMIS, and TES data to target HiRISE often produces interesting images. Fig. 11 shows layered deposits inside a crater that have a spectrum consistent with the presence of kaolinite and alunite in OMEGA and CRISM data, suggestive of hydrothermal or low-temperature aqueous alteration (Swayze et al., 2008). The crater is around 70 km in diameter and located in the Terra Sirenum region at 202.5°E, 30°S. The image shows a layered mesa at the southern end of the floor of the larger structure. Bright and colorful altered material is seen in the slopes of the mesa. Several other images in this region have been acquired and await detailed analysis to establish the relationship of the observed features and the spectral data.

Third, the compositional diversity in Nili Fossae and Mawrth Vallis continues to attract considerable attention. On Earth, the formation of phyllosilicate minerals most frequently results from prolonged interaction between rock and water, so their presence on Mars, again first detected by the OMEGA experiment (Poulet et al., 2005; Bibring et al., 2006), may have significant implications for the planet's aqueous history (Mustard et al., 2008; Wray et al., 2008; Murchie et al., submitted for publication). Recent discovery of carbonate minerals in the Nili Fossae region (Ehlmann et al., 2008b) evidences further compositional diversity. Hence, these and similar sites are often discussed as potential landing sites for MSL and ExoMars. HiRISE images show that heterogeneity in the color of these regions frequently persists down to the meter scale, which suggests that, in some places, processes may be best elucidated by mapping this heterogeneity below the resolution limit of CRISM using HiRISE color (Delamere et al., 2009). Phyllosilicate-bearing materials have also been studied in the Meridiani region within this theme; examples include PSP_006860_1840 and PSP_009154_1835, which show variable-toned eroding rock filling an impact crater. Meridiani Planum remains a candidate landing site for ExoMars.

Finally, THEMIS observations suggest the presence of chlorides in the Noachian highlands (Osterloo et al., 2008). HiRISE has observed ~20 of these regions; an example is shown in Fig. 12. At the highest resolution, the relatively blue deposits are often found within relatively low-lying areas (possibly enclosed basins) and show polygonal cracks that may have formed from desiccation. Their occurrences sometimes include craters and inverted channel deposits within valley networks as seen in PSP_009318_1465, suggestive of water ponding and subsequent evaporation leading to their formation.

5.2. Impact cratering

Nearly 1000 PSP images have been returned that were assigned to the impact cratering theme (Table 2), and they have one of the most uniform global distributions of any science theme (Fig. 4). Most of these images feature relatively recent and well-preserved impact craters or their ejecta, containing meter-scale information relevant to understanding impact processes. There are also many images of relatively recent craters assigned to other themes, such as those targeting gullies, geologic contacts/stratigraphy, volcanology, or composition and photometry, where the craters provide good exposures of the bedrock. There are more than 100 images of central uplifts (peaks and/or pits or rings) designed to search for and characterize uplifted bedrock, but that also provide information on the formation of central uplifts. A large number of HiRISE images cover degraded impact craters for the study of

Table 8
Completed HiRISE digital terrain models (DTMs).

HiRISE images	Description	DTM producer[a]	Relevant publications
PSP_001414_1780			
PSP_001612_1780	Victoria crater with *Opportunity* rover	USGS	Grant et al. (2008b) and Geissler et al. (2008)
PSP_001777_1650			
PSP_001513_1655	Columbia Hills with *Spirit* rover	USGS	Squyres et al. (2008) and Arvidson et al. (2008b)
PSP_001959_2485 PSP_002091_2485	Phoenix candidate landing site	USGS	Arvidson et al. (2008a)
PSP_001919_2470 PSP_001932_2470	Phoenix candidate landing site	USGS	Arvidson et al. (2008a)
PSP_001945_2515 PSP_002077_2515	Phoenix candidate landing site	USGS	Arvidson et al. (2008a)
TRA_000894_2475 TRA_000881_2475	Phoenix candidate landing site	USGS	Arvidson et al. (2008a)
PSP_008143_2480 PSP_008301_2480	Phoenix candidate landing site	USGS	Arvidson et al. (2008a)
PSP_008644_2485 PSP_008591_2485	Actual Phoenix landing site	USGS	
PSP_001846_1415			
PSP_001714_1415	Gullies in Hellas/Centauri Montes region	USGS	Pelletier et al. (2008) and Kolb et al. (2009)
PSP_002074_2025			
PSP_002140_2025	Mawrth Vallis phyllosilicate stratigraphy	USGS	Wray et al. (2008)
PSP_009505_1755			
PSP_009571_1755	Candidate MSL landing site in Gale crater	USGS	Griffes et al. (2008)
PSP_007191_1535			
PSP_007903_1535	Candidate MSL landing site in Holden crater	USGS	Grant et al. (2008a)
PSP_006676_2045			
PSP_007612_2045	Candidate MSL landing site in Mawrth 2 region	USGS	Griffes et al. (2008)
PSP_006887_2050			
PSP_007823_2050	Candidate MSL landing site in Mawrth 4 region	USGS	Griffes et al. (2008)
PSP_001871_2670 PSP_001738_2670	north polar layered deposits stratigraphy	USGS	Fishbaugh et al. (submitted for publication)
PSP_001918_1735 PSP_001984_1735	Light-toned layered deposits in west Candor Chasma	USGS	Okubo et al. (2008b) Chan et al. (2009)
PSP_001481_1875 PSP_002167_1880	Mojave crater terraces and alluvial fans	USGS	Tornabene et al. (2007)
PSP_002661_1895 PSP_003294_1895	Topography in Athabasca Valles	USGS	Jaeger et al. (submitted for publication)
PSP_001938_2265 PSP_002439_2265	Scalloped depressions and polygons in Utopia	USGS	Lefort et al. (2009)
PSP_001432_2015 PSP_001630_2015	Basal scarp of Olympus Mons	USGS	Keszthelyi et al. (2008)
PSP_003542_2035 PSP_005599_2035	Olympus Mons slope streak with topography	USGS	Phillips et al. (2007)
PSP_001472_2785 PSP_1710_2785	Angular unconformities in north polar layered deposits	USGS	Fishbaugh et al. (submitted for publication)
PSP_003434_1755 PSP_003579_1755	Layered deposits on plains next to Juventae Chasma	USGS	Weitz et al. (2008, 2009)
PSP_003460_2015 PSP_003605_2015	Rotational landslides in Bahram Vallis	USGS	Chuang et al. (2007)
PSP_001488_1750 PSP_001752_1750	Gale crater interior mound	USGS	Thomson et al. (2008b)
PSP_006774_2020 PSP_007341_2020	Columnar jointing in crater wall in Marte Valles	UA	Milazzo et al. (2009)
PSP_003418_1335 PSP_003708_1335	Gullies within small crater within Kaiser crater	UA	Lanza et al. (2009)
PSP_004060_1440 PSP_005550_1440	Fresh crater inside older crater in southern highlands	UA	Lanza et al. (2009)
PSP_007018_1255 PSP_007229_1255	Channels on Russell crater dunes	UA	Hansen et al. (submitted for publication)
PSP_002620_1410 PSP_002686_1410	Gullies at multiple topographic levels	UA	Kolb et al. (2009)
PSP_004106_1245 PSP_003816_1245	Layered sinuous ridge in Argyre planitia	UA	
PSP_005609_1470 PSP_005754_1470	Channels emanating from Hale crater ejecta	UA	Philippoff et al. (2009)
PSP_006668_1470 PSP_005811_1470	Candidate chloride salt deposit in Terra Sirenum	UA	Osterloo et al. (2008)
PSP_005429_1510			
PSP_005851_1510	Columbus crater layered clays and salts	UA	Wray et al. (2008)
PSP_005372_1515 PSP_006005_1515	Ritchey crater central peak megabreccia	UA	McEwen et al. (2008)
PSP_003611_1970 PSP_004244_1970	Floor of rayed crater Corinto	UA	Bray et al. (2009)
PSP_002118_1510 PSP_003608_1510	Rayed crater Zumba	UA	
PSP_002076_1735 PSP_002498_1735	Faulted and folded deposits in west Candor Chasma	Caltech and UA	Okubo et al. (2008b)
PSP_001401_1850 PSP_002021_1850	Layered stepped buttes in Crommelin crater	Caltech	Lewis et al. (2008)
PSP_001902_1890			
PSP_002047_1890	Crater in western Arabia Terra with stair-stepped hills	Caltech	Lewis et al. (2008)
PSP_002733_1880			
PSP_002878_1880	Faulted layers in impact crater in Meridiani Planum	Caltech	Lewis et al. (2008)
PSP_001546_2015			
PSP_001955_2015	Very long sequence of layering in Becquerel crater	Caltech	Lewis et al. (2008)
PSP_002932_1445 PSP_003209_1445	Light-toned gully materials on Hale crater wall	Caltech	Kolb et al. (submitted for publication)
PSP_004066_1530 PSP_003077_1530	Fan in southern Holden crater	Caltech	Grant et al. (2008a)
PSP_003288_1530 PSP_003710_1530	Uzboi Vallis breach in Holden crater rim	Caltech	Grant et al. (2008a)
PSP_001468_1535 PSP_002154_1530	Best fan surfaces in west Holden crater	Caltech	Grant et al. (2008a)
PSP_004000_1560 PSP_004356_1560	Measurement of stratal dips in possible delta-lake transition, Eberswalde	Caltech	Griffes et al. (2008)
PSP_002233_1560 PSP_001600_1560	Eberswalde crater, just east of candidate MSL landing site	Caltech	Griffes et al. (2008)
PSP_006633_2010 PSP_007556_2010	Characterize surface hazards at Nili Fossae candidate MSL landing site	Caltech	Griffes et al. (2008)
PSP_003086_2015 PSP_003587_2015	Nili Fossae phyllosilicates, go-to site for candidate MSL landing site	Caltech	Mustard et al. (2008)
PSP_001882_1920 PSP_002594_1920	Pettit crater wind streaks and intercrater dunes	Caltech	
PSP_007087_1700 PSP_007667_1700	Finely layered fan deposit of possible subaqueous origin	Caltech	Metz et al. (2008)
PSP_005771_2035 PSP_007406_2035	Tooting crater inner SW wall	UH	Garbeil et al. (2007)
PSP_001538_2035 PSP_002158_2035	Tooting crater cavity	UH	Garbeil et al. (2007)

(*continued on next page*)

Table 8 (*continued*)

HiRISE images	Description	DTM producer[a]	Relevant publications
PSP_002580_2035 PSP_002646_2035	Tooting crater west rim	UH	Garbeil et al. (2007)
PSP_006750_2130 PSP_007462_2130	Bacolor crater, cavity and southern ejecta layer	UH	
PSP_005813_2150 PSP_005879_2150	Odd craters near Hrad Vallis	UH	Keszthelyi et al. (submitted for publication)
PSP_008823_2310 PSP_009245_2310 PSP_004060_1440	Central peak of Lyot crater	Ames/SETI	Hart et al. (2009)
PSP_005550_1440	Fresh gullied crater inside older crater	Ames/SETI	Kolb et al. (2009)

[a] DTM producers: USGS = R. Kirk's group at the US Geological Survey in Flagstaff, AZ; UA = A. McEwen's group at the University of Arizona; Caltech = O. Aharonson's group at the California Institute of Technology; UH = P. Mouginis-Mark's group at the University of Hawaii at Manoa; Ames/SETI = R. Beyer's group at NASA Ames Research Center/SETI Institute.

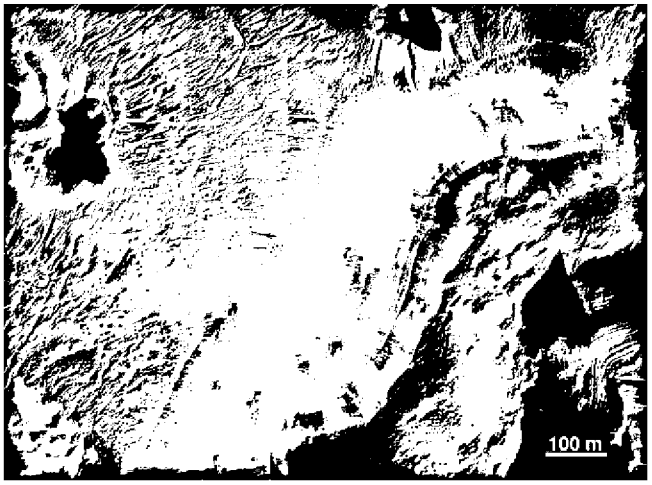

Fig. 11. Enhanced IRB color of a portion of PSP_010228_1490 showing a region targeted because of the presence of likely kaolinite and alunite in *Mars Express*/OMEGA and CRISM spectra. The image shows layers exposed in a mesa inside a 70-km diameter crater; image center is 30.7°S, 202.2°E. Illumination is from the upper left (northwest).

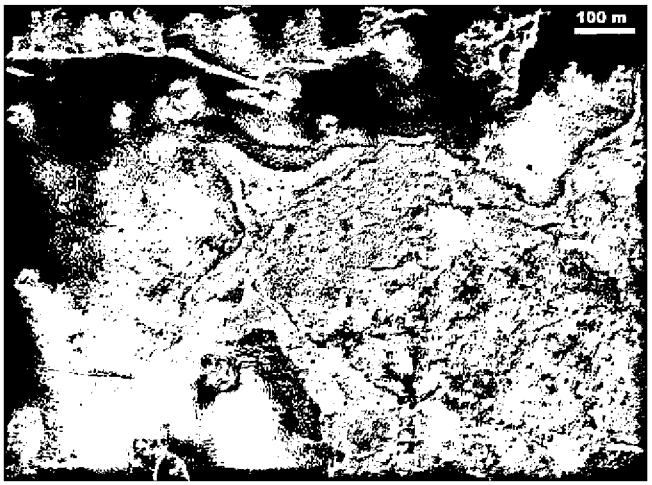

Fig. 12. Section of PSP_008780_1735. This image was acquired of a site suggested by the THEMIS team as having exposed chloride salts. This color composite shows distinct surface units. At the highest resolution, the apparently blue material shows a cracked surface structure.

aeolian, seasonal, mass wasting, fluvial, tectonic, and other processes. In general images of degraded craters do not provide much information about the impact cratering process, but there are exceptions, especially where internal structures have been exposed (e.g., craters significantly eroded but bearing minimal infilling, partial impact craters on the walls of Valles Marineris, etc.). A good example is Hargraves crater (20.7°N, 75.8°E) where erosion has exposed the internal structures and diverse composition within megabreccia blocks of the crater ejecta (part of the Nili Fossae candidate MSL landing site).

More than 100 HiRISE images cover very small primary craters (diameters <50 m) that most likely formed in very recent years, including the impact sites identified by Malin et al. (2006). Most of these new impact sites are found by the CTX team, which then requests HiRISE coverage. More than half of these impact sites are clusters of craters resulting from atmospheric breakup, and their shape and dispersion provide information on the strengths and densities of the bolides (Ivanov et al., 2009). Measurement of

Fig. 13. A large new impact cluster in PSP_003172_1870 (left and full-resolution false-color inset) and PSP_007431_1870 (right). These images were acquired before and after the global-scale dust storms of 2007, and show that fresh and relatively dark impact markings can disappear by darkening of the surroundings from dust removal as well as from new dust deposition that homogenizes the albedo. Thousands of new small impact craters were created by this single event. Several other new impact sites imaged before and after the 2007 dust storms do not show obvious changes.

the current cratering rate enables dating of very young surfaces where contamination by secondary craters is unlikely, provided the present-day modification processes are understood (e.g., Smith et al., 2008a) and the nature of primary crater clusters are understood (Kreslavsky, 2008). These new impact sites will be re-imaged in future years to monitor changes (e.g., Fig. 13) and to provide information on the rates of ongoing aeolian and polar processes. In the northern summer of 2008 there has been a campaign to image all candidate impact craters (mostly discovered from CTX images) on the apparently very young north polar cap, to better understand its ongoing modification (Banks et al., 2009b).

We have imaged a number of well-preserved km-scale craters such as Winslow crater located at 59.16°E, 3.74°S in the Syrtis Major region (Fig. 14). This relatively youthful, approximately 1-km diameter impact crater is similar to Meteor crater in Northern Arizona, and is distinctive in THEMIS nighttime thermal infrared images (Wright and Ramsey, 2006). The crater exhibits a bright, warm ejecta blanket suggesting that it is rockier than the surrounding surface materials of Syrtis Major, which is indicative of it being a relatively fresh Martian crater. The first HiRISE image acquired of Winslow crater (PSP_004313_1760) shows that it possesses distinctive secondaries with dark surge deposits in the typical herringbone pattern, which is like those around fresh lunar craters. Also noteworthy are the large meter-to-decameter-sized boulders on the steep rim. This is also reminiscent of Meteor crater and examples of fresh simple craters on the Moon. Later, a second HiRISE image of Winslow (PSP_005658_1760) was taken to obtain a stereo pair. By chance this second image was taken after the dust storm that enveloped the planet in summer 2007. Dust deposited during this storm blanketed the region and largely obscured the albedo differences between the dark rays and the surrounding bright soil. Laboratory experiments on natural surfaces indicate that a layer of dust only a few tens of microns thick is sufficient to achieve such obscuration (Wells et al., 1984). The thin dark lines that cross the later image show that dust devils have already begun the work of cleansing the surface of dust and restoring the region to its previous appearance. An image acquired in the ESP (ESP_012356_1760) shows albedo patterns similar to those in PSP_004313_1760.

More than 100 images of candidate well-preserved large (>1 km) impact craters (McEwen et al., 2007b; Tornabene et al., 2007) have been acquired. These craters are informative about cratering processes as many of them retain their primary surfaces (i.e., those related to the impact process), including impact melts and fall-back breccia deposits, in addition to various morphologic signs of the role of subsurface volatiles (e.g., water and water–ice; Bray et al., 2009) and overland flow of water (Williams and Malin, 2008). These large fresh craters are also the source of huge numbers of secondary craters, some of which correlate with crater rays apparent in THEMIS nighttime images (e.g., McEwen and Bierhaus, 2006; Preblich et al., 2006; Tornabene et al., 2006). Recently, THEMIS and HiRISE co-analysis led to the discovery and confirmation of two newly recognized large crater ray systems on Elysium Mons. Corinto crater, which is located at 141.72°E, 16.95°N, is now the largest recognized rayed crater with an average diameter of 13.8 km and with distinctive ray segments extending over 2000 km from the primary cavity (Tornabene et al., 2008). One smaller, as of yet unnamed, 2.5-km diameter rayed crater located at 151.4°E, 22.5°N possesses ray segments traversing >170 km from the primary (possibly 2× that distance) or ~136 crater radii consistent with other Martian rayed crater systems (Tornabene et al., 2006). Both of these craters possess numerous ray segments that are prominent in THEMIS nighttime infrared images that correlate with dense clusters of secondaries in HiRISE images. We have found chains of secondary craters emanating from many other well-preserved craters, although extensive rays are not apparent at optical or IR wavelengths. Although distant secondary craters can greatly increase uncertainties in attempts to date surfaces with small craters, they can also provide extensive stratigraphic markers to show the relative ages of adjacent or widely separated terrains (e.g., Schon et al., 2009).

5.3. Volcanology

More than 600 images with "Volcanic Processes" as the primary science theme have been acquired during the PSP (Table 2). While early imaging emphasized sampling a variety of volcanic terrains, after about 6 months the focus shifted to well preserved or otherwise especially interesting localities (Fig. 4). The results of the early imaging of primary volcanic features are largely covered in Keszthelyi et al. (submitted for publication). Highlights include (a) unequivocal evidence for inflated lavas on Mars (Fig. 15), (b) detailed observations of near-vent deposits including perched lava ponds, cinder cones, and fountain-fed sheet flows, and (c) the discovery of a covered lava channel that forms a natural bridge (PSP_001420_2045). HiRISE color data led to the suggestion that the extensive "dust" mantle on the Tharsis volcanoes, which locally

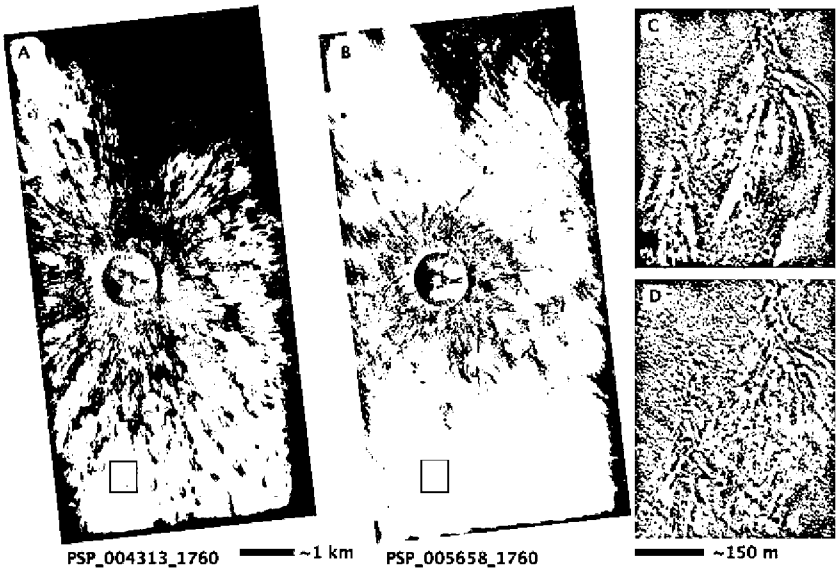

Fig. 14. HiRISE images of Winslow crater, showing changes before and after the dust storms of 2007. North is up in these equirectangular projections.

Fig. 15. Example of inflated lavas in the western margin of the Cerberus Palus lava flow that erupted from the head of Athabasca Valles, ~850 km to the east-northeast. Thin lobes of lava flowed around topographic obstacles, then inflated vertically, often to greater heights than the original obstacles. The many small bright-ejecta craters over areas not covered by the young lava are secondary craters from the rayed crater Corinto, ~735 km almost directly north of this location. Corinto rays are superimposed on this lava flow, but the detectability and retention of small craters varies with physical properties of the surfaces. PSP_007448_1845, equirectangular projection (north is up); illumination from the west (left).

reaches a thickness of several tens of meters, actually includes large volumes of volcanic airfall deposits.

A major area of volcanic research not discussed in Keszthelyi et al. (submitted for publication) is the interaction between lava and water. Jaeger et al. (2007, submitted for publication) report on the best-preserved phreatovolcanic features known on Mars, located in Athabasca Valles. These features provided strong evidence that the last material that flowed through Athabasca Valles and ponded in Cerberus Palus was lava, not water or ice. The extant equatorial frozen sea proposed by Murray et al. (2005) was thus shown to actually be an extremely voluminous single lava flow. Further confirmation has come from the Shallow Radar (SHARAD) experiment on MRO (Seu et al., 2007), which sees layering in this region but with loss tangents consistent with rock and incompatible with pure or dirty ice (Orosei et al., 2008). Continued studies of this flow (Jaeger et al., submitted for publication) show that the lava flow was emplaced as a short-lived turbulent flood. This style of eruption is fundamentally different than that observed for terrestrial continental flood basalts and points to significant (but still unresolved) differences in the subsurface plumbing system. Other evidence for lava-water interaction is summarized in Keszthelyi et al. (submitted for publication), with more details on "entablature" style columnar jointing in Milazzo et al. (2009), from cones in SW Elysium Planitia (Lanz and Saric, 2009), and from possible tuyas described by Martinez-Alonso et al. (submitted for publication).

As was revealed by Mariner 9, the scale of Martian volcanic features often dwarf similar features on Earth. HiRISE continues to expand the range of examples, including kilometer scale inflation features (Keszthelyi et al., submitted for publication) and voluminous turbulent floods of lava (Jaeger et al., submitted for publication). Overall, the variety of styles of mafic volcanic activity on Mars rivals, and in some areas exceeds, that seen on Earth. One of the most important lessons from the early imaging was that meter-scale volcanic features would not be discernable, should they exist, across vast parts of Mars. At higher latitudes, this is largely due to the volatile-rich mantling deposit and reworking of the surface by permafrost processes (Section 5.9). In equatorial areas, the mantle is mostly dust. In such areas, MRO's CTX camera, with ~30 km wide ~6 m/pixel images, is often more useful. However, HiRISE scale is useful for producing DTMs with sub-meter vertical precision, even when a mantle obscures sub-meter volcanic morphologies. Also, even in dust-mantled areas there may be steep scarps exposing lavas in cross-section; study of one such image (PSP_004412_1715) on the flank of Arsia Mons revealed an average of 17 layers with 51 m thickness (Mouginis-Mark and Rowland, 2008).

5.4. Tectonism

Studies pertaining to crustal deformation (e.g., folding, faulting, and related processes) fall under the theme of Tectonic Processes. By the end of the PSP 333 HiRISE images were acquired with Tectonic Processes as the primary science theme and more than 100 additional images were acquired with Tectonic Processes as the secondary science theme. Initial imaging for the Tectonic Processes science theme sampled classic, large scale, tectonic terrains such as wrinkle ridges in Hesperia and Solis plana and the Tharsis-radial graben and normal fault systems. These images immediately showed that the usefulness of the structural information that can be gained from data at HiRISE resolution is strongly affected by any post-tectonic modification (e.g., erosion, burial, periglacial processing, etc.). While not unexpected, these observations clearly demonstrate the importance of accounting for the effects of post-tectonic modification when drawing structural interpretations from larger-scale datasets (e.g., CTX, THEMIS, MOLA).

The first HiRISE image of Mars (AEB_000001_0000; see Fig. 16 of McEwen et al., 2007a) serendipitously covered a prominent thrust fault-related fold (wrinkle ridge) in Bosporos Planum. This image revealed abundant aeolian, fluvial, and periglacial features on the surface of the fold, but tectonic features that could be attributed to fold growth, such as patterns of axial fracturing, are not clearly resolved. Subsequent HiRISE observations of other Noachian and Hesperian-aged thrust faults (e.g., PSP_006508_1415, PSP_007614_2005) and normal faults (e.g., PSP_006770_2255, PSP_003251_1475) show similar results. That is, much of the primary tectonic geomorphologies of these ancient structures appear overprinted by subsequent geologic processes, to the extent that HiRISE images largely reveal details of this post-tectonic modification rather than the original tectonism. Thus, data from instruments with wider fields of view (e.g., CTX, THEMIS, HRSC) and spatial sampling (e.g., MOLA) are found to be generally better suited for studies of large-scale structures that are sufficiently old to have undergone significant post-tectonic modification. In these cases, HiRISE images are best used to characterize any such post-tectonic modifications to the surfaces of these tectonic features, which may affect interpretations drawn from larger-scale datasets.

In areas of minimal post-tectonic modification or of recent erosion exposing fresh bedrock, HiRISE data are valuable for investigating tectonic systems at scales much finer than could be resolved with earlier orbiter-based datasets. In these areas, the scale of features appropriate for study with HiRISE is constrained by the limit of resolution of tectonic structures. Analysis of sample HiRISE data shows that the location of a tie point on either side of a fracture (e.g., offset layers or asperities) can be resolved to within roughly 3-pixel accuracy. Thus, the relative displacement of the fracture walls can be measured to within a minimum of 6 pixels, or 1.8 m for 0.3 m pixel widths. A displacement of 1.8 m corresponds to a

minimum fault length of roughly 200 m, assuming a critical strain (maximum displacement to fracture length) of 6.7×10^{-3} (Wilkins et al., 2002) to $\sim 1 \times 10^{-2}$ (Hauber et al., 2007). For joints, this minimum length is ~360 m, assuming a critical strain for joints of $\sim 5 \times 10^{-3}$ (Okubo et al., 2007). Thus in order for fracture displacement to be measured in typical HiRISE images, the length of that fracture must be greater than ~200 m for faults and ~360 m for joints. Shorter fractures (with smaller displacements) can be detected down to a single pixel, which is often sufficient for studies that do not require measurements of fracture displacement, such as characterizing fracture densities and map-view orientations.

HiRISE's ability to image in color and at high resolution, as well as the MRO spacecraft's capability to point the camera off nadir for stereo imaging, are key attributes that make these data valuable for studies of Tectonic Processes. An early HiRISE image of Mars (TRA_000836_1740) revealed evidence of fluid flow along fractures within the interior layered deposits on Ceti Mensa, in west Candor Chasma (Okubo and McEwen, 2007). Subsequent HiRISE observations of other equatorial layered deposits revealed additional evidence of fluid flow along fractures (Okubo et al., 2008a). Here, fluid flow is evidenced by light-toned and dark-toned discolorations and apparent induration along the wallrock of the fracture. HiRISE stereo and color are crucial in distinguishing these diagenetic fingerprints from topographic shading. Recognizing this widespread occurrence of fracture-controlled fluid flow within the equatorial layered deposits is significant because evidence of past hydrologic, geochemical, and biologic processes are often concentrated and preserved in analogous fracture-fluid systems on Earth (e.g., Boles et al., 2004; Shipton et al., 2004, 2005; Souza-Egipsy et al., 2006; Bowen et al., 2007).

DTMs derived from stereo HiRISE observations (Kirk et al., 2008) are also an important new tool for investigating Tectonic Processes on Mars. These data have been used to investigate the meter-scale structure of the Light Toned Layered Deposits (LTLD) in southwest Candor Chasma, near the contact between the LTLD and the chasma wall (Fig. 16; Okubo et al., 2008b). The HiRISE DTM of this area, constructed with 1 m postings, allows the orientation of geologic structures (bedding, faults) to be confidently quantified at the scale of roughly 100 m. Through detailed structural mapping of the area, Okubo et al. (2008b) found an abundance of thrust faults, normal faults, and folds, many with discernable crosscutting relationships. Based on these observations, Okubo et al. (2008b) showed that evidence of large-scale normal faulting that can be attributed to chasma formation (e.g., Schultz and Lin, 2001) is not exposed at the surface in this area. Instead, an approximately 2 km thick, conformable stratigraphic sequence is exposed throughout their area. Thus at least several kilometers of LTLD were deposited in this part of Candor Chasma after any such chasma-related normal faulting. Okubo et al. (2008b) also found that these LTLD were most plausibly deposited in an existing basin. Further, the patterns of deformation that are observed are found to be strongly consistent with the erosional remnants of the basal part of a ~5 km-wide landslide within the LTLD.

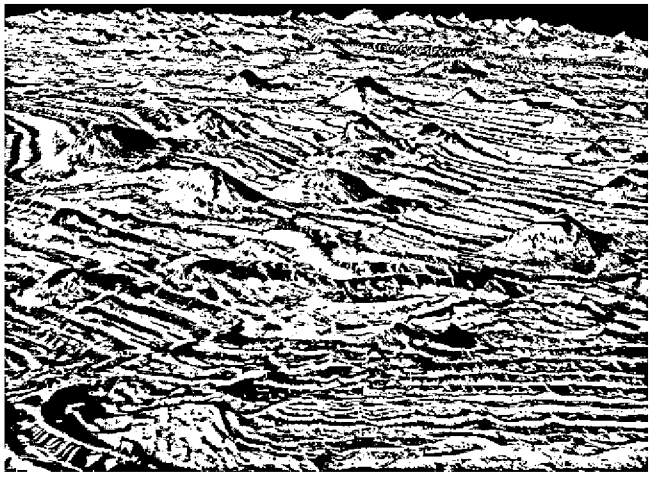

Fig. 16. Perspective view looking north in southwest Candor Chasma showing faulting and folding of the LTLD. View is from an altitude of 200 m above the surface, and the bottom of the image is approximately 1.5 km across. No vertical exaggeration; enhanced color. Image PSP_003474_1735.

5.5. Fluvial and hydrothermal processes

Fluvial processes has been a popular theme, with 777 PSP images (Table 2), although this number is somewhat inflated by the Quest images (Section 7). Also, many suggestions relevant to fluvial processes are assigned to other themes, such as composition and photometry, landscape evolution, and sedimentary/layering processes.

We have acquired more than 800 images that show geologically recent "gullies" (or ravines, debris flows, etc.), assigned to multiple themes. Of particular interest are the bright gully deposits that formed during the MGS era, and suggested to be evidence for water flowing on Mars in the present-day climate (Malin et al., 2006). Followup on these and other bright slope deposits by HiRISE and CRISM has shown that they can be explained as dry granular flows (McEwen et al., 2007b; Pelletier et al., 2008; Kolb et al., submitted for publication). Many other studies with HiRISE images have confirmed a likely role for water in the formation of at least some of the gully features, and have certainly shown that these are complicated, evolved landforms (e.g., Gulick et al., 2008; Welty et al., 2008; Head et al., 2008). Studies utilizing HiRISE topographic data seem particularly promising for understanding the origins of gullies (Lanza et al., 2009; Parsons et al., 2008; Howard et al., 2008; Kolb et al., submitted for publication). Putative evidence dating gully activity seen in PSP_002293_1450 at ~1 Ma (Schon et al., 2009) appears from a HiRISE stereo pair (http://hirise.lpl.arizona.edu/anaglyph/singula.php?ID=ESP_012314_1450) to instead provide an upper limit on the age of the two gully fans.

HiRISE has acquired many images of outflow channels, including cataracts (Davatzes and Gulick, 2007; Fig. 9). One hope for HiRISE was to finally resolve flood-transported boulders (McEwen et al., 2007a). The best target seemed to be the putative subaqueous dunes in Athabasca Valles (Burr et al., 2004), but HiRISE showed these features to consist of or to be coated by lava (Jaeger et al., 2007). However, boulders have been seen within features interpreted as subaqueous dunes in Holden crater (see Section 5.7). Boulders are commonly seen in association with sedimentary deposits of potential fluvial origin, but it is often unclear if these were transported or represent breakdown of indurated fine sediments.

There have been relatively few suggestions entered for hydrothermal processes, in part because it is difficult to recognize evidence for such processes in high-resolution images. CRISM detections of minerals such as kaolinite (e.g., Fig. 11) and other hydrous silicates, sometimes associated with impact craters (Mustard et al., 2008), particularly central peaks (see Sections 5.2 and 5.6), are perhaps a better guide to such targets. Allen and Oehler (2008) suggested there was evidence for spring mounds in PSP_002812_1855 in Vernal crater, in SW Arabia Terra, although a HiRISE stereo pair (PSP_002812_1855 and ESP_011844_1855) does not seem to confirm the existence of topographic mounds at this location.

5.6. Geologic contacts, stratigraphy, and layering processes

The geologic contacts/stratigraphy science theme accumulated 502 images by the end of the PSP. The suggestions span much of

the surface of Mars (Fig. 4) and include features such as central peaks and walls of impact craters, locations where distinct geologic units intersect, and places with exposed stratigraphy. The Sedimentary/Layering science theme has a total of 551 PSP images. Most of the suggestions are located where layered deposits are exposed, such as inside and around Valles Marineris, Meridiani Planum, and Mawrth Vallis (Fig. 4).

5.6.1. Geologic Contacts/Stratigraphy

We are in the midst of a paradigm shift with respect to the Noachian (>3.8 Gyr) crust of Mars. Imaging spectrometers (Bibring et al., 2006; Mustard et al., 2008; Murchie et al., submitted for publication) have shown that hydrous alteration is ubiquitous. With the high-resolution observations of MRO it is apparent that much of and perhaps most of the Noachian bedrock is at least partly altered. Although alteration is widespread, unaltered bedrock may comprise a much greater volume of the Noachian crust (Christensen et al., 2005b). There are only small-scale exposures except in a few locations (Mawrth Vallis, Nili Fossae regions); the surface is largely covered by up to ~100 m of younger materials, probably a mixture of impact-generated regolith and volcanic and aeolian materials. Below this mantling layer the crust appears indurated, supporting steep slopes, unlike the lunar highlands. HiRISE has discovered megabreccia (Grant et al., 2008a; McEwen et al., 2008) especially in central peaks and near impact basins such as Nili Fossae (near Isidis basin), but appears to be indurated, probably by interaction with groundwater (e.g., diagenetic and hydrothermal alteration). Fluid-filled fractures are common in Valles Marineris (Okubo and McEwen, 2007) and many other locations, from the action of groundwater. The central peaks of large impact craters often expose bedrock and are often imaged by HiRISE and CRISM (Fig. 17). HiRISE images are revealing distinctive textures (Edwards et al., 2008) and colors (Delamere et al., 2009) of olivine-rich bedrock.

Fig. 17. Portion of HiRISE enhanced-color image PSP_007694_1700 showing layered beds exposed in the central peak of Oudemans crater. The strata must have been brought up from several kilometers depth, which suggests that areas beneath the Hesperian lava plains around Valles Marineris may be layered bedrock that is light-toned in nature.

5.6.2. Sedimentary/layered deposits

Finely layered deposits of likely sedimentary origin (aqueous, aeolian, pyroclastic, or from impact sedimentary processes) have been high-priority targets. Horizontal layers associated with fluvial-lacustrine settings have been studied in Holden (Grant et al., 2008a), Gale (Thomson et al., 2008b), Jezero (Ehlmann et al., 2008a), and Columbus (Wray et al., 2009) craters, and in the larger Xanthe Terra (Hauber et al., 2008). Melas Chasma contains fans with morphologies similar to submarine fans in the Gulf of Mexico (Metz et al., 2008). There are extensive light-toned sedimentary layers inside the Valles Marineris, for which HiRISE is revealing new details (Chojnacki and Hynek, 2008; Fueten et al., 2008; Murchie et al., submitted for publication). Study of a HiRISE DTM in western Candor Chasma has demonstrated that these sulfate-rich deposits post-date the opening of the canyon, as discussed in Section 5.4 (Okubo et al., 2008b; Fig. 16). Extensive fine-layered deposits with distinctive morphologic and spectral properties have been revealed on the high plateaus surrounding Valles Marineris (Milliken et al., 2008; Weitz et al., 2008, 2009). Several equatorial craters contain remarkably periodic layers, perhaps driven by astronomical cycles (Fergason and Christensen, 2008; Lewis et al., 2008; Fig. 18). The potential chloride salt deposits scattered through the highlands have distinctive morphologic and color signatures in HiRISE data (Osterloo et al., 2008; Fig. 12). The diverse hydrated silicates detected by CRISM near and within Mawrth Vallis occur in a distinct stratigraphic sequence, with the uppermost horizons conforming to pre-existing topography over an area of $\sim 10^6$ km (Wray et al., 2008; Bishop et al., 2008; Noe Dobrea et al., submitted for publication). A 100–200 m thick deposit of fine-grained sediments draping kilometers of relief in the Electris region may have resulted from airfall of volcanic ash (Grant et al., 2009).

5.7. Landscape evolution

HiRISE images falling in the landscape evolution category cover a range of surface characteristics and are often submitted with the

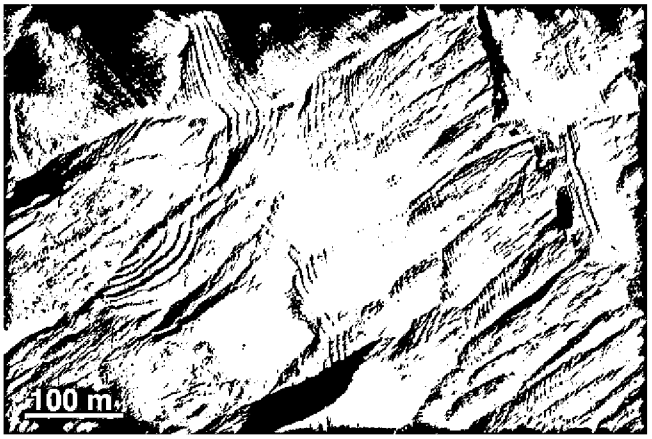

Fig. 18. Portion of HiRISE image PSP_008002_1750 showing quasi-periodic or evenly spaced layering at the top of the large mound in Gale crater.

intent of understanding the processes responsible for evolution of a particular set of landforms or exposed layers. As might be expected, landscape evolution images are scattered across the planet (Fig. 4) and lack the concentration around particular landforms or regions that is associated with some other science themes. More than 330 images were acquired in this science theme by the end of the PSP and have assisted in evaluation of the depositional settings across the planet. One example study combining HiRISE and MER *Opportunity* observations is that of the degradation of Victoria crater (Grant et al., 2008b). Two detailed examples of how these images have been used to evaluate diverse depositional settings follow.

Sinuous ridges with dendritic and braided morphologies form an anastomosing network in southern Argyre Planitia (Kargel and Strom, 1992). Interpretation of HiRISE images within the framework created by other datasets (e.g., CTX and MOLA) helps to distinguish between candidate processes that contributed to their formation. Most characteristics of the ridges are consistent with sub-ice fluvial processes and suggest the ridges are most likely eskers (Banks et al., 2009a). HiRISE reveals apparently flat-lying layers in several ridges that appear to alternate between resistant and less resistant layers. Some layers are discontinuous while others are laterally continuous for several kilometers and some clearly extend across the width of the ridge. HiRISE also resolves large, often angular boulders, some more than 8 m across, distributed in layers and scattered on ridge surfaces. The more angular boulders appear to be eroding out of indurated layers and it is not clear whether other boulders were transported. MOLA shows that variations in ridge height are apparently related to the surrounding surface slope with ridge height increasing on descending slopes and decreasing on ascending slopes; this is a characteristic observed in terrestrial eskers (Shreve, 1985). The size, aspect ratio, and extent of the ridges imply significant water was available for their formation, and that southern Argyre was covered by a thick, stagnating or retreating glacier.

HiRISE images of layered deposits in the 154 km diameter Holden crater (26°S, 326°E) resolved sub-meter bedding whose characteristics enable definition of depositional setting (Fig. 19). Numerous HiRISE images at 26–56 cm/pixel scale reveal megabreccia beneath two sedimentary facies emplaced during two Noachian wet alluvial/lacustrine phases. As summarized from Grant et al. (2008a), the first wet phase was associated with early, prolonged erosion of crater walls and saw deposition in fans and a relatively thick lower unit on the crater floor. The second wet phase was caused by high-magnitude flooding when Uzboi Vallis breached the crater rim in the Late Noachian and deposited a thinner upper unit.

The lower unit overlies the megabreccia and includes three members distinguished by varying reflectance, bed thickness, and phyllosilicate spectral signature from CRISM. The lower and middle members of the lower unit display meter-scale flat-lying beds apparently devoid of complex stratal geometries (e.g., truncating beds). Lower unit beds are typically dark and traceable for hundreds of meters, whereas middle member beds are brighter and can be traced for up to kilometers along more extensive outcrops. Upper member beds are flat lying and thinner than middle and lower member beds and are sometimes separated by meter-scale darker-toned blocks. The thin bedding, lateral continuity, and restriction below a common elevation point to a water-lain origin for all the lower unit beds in a distal alluvial or lacustrine setting.

The upper dark unit includes low angle fans composed of coarse bedded deposits and capped by flat-lying beds that are approximately radial to the breach where discharge from Uzboi Vallis drained into the crater. The largest fan reaches 60 m above the surrounding surface and much of it is covered by bedforms that incorporate meter-scale blocks and that are interpreted to be subaqueous dunes. Beyond the fans, the upper unit consists of tens of meters of crudely layered beds that unconformably drape the lower unit and become more continuous and parallel towards the crater center. Blocks up to 100 m across of lower unit deposits are enveloped in the upper unit and point to a high magnitude flood event.

5.8. Aeolian processes and landforms

Mars, with a dynamic atmosphere and a range of particles that are harnessed by the wind, has a greater known diversity of aeolian (wind) processes and landforms than any other world besides Earth. The high resolution and clarity of HiRISE images has increased our understanding of previously documented aeolian landforms and shown unexpected features that in some cases indicate geologic processes unique to Mars.

By the end of the PSP, 309 images assigned to the aeolian theme were acquired. However, nearly all HiRISE images of Mars have bedforms, yardangs, and other aeolian features within them, and many of the discoveries reported here and in other papers were from images not assigned to the aeolian theme. Some of these initial findings were published in Bridges et al. (2007) and include (1) fine-scale 2nd and 3rd order superposed bedforms on dunes and ripples, (2) bedforms located in relatively young craters and gullies, a constraint on the rates of aeolian modification of the surface, (3) diverse yardang textures indicative of multiple modes of formation or modification, (4) unexpected "reticulate" bedforms in the Tharsis and Elysium Montes, and (5) evidence for current sand movement at Victoria crater. More detailed investigations of items 4 and 5 are reported by Bridges et al. (2009) and Geissler et al. (2008). The latter study effectively combines results from the MER *Opportunity* rover with HiRISE data and shows that basaltic sand is actively being blown out of Victoria crater, forming the dark streaks on the adjacent plains. Similarly, Thomson et al. (2008a;

Fig. 19. Portion of HiRISE image PSP_002721_1530 in Holden crater showing sub-meter thick and laterally continuous beds of the upper member of the lower unit. Characteristics of these deposits discernable in HiRISE images enable their depositional setting to be constrained to a distal alluvial or lacustrine aqueous environment.

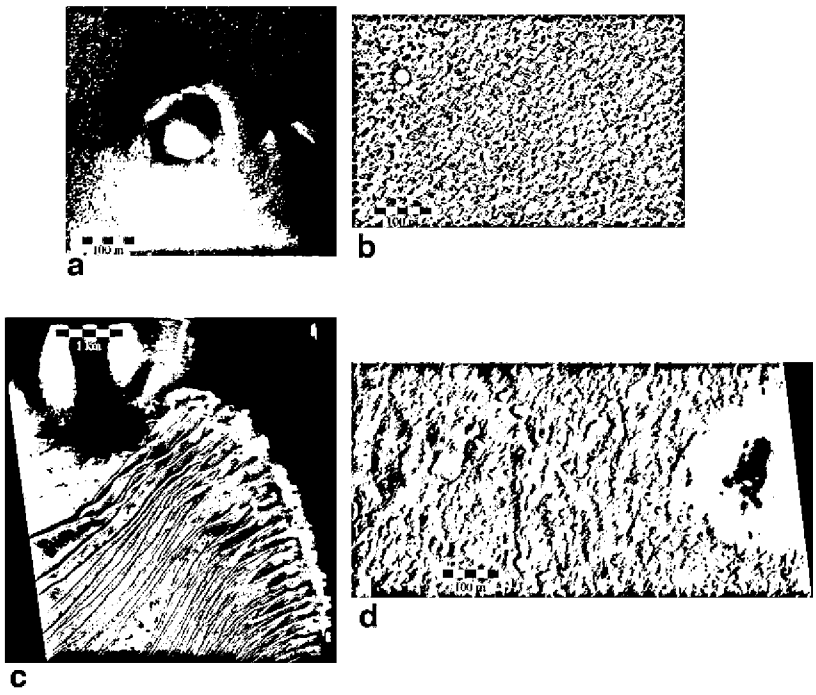

Fig. 20. Representative HiRISE images of recent aeolian findings. (a) Dunes in the north polar erg with downwind sand streaks (PSP_009295_2565), (b) ice streak downwind of ice-filled crater (PSP_009189_2645), (c) Russell crater dunes in late southern winter (PSP_010301_1255), (d) dust devil in Amazonis Planitia (PSP_009819_2130), local time 3:26 P.M.

see also Greeley et al., 2008) used MER *Spirit* Pancam and Navcam images to map out the orientation of ventifact features in the Columbia Hills. Using HiRISE images, they showed that the ventifact orientation was predominantly aligned with 2nd order (T_2) ripple trends, that is, ripples superposing the main ripple set. They concluded that T_2 aligned winds, not those perpendicular to the main ripples, have been the dominant drivers of sand movement and abrasion in this region.

There are several other noteworthy discoveries not reported in the above publications:

Ice-cored dune abrasion. Some north polar erg dunes have dark wind streaks, indicative of abrasion of ice-cemented sand (Fig. 20a). This is consistent with the observations of Bourke et al. (2008) of dune shrinkage and erasure in this region.

Ice streaks. Bright streaks are seen in the lee of some craters that contain seasonal ice deposits (Fig. 20b). We interpret these as deposits of ice grains liberated by near surface winds. This suggests that the ice in these craters, or at least that composing the upper surface, is of a particulate nature, with some particles of a size that will not go into suspension, therefore on the order of a few hundred microns in diameter.

Channels on dunes. HiRISE continues to monitor the seasonal volatile changes on dunes that contain enigmatic channel/gully features, such as those in Richardson and Russell craters (Fig. 20c). Of relevance to aeolian studies, these dunes contain a diversity of fine-scale superposed bedforms that may change over time from processes due to wind or those responsible for channel formation.

Dust devils. Several active dust devils have been imaged by HiRISE, providing high-resolution morphologic and color information from the overhead perspective (Fig. 20d). The CTX experiment is providing a record of dust-devil activity near 3:00 P.M. at a variety of latitudes.

Change detection. MRO completed a bit more than 1 Mars year during the PSP. We are therefore now getting HiRISE images of previously imaged regions of the planet under similar lighting geometries. Comparison of images separated by a year or more may show dune or ripple migration. So far, no changes have been found, but precision geometric corrections (see Section 4.3) may reveal small changes. Change detection is a primary goal of the ESP.

5.9. Glacial/periglacial processes and rocks/regolith

By the end of the PSP, 873 images in the glacial/periglacial theme had been acquired. Ice-rich permafrost on Mars is widespread throughout the middle and high latitudes and represents a major reservoir of near-surface water (Boynton et al., 2002; Feldman et al., 2008a). Likewise, non-polar surface deposits of ice and snow, while unstable today unless buried by a protective veneer of soil, have left a signature on the Martian landscape (e.g., Kargel and Strom, 1992; Holt et al., 2008). This ice, surface or subsurface, can be quite dynamic, both in its impact on the geologic character of the landscape and by its ability to come and go with changes in the Martian orbit and global climate (e.g., Mellon and Jakosky, 1995). Understanding the current distribution and history of surface and subsurface water ice, how the different reservoirs of water (surface ice, ground ice, ground water, atmospheric vapor) exchange with one another, and how ice deposits have changed over time is central to our understanding of the Martian climate and its history.

High latitude HiRISE images have revealed never before seen patterns indicative of an ice-rich subsurface. Small 5-m-scale polygonal patterned ground (Fig. 21a) completely covers the surface in nearly every image in the Martian northern plains (Mellon et al., 2008; Levy et al., 2008, 2009). Such patterns are typically associated with thermal contraction cracking in ice-rich permafrost and their presence and detailed characteristics can be related to the subsurface distribution of ice and ice-rich-soil deposits (e.g., Lachenbruch, 1962). Larger tens-of-meter-scale polygons have been previously observed in select locations within lower-resolution MOC images (Malin and Edgett, 2001; Mangold, 2005). However, the ubiquitous small 5-m-scale polygons had not been

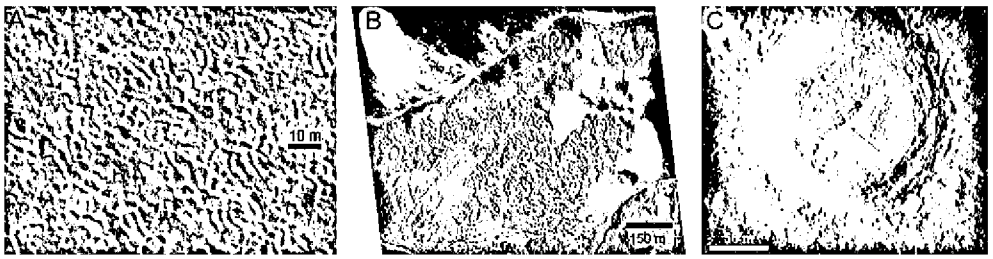

Fig. 21. Examples of HiRISE images of periglacial landforms: (a) small 5-m-scale polygonal patterned ground and rocks sorted into small regularly spaced piles (PSP_002025_2485); (b) dissected mantle terrain (PSP_004059_1410); and (c) fractured mound (PSP_001503_2180). Illumination in (a) and (c) is from the left and from the upper left in (b).

previously observed from orbit, and appear to represent the most recent stage in the evolution of the permafrost. In conjunction with polygon patterns, HiRISE images have revealed a variety of sorted boulders and rocks of a style never before observed on Mars (Mellon et al., 2008). These patterns may be analogous to sorted rock patterns that form in terrestrial frozen soils as a result of convective cycles in the soil driven by freezing or subfreezing processes. Sorted rocks and boulders are also a valuable indicator of permafrost processes and the history of permafrost. However, isolated stone circles may occur in locations unlikely to have experienced periglacial processes (Balme et al., 2009).

Much of the middle latitudes of Mars are mantled by a few meter thick layer of dust that, in places, appears dissected. This "dissected mantle terrain" (Fig. 21b), first seen in MOC images, is defined as a distinct disaggregated, eroded surface with a hummocky pitted appearance that is characterized by a strong latitudinal dependence (Mustard et al., 2001). The leading hypothesis has been that the mantle consists of ice-rich dust deposited during the most recent period of high obliquity ($<10^5$ years ago), and the dissected regions have now lost the ice cement in the current climate, resulting in the characteristic morphology. HiRISE imaging of dissected mantle terrain shows a number of features, such as small craters, surface rocks atop the mantle, and fissures within the mantle, that suggest at least some these mantle deposits are in fact older than previously thought (Searls et al., 2008). Additionally, HiRISE images reveal small aeolian bedforms among the dissected knobs and collapse pits, also suggesting a greater age of the dissection process. Examination of the distribution of these features shows that dissection preferentially occurs on poleward facing slopes, where ice would be preferentially stable. A new hypothesis has emerged (Searls et al., 2008) in which dissected regions indicate areas of preferred surface-ice stability (snow pack) during an earlier climate that was then covered by a uniform dusty mantle. These relatively clean ice deposits have since destabilized resulting in the collapse of the overlying dusty mantle.

HiRISE images of mid-latitude mounds have revealed a variety of summit fractures (Fig. 21c) suggesting that these mounds result from internal inflation and uplift (Dundas et al., 2008; Dundas and McEwen, 2009). Some of the mounds resemble terrestrial "pingos," ice cored mounds up to a few hundred meters in scale that form as a result of groundwater freezing under pressure. Additionally, the association of Martian mounds with gullies, and their occurrence at latitudes (~40°) where other periglacial landforms are common, lends support to the hypothesis of an ice-related origin. The significance of these features is twofold. Their presence could indicate present-day large masses of subsurface ice. Also, because their formation, if like terrestrial pingos, requires generation of freezing pressures in a local ground water system, these features could indicate a recent past occurrence of subsurface liquid water. This might support the shallow groundwater model for the origin of gullies (Mellon and Phillips, 2001). Additional HiRISE-based evidence that the moderately high latitudes (40–60°N and °S) are rich in ice includes the detailed morphology and topography of scalloped terrain (Lefort et al., 2009a,b) and from marginal pits around pedestal craters (Kadish et al., 2008).

HiRISE observations of the Argyre basin exhibit evidence of past glaciation. Surface striations, parallel groves, and streamlined hills suggest episodes of wet-based glaciation (Banks et al., 2008). Striations consist of meter-scale grooves trending downhill for up to hundreds of meters, indicative of glacial erosion of bedrock. Post-glacial modification in the form of polygonal patterned troughs and sorted boulder distributions are also observed (Banks et al., 2008). The sinuous ridges in Argyre, interpreted as eskers, suggest thick glaciers were present, as discussed in Section 5.7. Additional evidence for thick (~1 km thick) glaciers comes from analysis of HiRISE images of lineated valley fill near the dichotomy boundary (Dickson et al., 2008).

Most HiRISE images provide information about rocks and regolith, but more than 250 images were specifically assigned to this theme. Many of these are for full-resolution sampling of thermophysical (albedo and thermal inertia) "end-members" from Putzig et al. (2005). These images often show that various mixtures of dust, sand, rocks, and duricrust are present, so true end-members are typically not resolved by Thermal Emission Spectrometer (TES) data, except for dust. Rocks at the Phoenix landing site have been shown to influence depth to the ice table (Sizemore et al., 2009).

5.10. Mass wasting

The mass wasting science theme is focused on understanding the downslope movement of rocks and fine particles under the force of Martian gravity. Since landscapes are bounded by slopes, their evolution may be best understood through the study of slopes and the factors controlling their character and development (Sharp, 1982). Although the Martian landscape is largely static, slopes are some of the most active and dynamic surface environments available for study on short observational time scales. By the end of the PSP, 186 HiRISE observations assigned to the mass wasting theme were acquired. Targeted regions include steep inclines in high albedo regions that are marked with slope streaks, small rockfalls, and large landslides and landslide source areas. Observations of the intriguing gully systems are partly included in this science theme but are also targeted in other themes. Additional targets with a mass-wasting component, such as the slipfaces of dunes and smaller bedforms, are primarily assigned to the aeolian processes science theme.

HiRISE images of Martian slope streaks, which are recently formed surface disturbances on steep slopes over dust-mantled regions of Mars, have revealed a wealth of detail that have helped elucidate their origin and evolution (Chuang and Beyer, submitted for publication). For example, low Sun angle images reveal that

many dark slope streaks have detectable topographic edge relief, a characteristic that is consistent with a dry dust avalanche formation (e.g., Sullivan et al., 2001). Furthermore, HiRISE images have revealed evidence for several previously unresolved slope streak triggering mechanisms, including recent impact craters, boulders tumbling downslope in small rockfalls, and zones of local oversteepening below meter-scale topographic knobs (Chuang et al., 2007; Phillips et al., 2007).

HiRISE images of gullies (or ravines) have revealed a wealth of new details. Some Martian gullies at all latitudes have simple morphologies similar to debris chutes and probably result from dry granular flow on steep slopes. But in the middle latitudes there are complex gully/channel systems that display fluvial-like bedforms including cut bank-point bars, incised meanders and inner channels, braiding in middle reaches, stream terracing, levees, distributary alluvial/debris fans, and delta-like forms (Gulick et al., 2008).

5.11. Polar geology

A total of 883 images acquired during the PSP were assigned to the polar geology theme (Table 2).

5.11.1. North polar region

The polar layered deposits on Mars are widely believed to record recent global climate variations (e.g., Thomas et al., 1992; Laskar et al., 2004; Levrard et al., 2007). HiRISE observations show that the north polar layered deposits (NPLD) are divided into an upper, unfractured section and a lower, polygonally fractured section that is interbedded with the dark, basal unit. Blocks wasted from the fractured section appear to erode rapidly, consistent with the ice-rich composition indicated by CRISM observations (Herkenhoff et al., 2007).

DTMs derived from HiRISE stereo images (Table 8) allow meter-scale topographic measurements in the Planum Boreum 1 unit (Tanaka et al., 2008) of the NPLD and distinction of slope vs. albedo effects on apparent brightness of individual layers. The DTMs allow the thickness of polar layers to be measured with sub-meter precision, but HiRISE images do not show thin layers at the limit of resolution. Rather, fine layering, if it exists, appears to have been obscured by a more dust rich mantling deposit which itself shows signs of aeolian erosion and slumping. Stratigraphic sequences within the NPLD appear to be repeated within exposures observed by HiRISE, indicative of a record of periodic climate changes (Fishbaugh et al., submitted for publication).

The dark, basal unit, consisting of the Rupes Tenuis and Boreum Cavus units (Tanaka et al., 2008) appears to be cross-bedded, indicative of formation by saltating grains between periods of burial by the NPLD. More recently, deposition of the NPLD has not been interrupted by the influx of dark sand, either because the source was exhausted or because winds were no longer capable of transporting the dark grains into the north-polar region. Granular flow deposits sourced from within the dark, basal unit are suggestive of, but do not require, the presence of water during their formation (Herkenhoff et al., 2007). Active mass wasting of frost and dust has been observed on steep scarps in early spring (Fig. 22; Russell et al., 2008b).

Relatively dark patches observed within the north polar residual cap (NRC) during the summer indicate that the cap is relatively thin or transparent in places, or that dust has collected in the low areas. A graben within the area covered by the NRC indicates that recent tectonic extension has affected the north polar plateau (Byrne et al., 2007; Tanaka et al., 2008).

5.11.2. South polar region

HiRISE has observed the south-polar region throughout the spring and summer seasons on Mars. Multiple HiRISE observations of the south polar residual cap (SRC) permit more accurate measurements of the expansion rate of pits in the carbon dioxide cap. Comparisons with measurements of MOC images show that the carbon dioxide ice responds sensitively to interannual variations in the current climate. These results are being used to better constrain landscape evolution models of the SRC (Byrne et al., 2008).

As noted by Milkovich and Plaut (2008) from THEMIS images, layering in the SPLD appears more degraded than in the NPLD, complicating stratigraphic analyses. HiRISE images of the SPLD show interesting features, such as rectilinear fractures (Fig. 23), with greater spacing between fractures than observed in the NPLD. The fractures are continuous across several layers and their orientation is not affected by the topography of the exposure, suggesting that they were formed before erosion of the SPLD in this area. They

Fig. 22. IRB enhanced-color image of frost-dust avalanche at 83.8° N, 235° E. Cliff of NPLD has slope >60° and is ~700 m high. Subframe of PSP_007338_2640, up-slope toward left, illumination from upper right, taken at $L_s = 34°$ (northern spring).

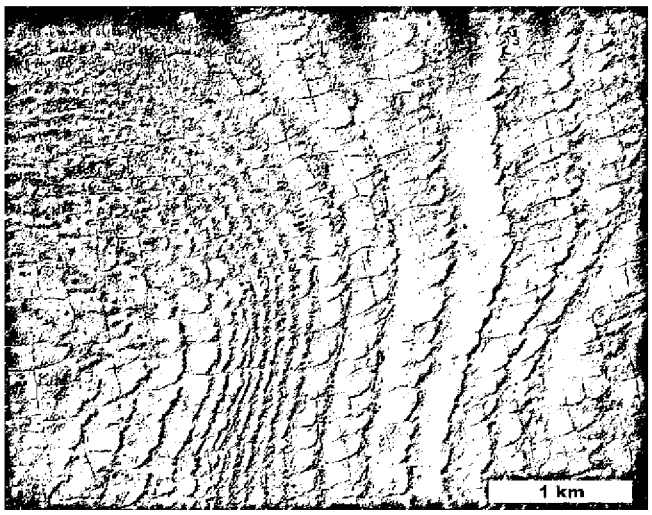

Fig. 23. Part of HiRISE image PSP_004959_0865 showing rectilinear fractures on an exposure of SPLD. Illumination is from the top.

appear to extend laterally and vertically through the SPLD, like a joint set. Volume scattering from this pervasive network of cracks may be the reason that SHARAD radar observations do not, in general, penetrate to the base of the SPLD (Seu et al., 2007). Another example of brittle deformation of the SPLD comes from previously recognized faults. Several faults have been observed by HiRISE in the SPLD, showing structural details including reverse fault splays that merge into bedding planes and possible evidence for thrust duplication. The faults may be the result of basal sliding (decollements) ramping into thrust faults near the margin of the SPLD (Herkenhoff et al., 2008).

5.12. Seasonal processes

CO_2 condenses to form a seasonal polar cap in the fall, subsequently shrouded in winter darkness. In the late winter and spring, sublimation of the CO_2 ice is a dynamic process, not a simple gradual disappearance of ice. Dramatic changes are seen on very short timescales. HiRISE carried out campaigns to image the activity during the spring season in both the south and north polar regions, acquiring a total of 570 images in the PSP. The sensitivity of the HiRISE camera allowed us to start imaging at low light levels as soon as the Sun was above the horizon, or even just below the horizon. The ability of the MRO spacecraft to turn off-nadir enabled repeat imaging of selected high latitude sites at frequencies of hours to weeks.

HiRISE studies of the seasonal sublimation of the southern cap began in December 2006, late winter in the southern hemisphere. HiRISE imaged a variety of locations repeatedly to study the evolution of the spots and fans that develop as the cap sublimates. Unique spider-like channels are eroded into the surface, most likely by CO_2 gas escaping from under the ice (Kieffer, 2000, 2007; Piqueux et al., 2003; Christensen et al., 2005a; Kieffer et al., 2006) and entraining loose material. Analysis of HiRISE data has fleshed out the details of this process and models of key steps in the process are reported (Hansen et al., submitted for publication; Thomas et al., 2009a; Portyankina et al., submitted for publication). A particularly well-monitored site is a portion of the dunes in Richardson crater (Fig. 24), repeatedly imaged by CTX and HiRISE to continue earlier monitoring (Supulver et al., 2001).

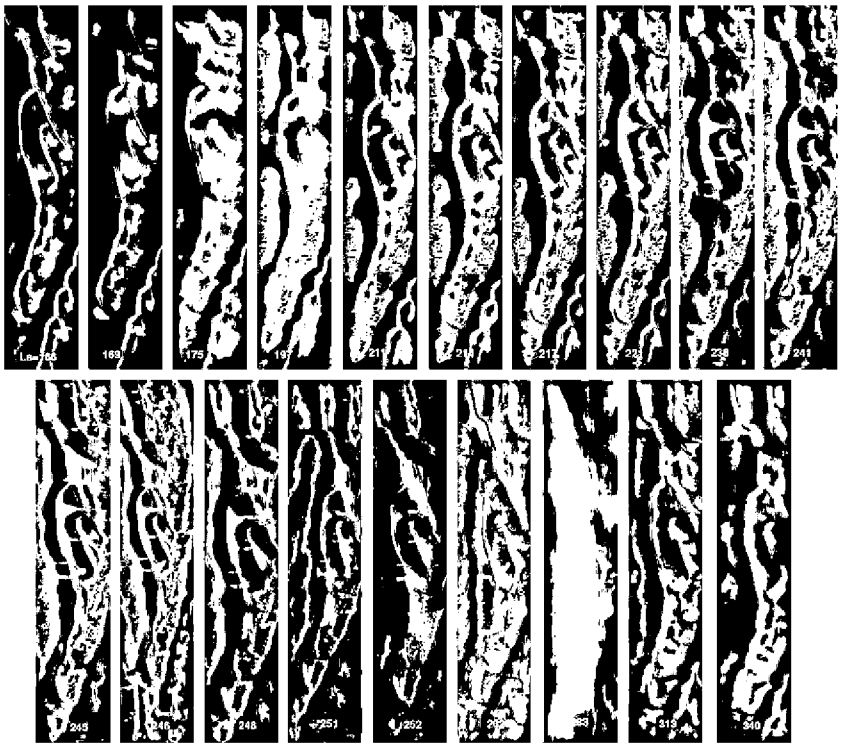

Fig. 24. Sequence of images monitoring seasonal changes over a portion of the Richardson crater dunes at 72.0°S, 179.4°E. Each image is a reduced-scale portion of the RGB "NOMAP" product (raw geometry with north down) with a relative stretch in each color to maximize contrast. L_s values are listed at the bottom of each frame; the sequence extends from late southern winter to late southern summer. The image acquired at L_s 283 is obscured by atmospheric dust and is part of the RED-filter image rather than RGB color. The relative stretches are comparable for images ranging from L_s 166–252 where there is bright frost to control the maximum values (stretched to white); the surface is actually much darker and redder (relative to frosted scenes) in the last four images. Each image covers a swath ~1 km wide on Mars. Illumination is from the bottom right, with the Sun elevation ranging from 3° above the horizon at L_s = 166,36° at L_s = 283, then decreasing to 21° at L_s = 340.

Observations of the sublimation of the northern seasonal cap began in January 2008 at $L_s = 13$ after the dissipation of the polar hood. The images show a number of interesting phenomena associated with the dunes in the north polar erg, including slope streaks, banded defrosting features, and star-like patterns suggesting explosive gas release. Time-lapse sequences show how these features evolve through the spring as the seasonal frost disappears.

Slope streaks appear to be mobilized by the vigorous activity associated with the sublimation of the CO_2 ice. Streaks are observed to lengthen as the season progresses, and mass wasting from the crests of the dunes is implicated (Fig. 25; Mangold et al., 2008). Frosted granular flow is a possible mechanism (Hugenholtz, 2008), but seepage of water melted by a solid-state greenhouse effect has also been proposed for this type of feature (Kereszturi et al., 2009). Banded features associated with defrosting show alternating bright and dark rings (Fig. 25). They are found at the crests of dunes, and at the interface of the bottom of the dunes with the substrate. The contrast is most pronounced early in the spring and gradually fades as more and more ice is sublimated. This is detected by HiRISE from the changing albedo, presumably due to different degrees of frost and dust covering the surface. Topographic changes have not yet been detected by HiRISE but will be studied by acquiring images of the same sites in future Mars years.

The properties of the substrate below the seasonal ice layer have an effect on sublimation features: mobilization of material is found on dunes, not on the surface beneath the dunes (cf. Feldman et al., 2008b). Images of dunes show numerous small dark star-shaped features that look like dust being explosively strewn in multiple directions from a source point (Fig. 26). This may be evidence for gas pressure building up below the seasonal ice layer and being released suddenly through a weak point.

Some evidence for translucent CO_2 ice with properties similar to the seasonal ice found at southern high latitudes has been found at northern (non-dune) sites suggested by Piqueux and Christensen (2008). Dark and bright streaks are observed with orientations determined by the prevailing wind. We have not observed the terrain with spider-like channels, found in many locations in the south polar region, in the north polar region.

5.13. Non-aeolian surface changes and potential Climate Change

High-resolution imaging and high-stability, off-nadir pointing capabilities allow HiRISE to continue, and improve upon, monitoring by MOC (1998–2007) of potentially currently evolving surface features. The theme of Climate Change is specifically focused toward detection of morphological change from one year to the next in response to climatic conditions and variability. In contrast, the seasonal processes theme (Section 5.12) focuses on cycles of changes that likely occur every year. Clearly, the repeat-imaging aspect of both themes ties them closely together, and investigating the intra- as well as the inter-annual aspects of activity will lead to a more integrated understanding of processes.

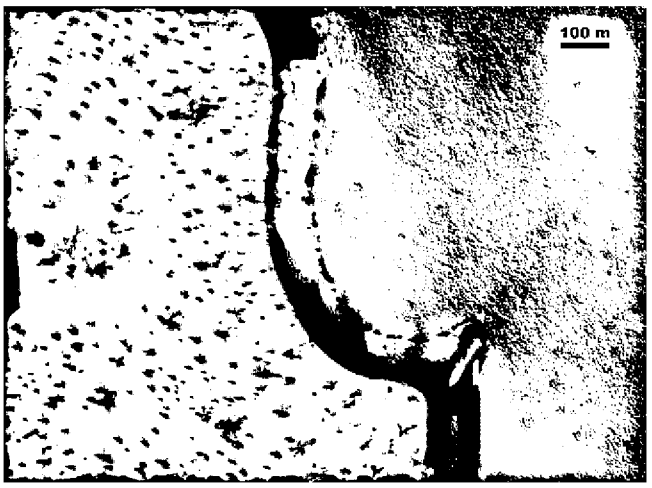

Fig. 26. Defrosting patterns seen on the dunes (left) but absent on the underlying surface (right). Part of PSP_007725_2600 with enhanced IRB color, taken at $L_s = 47.5$. North is approximately up and illumination is from the lower left.

Features are primarily targeted and assigned to the Climate Change theme based on their potential to exhibit detectable evolution due to exchange of volatiles (CO_2, H_2O) with the atmosphere, resulting in a concentration of efforts in the polar and mid- to high-latitude regions. Of primary interest are: "Swiss-cheese" terrain of the CO_2-rich south polar residual ice cap (SRC); dissected mantle terrain of mid-latitudes that may be actively losing interstitial H_2O ice; scarps, troughs, and other features of the H_2O ice-rich polar layered deposits (PLD) that may be undergoing net sublimation or accumulation; the fine texture of the H_2O-ice north polar residual cap; and other periglacial terrains and circumpolar deposits that may contain ice or host frost cover. Broad-scale goals include constraining volatile budgets and transport pathways, active atmospheric processes, polar and global energy balance, and climate models. Of secondary interest to the Climate Change theme are targets of features that the suggestor believes are, or will prove to be, indicators of a different past climate or past climate shift. While evidence of such Climate Change may be the primary motivator of the investigator, these sites will inevitably overlap with themes centered on the primary feature, such as fluvial processes, periglacial processes, etc. A total of 146 images assigned to the Climate Change theme were acquired during the PSP.

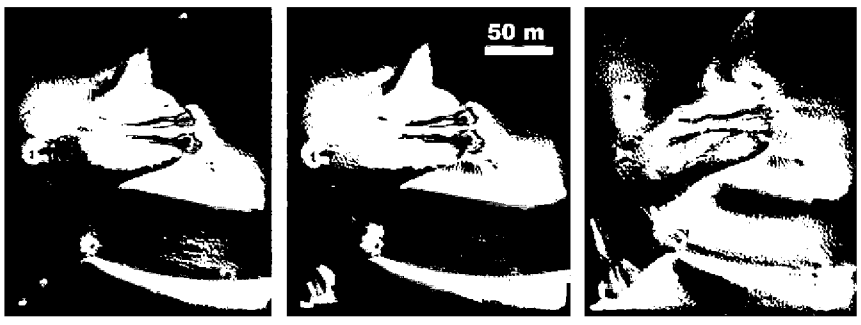

Fig. 25. Slope streaks emanating from dune crests. These are sub-images of PSP_007193_2640 (left, $L_s = 28.8$), PSP_007404_2640 (middle, $L_s = 36.3$), and PSP_007905_2640 (right, $L_s = 53.7$), at 84°N, 233°E. The slope streaks are observed to lengthen and flow around small undulations in the surface. Bright – dark banding is observed on both sides of the dune crest. Illumination from the lower left; north is approximately up; enhanced IRB color.

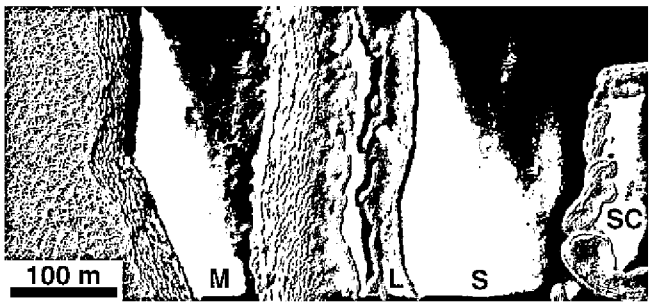

Fig. 27. Features of the SRC viewed with HiRISE (PSP_002602_0930), including: rounded "Swiss cheese"-like depressions (SC) with circumference-parallel, segment-wise, interior-edge collapse; linear depression (L); smooth SRC surface (S) with superposed thin ridges; thick remnant mesa (M) with superposed thin grooves, possibly comprising ~10 individual layers. Illumination is from the lower right.

The SRC contains a variety of features that range from quasi-circular depressions ("Swiss-cheese" features) to closely spaced linear troughs (fingerprint terrain) (Thomas et al., 2000) (Fig. 27). The depressions have been observed to expand by an average of ~2–6 m/year over the 3 Mars years of MOC observation (Malin et al., 2001b; Thomas et al., 2005). HiRISE has revealed such inter-annual evolution to be continuing at comparable rates (Thomas et al., 2009b). A smaller collection of measurements, however, suggests that the rate of inter-annual expansion between the last MOC year and the first HiRISE year may have been less than half that of the previous few MOC years, possibly due to the thermal input of major dust–lifting events in those MOC years (Byrne et al., 2008). Among the most important new SRC discoveries is that depressions expand not solely by gradual, uniform sublimation but to a large degree by undercutting of the surface layer and segment-wise failure of depression rims, resulting in a series of detached blocks or ridges ringing the interior of the depression (Byrne et al., 2008; Thomas et al., 2009b). HiRISE has also revealed up to ~10 internal layers visible within margins of depressions and remnant mesas and faint ⩽1 m-wide polygonal ridges on the smooth SRC surface (Byrne et al., 2008). The meter-scale annual expansion of depressions, the potential influence of atmospheric dust load on these expansion rates, and the presence of fine layers indicate that SRC behavior is an important and sensitive indicator of current polar atmospheric conditions. Thus, depositional and erosional relationships observed within the SRC may be a valuable record of recent climatic variability on Mars. Previous studies have suggested that the timescale associated with the generation of the current Swiss-cheese features is on the order of decades to centuries (Byrne and Ingersoll, 2003a,b; Thomas et al., 2005, 2009b) and that the very existence of the SRC is anomalous and tenuous (Jakosky and Haberle, 1990). However, recent numerical modeling and HiRISE-enabled comparison with sub-meter scale morphology suggest that the SRC and the "Swiss-cheese" features are in a state of dynamic equilibrium: accumulating CO_2 ice sheets are being eroded by expanding "Swiss-cheese" features such that the volume of the SRC itself is stable over the long-term, with no net loss or gain of CO_2 required (Byrne et al., 2008). Of ~150 HiRISE images that intersect with the SRC, many are dedicated to "Swiss-cheese" terrain. Seven such sites have 3–7 images over the spring-summer season. Many sites will be re-imaged next southern summer and several will again be targeted multiple times per year in order to better constrain the timing and mechanism of volatile and energy exchange between the surface and atmosphere and the effect of significant atmospheric events, such as dust-lifting episodes.

The dissected mantle terrain is probably the partially eroded, mid-latitude (30–60°) expression of an ice- and dust-rich mantling deposit in both hemispheres (Kreslavsky and Head, 2000, 2002; Mustard et al., 2001; Section 5.9). The combination of the neutron-based detection of significant near-surface water at high latitudes (e.g., Feldman et al., 2004) and the theoretically predicted geographic distribution of ground-ice stability (Mellon and Jakosky, 1993; Mellon et al., 2004) suggests that the margin of currently present, yet unstable ice is roughly coincident with the latitudinal band characterized by erosional features. During the second and ensuing Mars years of operations, looking for <1 m-scale change in these erosional textures may help resolve the issue of whether a reservoir of ground ice is in active exchange with the atmosphere. We have identified several locations within the dissected mantle terrain between 35° and 45° latitude for re-imaging within the coming months and years.

Having recently concluded imaging in the second north polar season, analysis of the modification of H_2O ice-rich features over time is in progress. The feature with the most potential for exhibiting small-scale change may be the north polar residual ice cap, which is pitted and ridged on the meter scale. Judging the amount of retreat or deposition at a trough or scarp due to sublimation may be difficult if there is no stable reference feature. More likely, we may be able to assess the amount of relative and qualitative change in outcrop expression or texture among layers of the PLD, which would provide information on relative layer properties such as composition, coherence, and structure. In particular, high-relief features such as rare, small craters and a unique extensional fracture in the PLD (Byrne et al., 2007) are better candidates for detectable change. One of the most notable HiRISE discoveries in the north-polar region is that mass wasting of blocks from the fractured, basal-unit and lower PLD layers is a significant mode of erosion (Herkenhoff et al., 2007; Section 5.11). The occurrence of one such event, involving the appearance of 3 ~ 1–2 m blocks and smaller debris on a relatively dark slope and the corresponding disappearance of an edge section of the fractured, relatively bright layer immediately above, occurred between two images taken ~6 weeks apart last Mars northern summer (Russell et al., 2008a; Fig. 28). Constraining the rates of this type of erosion is an important and promising aspect of the imaging campaign for this and coming years. Also important is to monitor relatively low-latitude ice deposits, such as crater-interior mounds (e.g., Louth crater, Brown et al., 2008; Korolev crater, Armstrong et al., 2005, and others in both hemispheres, Russell et al., 2004).

6. Imaging of past, present, and future landing sites

Imaging of landing sites, both to aid future landed exploration and to extrapolate landed results globally, is a major objective of HiRISE (McEwen et al., 2007a). Fig. 4 shows the distribution of

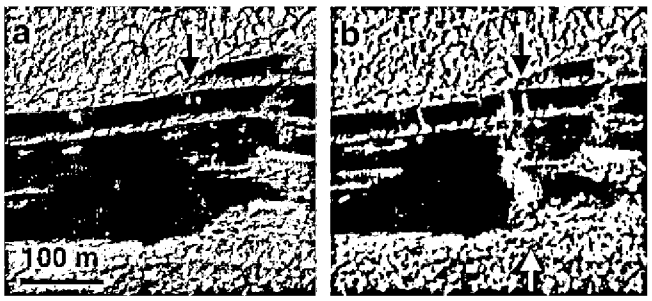

Fig. 28. Portions of (a) TRA_000845_2645 and (b) PSP_001412_2650, taken before and after, respectively, the occurrence of a block fall within the north polar basal unit. Three largest blocks appearing in (b) are ~2–3 m across (above white arrow). Images separated by ~44 days. Disappearance of block in edge of upslope fractured bright layer is the likely source (black arrows). Up-slope toward top; illumination from lower right.

images acquired for the theme future exploration/landing sites. In many cases a dot represents multiple images. A total of 400 images were acquired within this theme in the PSP, typically large, full-resolution images that require significantly (~5×) more data volume than the average image size.

6.1. Viking, MPL, MER

One of the very first images HiRISE acquired when in the final mapping orbit, during the transition phase in October 2006, was of the *Opportunity* rover, which had just arrived at Victoria crater. This image suffered many telemetry gaps, including most of the IR data and some of the BG data in the channel covering the rover. As a result the colors were not properly registered in the initial RGB color image that has been seen by millions of people. Within hours of image acquisition on the ground, it was utilized by the MER team to decide how to begin traversing the rim of the crater. Within months of the start of the PSP we imaged the *Opportunity* (Meridiani Planum) and *Spirit* (Gusev crater) sites in stereo and produced DTMs to assist the MER mission. HiRISE images have assisted the MER team with science analysis and mission planning (Squyres et al., 2008; Arvidson et al., 2008b; Sullivan et al., 2008; Geissler et al., 2008; McCoy et al., 2008). We recently acquired a stereo pair over the west rim of Endeavour crater (Fig. 29), which is a target of *Opportunity*. HiRISE images over parts of Endeavour crater show fine layers with fracture patterns a few meters in scale, similar to deposits elsewhere on Mars that correspond to phyllosilicate detections by CRISM (e.g., Wray et al., 2008).

We imaged the landing sites of Viking 1 and 2 and Mars Pathfinder within the first few months of the PSP (Parker et al., 2007), and comparison of these data with rock counts made by the landers enabled calibration of rock counts and permits derivation of rock counts from elsewhere on Mars using HiRISE images (Golombek et al., 2008). The Viking landers had not been correctly identified in previous orbital images. We located the backshells from all five successful landing sites, as well as the heat shields from MER and Pathfinder and (more tentatively) for the Viking landers. The parachutes were clearly seen attached to the backshells in all cases except Viking 2.

6.2. Searches for Mars Polar Lander (MPL) and Beagle-2

Locating flight hardware from past unsuccessful landing attempts has proven much more difficult, with no good candidates so far. Accurate locations for these landers are not known, so many images are needed. We covered about half of the "2-sigma" MPL landing ellipse before the light faded, and may resume the imaging next southern summer. The MPL region is covered by many bright and dark features about the scale of the flight hardware, so it may be well camouflaged. Five images have been acquired within the large landing ellipse for Beagle-2 (Bridges et al., 2003), in spite of no MRO project "must-have" requests in this case. Another difficulty is the unknown states of the hardware. Did the parachutes open or should we look for fresh impact sites? Did the heat shields or backshells separate? Did they land safely and deploy the lander before failing to communicate? We have also taken some images in the general vicinity of some of the past USSR Mars landing attempts, but success in locating this hardware seems especially unlikely.

Fig. 29. Stereo anaglyph of layered deposits near the NW margin of Endeavour crater, a possible destination for *Opportunity* rover. Portions of PSP_010341_1775 and PSP_010486_1775 reduced to 0.5 m/pixel.

6.3. Phoenix

HiRISE engaged in an intensive effort to find a safe landing site for the Phoenix mission (Smith et al., 2008b) in 2006 through early 2007, before the onset of northern winter. This effort was successful, and many more HiRISE images of the final landing site were acquired in early 2008 in order to tweak the exact placement of the landing ellipse (Arvidson et al., 2008a; Golombek et al., 2008). In addition, HiRISE acquired the wonderful image of Phoenix descending on the parachute (see Section 3.4 and Fig. 8), and many images of Phoenix hardware on the ground at different local times, monitoring the site for diurnal and seasonal changes. HiRISE images have been use to study the geomorphology and periglacial processes of the region (Seelos et al., 2008; Mellon et al., 2008). We expect to continue imaging the landing site in future years, as this is now a well-studied site for monitoring seasonal change.

6.4. Candidate landing sites for MSL

HiRISE has sampled almost all of the more than 50 landing sites initially proposed for the Mars Science Laboratory (MSL). These data enable unprecedented consideration of their geologic setting in advance of landing. To date, the HiRISE camera has obtained more than 110 images of the candidate landing sites that complement comparable numbers of images obtained by the CRISM and CTX instruments. Some of these images are intentionally overlapping, thereby enabling construction of DTMs (Table 8) to quantitatively assess the orientation and juxtaposition of exposed stratigraphy and permit modeling of any potential hazards for landing or driving MSL.

Many HiRISE images have been targeted over the 20 km by 25 km landing ellipses proposed for the seven sites remaining under consideration in advance of a third community workshop held in September 2008. These sites include Holden crater (26.4°S, 325.1°E), Eberswalde crater (23.9°S, 326.7°E), Gale crater (4.5°S, 137.4° E), Mawrth Vallis (24.7°N, 340.1°E), Miyamoto crater (3.3°S, 352.3°E), Nili Fossae trough (21.0°N, 74.5°E), and south Meridiani (3.3°S, 354.4°E).

HiRISE data reveal morphologic detail at each site that helps constrain past depositional environments. For example, when considered together with CRISM and CTX data, HiRISE images reveal laterally extensive, sub-meter and phyllosilicate-bearing stratigraphy in Holden crater indicative of emplacement in a distal alluvial and/or lacustrine setting (Figs. 19 and 30). Although these finely bedded deposits comprise the ultimate attraction of the Holden crater site, landing may only be possible on an alluvial bajada to the west and would provide more immediate access to sediments in inverted channels and associated deposits derived via erosion of the crater walls. In Eberswalde crater, the distribution and orientation of phyllosilicate-bearing beds appears consistent with the past presence of a long-lived fluvial-deltaic system (Fig. 30). Like at Hol-

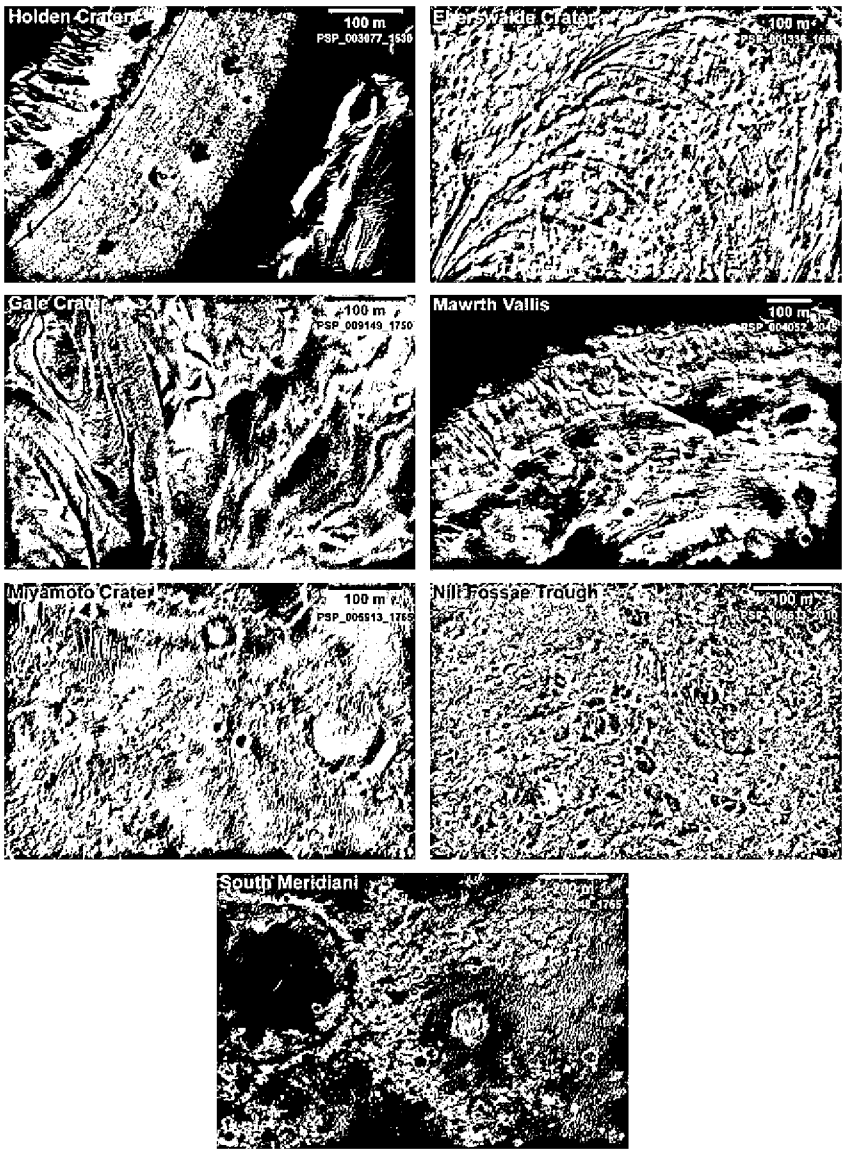

Fig. 30. Examples of the surfaces within each of the final seven candidate landing sites for the MSL as viewed by HiRISE. Holden crater image is modified from Fig. 4 in Grant et al. (2008a).

den, however, a landing in Eberswalde would occur near and beyond the distal edge of the delta deposits, but may provide access to lacustrine sediments and megabreccia-rich ejecta from nearby Holden crater. Gale crater exposes a thick sequence of finely bedded deposits with phyllosilicate-bearing rocks beneath possible sulfate-bearing rocks that may incorporate aeolian bedforms and displays evidence for local fluvial modification (Thomson et al., 2008b; Milliken et al., 2009). Landing would occur to the north of the sediment mound on the crater floor in an area that includes alluvium transported from the northern crater wall (Fig. 30). The multiple candidate landing ellipses in Mawrth Vallis display an especially distinctive stratigraphy of Mg–Fe smectites and Al-rich phyllosilicates, but the origin(s) of these layers remains uncertain (Bishop et al., 2008; Wray et al., 2008; Noe Dobrea et al., submitted for publication; Fig. 30). The floor of Miyamoto crater reveals an ancient stripped surface likely exhumed from beneath hematite-bearing plains materials comprising Meridiani Planum to the east. Morphology at Miyamoto (Fig. 30) may record an ancient fluvial setting that would be consistent with occurrence of phyllosilicate-bearing and presumably aqueously altered materials that are present (Newsom et al., submitted for publication). Nili Fossae trough reveals Noachian stratigraphy, with unaltered basaltic and olivine-rich materials overlying diverse phyllosilicate-bearing rocks that may correspond to aqueously altered ejecta from nearby Isidis basin or altered crustal materials (Mustard et al., 2008; Murchie et al., submitted for publication). Landing would occur on the floor of the trough (Fig. 30) with immediate access to infilling materials that include megabreccia-rich ejecta from Hargraves crater to the east. Finally, south Meridiani Planum includes hematite-bearing, sulfate-rich evaporite sediments that are likely similar to the materials explored by the Mars Exploration Rover *Opportunity* farther to the north. The hematite-bearing materials unconformably overlie in place, ancient polygonally fractured, phyllosilicate-bearing and incised bedrock outside of the proposed landing ellipse (Fig. 30) whose access could enable assessing changing conditions responsible for deposition of the sulfate-rich versus phyllosilicate-bearing materials.

The final seven sites under consideration as the landing site for MSL highlight the capabilities of HIRISE to detail diverse morphologic attributes characterizing ancient Mars to help better understand the planet's potential habitability. HiRISE's ability to resolve sub-meter scale features on the surface confirms that each

of the final candidate landing sites for MSL represent compelling targets for in situ exploration.

7. Education and Public Outreach (E/PO)

An E/PO highlight has been our student image suggestion program, conducted in association with NASA Quest as HiRISE Image Challenges (http://quest.arc.nasa.gov/challenges/hirise/). During challenges, students—either individually or as part of a collaborative classroom or group—learn about Mars through our webcasts, web chats and our educational material. They use HiWeb, HiRISE's image suggestion facility, to submit image suggestions and include a short rationale for why their target is interesting. The HiRISE team gives priority to obtaining a sampling of these suggestions as quickly as possible so that the acquired images can be examined during the exercise. During the challenge, a special web site (http://marsoweb.nas.nasa.gov/hirise/quest/) allows participants to view their returned images and to write captions. Finished captions are then posted and highlighted on the HiRISE web site (http://hirise.lpl.arizona.edu) along with their class, teacher's name and the name of their school. Through these HiRISE challenges, students and teachers become virtual science team members, participating in the same process (selecting and justifying targets, analyzing and writing captions for acquired images), and using the same software tools as the HiRISE team. To date, we have completed four HiRISE challenges. More than 200 image suggestions were submitted during the challenges and over 85 of these image requests have been acquired. Over 675 participants from 45 states and 42 countries have registered for the challenges. These participants represent over 8000 students in grades 2 through 14 and consist primarily of teachers, parents of home schoolers and student clubs, college students, and life-long learners.

One part of our original plan that has not (yet) worked out is accepting target suggestions from individuals outside the HiRISE team, except those participating in the Quest challenges. HiWeb was intended to be a tool that we could freely distribute, but it evolved into a tool that is integrated with uplink planning, and thus poses a security risk to mission critical data. We are now working on a separate web-based tool that can be used for public targets; release is expected in 2009.

HiRISE Clickworkers (http://clickworkers.arc.nasa.gov/hirise), a citizen science effort, is also part of our E/PO program, where volunteers identify geologic features (e.g., dunes, craters, wind streaks, gullies, etc.) in the HiRISE images and help generate searchable image databases. We have also developed the HiRISE online image viewer (http://marsoweb.nas.nasa.gov/HiRISE/hirise_images/) where users can browse, pan, and zoom through some of the very large HiRISE images from within their web browser. Educational materials include an assortment of K through college level, standards-based activity books, a K-3 coloring/story book, a middle school level comic book, several large HiRISE science posters and several interactive educational games, including Mars jigsaw puzzles, crosswords, word searches and flash cards (http://hirise.seti.org/epo). HiRISE team members have given numerous classroom presentations and participated in many other informal educational and public events (e.g., Sally Ride Science Festivals, CA Science teachers conference workshops, NASA's Yuri's Night, Xprize events, University of Arizona's Mars Mania and Phoenix public events). The HiRISE operations team maintains a blog (HiBlog) (http://hirise.lpl.arizona.edu/HiBlog/) providing insights to the pulse of daily activities within the operations center as well as useful information about HiRISE.

The HiROC group has participated in a dozen public education and outreach activities, the most visible being participation in the Phoenix landing event on 25 May 2008. We have used these opportunities to advance knowledge of the Mars Reconnaissance Orbiter, Mars exploration, and specifically, our own products that we release via our Web site. We have conducted tours and presentations for several diverse groups: middle and high school, as well as teachers from across the country who are interested in how to present science to their classrooms. Working with our partners like Lunar and Planetary Laboratory and Flandrau Science Center, we have participated in activities designed to promote science and the University of Arizona's role in scientific education. We have also had the opportunity to deal directly with the media, including local news affiliates as well as national and international outlets, such as Sky and Telescope (BBC England), Ciet et Espace (France) and National Geographic.

8. Instrument performance

The in-flight performance of the HiRISE instrument has been exceptionally good in most ways. The telescope has performed flawlessly, achieving the expected point-spread function (PSF) and allowing negligible stray/scattered light. The robust thermal control system is keeping all components close to nominal temperatures. Having the focal-plane electronics off for most of the time works well to keep the power consumption and electronics temperatures modest. There is no observed external electronic noise induced by the spacecraft or other instruments. In addition, the camera does not interfere with the spacecraft or other instruments, thus HiRISE was left on during the critical EDL phase of the Phoenix mission. HiRISE instrument performance has not been nominal in just two areas: rare down-track smearing in the images from CCD BG13, and, more significantly, anomalous bit flips in the images from half of the 28 data channels.

8.1. BG13 images

In pre-flight testing we found that the computer processing/memory module (CPMM) for one of the blue-green CCDs (BG13) did not work correctly most of the time when returning data from 128 or 64 TDI lines, resulting in down-column smearing of the data. To mitigate this problem during science observing, we initially planned to restrict BG13 to no more than 32 TDI lines, which usually meant using 4×4 binning to achieve an acceptable SNR. As a result, many images from the first 2 months of the PSP have different TDI and binning modes in BG13 and BG12. Once we decided to test the use of 64 and 128 TDI lines on BG13 when at Mars, we found that it behaved nominally and reverted to using its full capability. We have seen several occurrences of smeared BG13 images at Mars, always in just the very first image acquired after the HiRISE instrument is powered on.

8.2. Image DN bit flips

Under relatively cold operating conditions, and worsening over time, some of the channels produce erroneous data due to flipping bits (i.e., from 0 to 1 and vice versa) in the digital number (DN) values of the images, especially in certain image columns (Figs. 31 and 32). In the initial stages the least significant bits start to flip erroneously, increasing the low-level noise of the images. As it worsens over time or at lower FPE temperatures the more significant bits begin to flip, eventually leading to out-of-bounds values that are encoded as zeros. The anomalous behavior was never seen in ground testing, but was discovered in channel IR10_1 in the first post-launch HiRISE images acquired at very low FPS temperatures. In addition to IR10_1 some anomalous behavior at very low temperatures was seen during cruise in Channel 1 of both RED3 and RED0. Soon after MRO achieved the proper orbit for sci-

Fig. 31. Example image anomalies in RED9 of PSP_002204_1655, raw data. The bad (mostly dark) DN values are concentrated after video pause columns. Channel 1 (right) is worse than channel 0 (left).

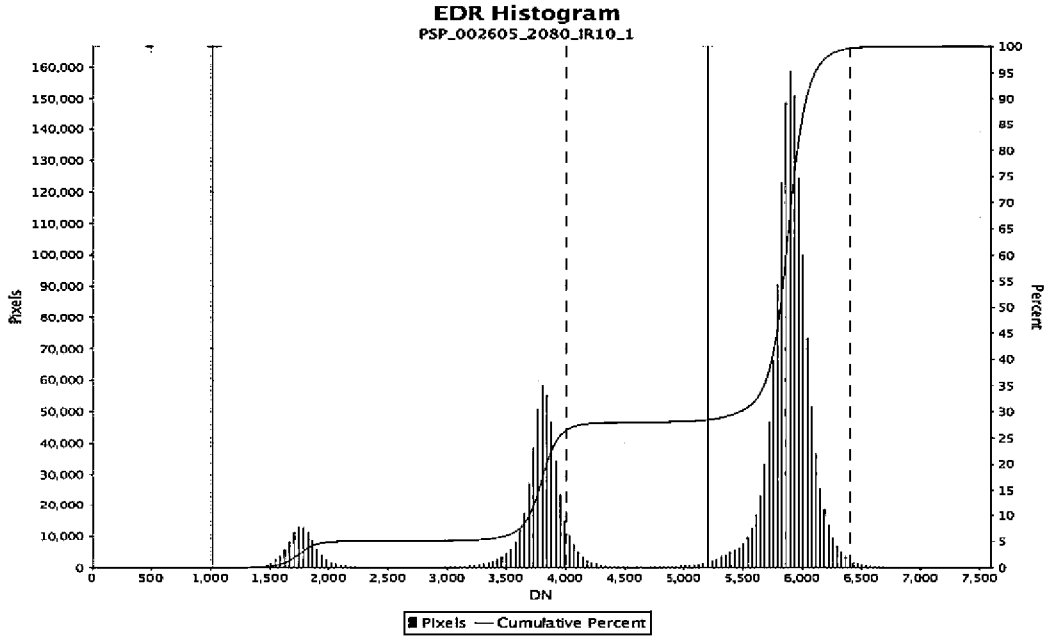

Fig. 32. Histogram of the EDR (raw data) for IR10_1 of PSP_002605_2080. This is an especially uniform (dust-covered) scene, so the effect of flipped bits is apparent. Those values near 6000 DN are correct, and the DNs at lower values are erroneous, as are 23.8% of the DNs that were encoded as zeros (not shown in the histogram). The image was LUT-compressed to 8 bits in the camera, then uncompressed on the ground to give the 14-bit DN values.

ence observations, HiRISE data in late November of 2006 showed a rapid and significant degradation in channel RED9_1 that had previously been operating nominally (Fig. 33). IR10_0 began degrading at about the same time as RED9_1 and RED9_0 soon followed. Testing in February 2007 at slightly colder FPS temperatures (15 °C rather than 20 °C) revealed smaller anomalies in RED0_1, RED1_1, RED3_1, and both channels of RED_8, for a total of nine affected channels. Towards the end of the PSP erroneous bits in RED1_0, RED2 (both channels), RED3_0, and RED7_1 were found in the performance monitoring images acquired with short warm-up times. The remaining 14 channels have shown no anomalies.

Options for operation were exercised early in this process because the data showed that the anomalous behavior disappeared at higher FPS temperatures. The initial normal operation called for approximately 30 s of CCD reverse clocking to flush the CCDs of charge and warm-up the electronics before taking an image. A simple change was required to extend that reverse clock time and in the process further warm the CCD electronics prior to data collection. In-flight data in early 2007 showed that a 200 s warm-up caused the anomalous behavior to cease except in IR10_1. A side effect was that we lost any sensitive measure of continued degradation. This was mitigated by periodically taking "stimulation-lamp" images during night side passage with the original 30-s reverse clocking to monitor the anomalous behavior under consistent temperature conditions. The typical history consists of rapid initial degradation of a particular channel followed by gradual continued worsening. In the summer of 2008, we increased the warm-up time to 300 s to eliminate artifacts that had appeared in several channels from the slow continued degradation. Increasing the warm-up time beyond 300 s is problematic for operational reasons, and produces diminishing returns. A better option is to keep the FPS warm between images, but we are near 100% duty cycle on the heaters and wish to continue taking one cold "stimulation lamp" image per cycle for consistent monitoring of the anomaly. The alternative is to stay warm by imaging, and in September

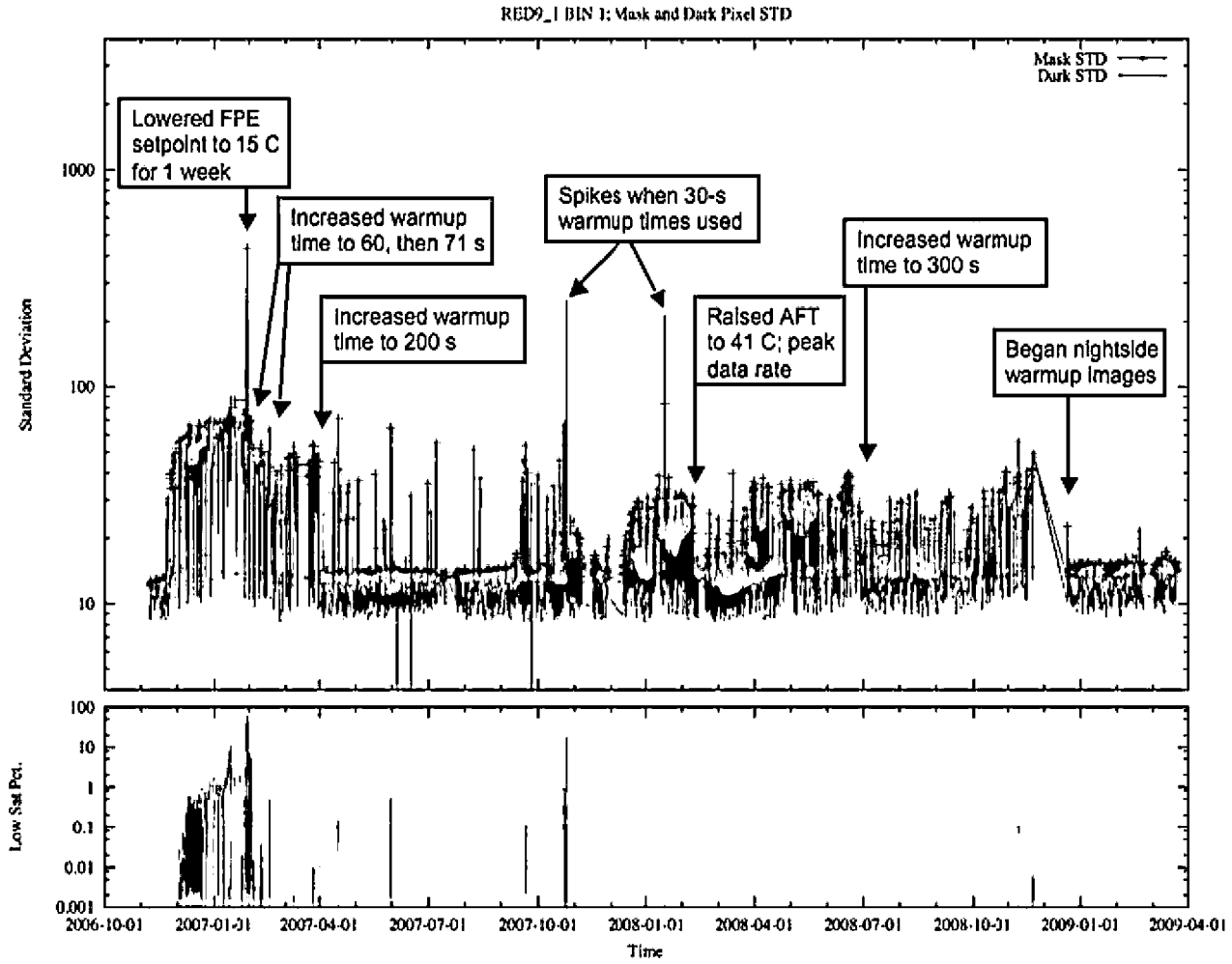

Fig. 33. History of bit-flip anomalies in Red 9_1 images of Mars from the PSP. The Mask and Dark pixel areas contain no signal and should have low standard deviations, except when anomalies occur. The bottom graph shows the percentage of pixels erroneously encoded to zeros. The RED9_1 images began the PSP with no apparent problem at an FPE set point of 20 °C and 30-s warm-up time before each image, but exhibited rapid degradation in late November 2006. The low data points from 11/26/06 until the warm-up time was increased to 200 s correspond to images acquired with a relatively warm FPE box temperatures from recent prior images. The high data points from 4/2007 until 10/2007 are due to images acquired with warm-up times shorter than 200 s. Raising the FPE allowable flight temperature (AFT) combined with peak data rate usually kept the FPE temperature above ~23 °C, resulting in fewer anomalies for a few months. Increasing the warm-up time to 300 s provided a modest improvement, whereas use of nighttime warm-up images (in the ESP) has essentially eliminated the bad data. Gaps in time represent spacecraft safing events or solar conjunction when no images were acquired.

2008 we began adding many small image samples (~10 extra images per day on average) for the purpose of keeping the flight FPE warm, which provided further mitigation. However, for the ESP we have substituted a simpler and more effective strategy of taking a long-duration but very low data volume image on most nightside passes to keep the FPE warm. An extended life test on the engineering model FPS at Ball Aerospace and Technology Corporation (BATC) has shown that extended operation at elevated temperatures actually reverses the degradation, so we are confident that we can mitigate this problem and return high-quality images for many years.

9. Future plans

A 2-year Extended Science Phase (ESP) has been approved for MRO, so we are continuing HiRISE. Much remains to be done, such as imaging high-priority targets over the other 99.45% of Mars' surface and acquisition of repeat observations to search for longer-term changes such as dune migration and new or enlarged sublimation pits. Quantitative measurement of the rates of surface changes would be a major advance in understanding present-day Mars and interpretations of past Mars. We expect to continue characterization of candidate landing sites for MSL and for ExoMars (Rover Team, 2006) and perhaps other future rovers, landers, and sample return. MRO has sufficient fuel to continue science operations for a decade or longer, which will hopefully be realized because NASA has no current plans for a future Mars orbiter with capable remote sensing of the surface.

Acknowledgments

We thank everyone who has made HiRISE possible, including those at NASA, JPL, Lockheed–Martin, BATC and subcontractors, and the University of Arizona. A.S.M. especially thanks Larry Soderblom (USGS) and the late Gene Shoemaker for providing examples of doing what's best for the science community. For constructive reviews we thank E. Hauber, J. Johnson, L. Soderblom, and an undisclosed reviewer. This work was supported by the NASA/JPL MRO project.

References

Allen, C.C., Oehler, D.Z., 2008. A case for ancient springs in Arabia Terra, Mars. Astrobiology 8, 1093–1112.

Anderson, J.A., Sides, S.C., Soltesz, D.L., Sucharski, T.L., Becker, K.J., 2004. Modernization of the integrated software for imagers and spectrometers. Lunar Planet. Sci. XXXV, 2039 (abstract).

Armstrong, J.C., Titus, T.N., Kieffer, H.H., 2005. Evidence for subsurface water ice in Korolev crater, Mars. Icarus 174, 360–372.

Arvidson, R., and 12 colleagues, 2008a. Mars Exploration Program 2007 Phoenix landing site selection and characteristics. J. Geophys. Res. 113, E00A03. doi:10.1029/2007JE003021.

Arvidson, R.E., and 32 colleagues, 2008b. Spirit Mars Rover Mission to the Columbia Hills, Gusev crater: Mission overview and selected results from the Cumberland Ridge to Home Plate. J. Geophys. Res. 113, E00A03. doi:10.1029/2008JE003183.

Balme, M.R., Gallagher, C.J., Page, D.P., Murray, J.B., Muller, J.-P., 2009. Sorted stone circles in Elysium Planitia, Mars: Implications for recent martian climate. Icarus 200, 30–38.

Banks, M.E., and 10 colleagues, 2008. High Resolution Imaging Science Experiment (HiRISE) observations of glacial and periglacial morphologies in the circum-Argyre Planitia highlands, Mars. J. Geophy. Res. 113, E12015. doi:10.1029/2007JE002994.

Banks, M.E., Lang, N.P., Kargel, J.S., McEwen, A.S., Baker, V.R., Grant, J.A., Pelletier, J.D., Strom, R.G., 2009a. An analysis of the sinuous ridges in the southern Argyre Planitia, Mars using HiRISE and CTX images and MOLA data. J. Geophys. Res., in press.

Banks, M.E., Galla, K.G., Bryne, S., Murray, B.C., McEwen, A.S.and the HiRISE Team, 2009b. Crater population and resurfacing of the martian north polar cap. Lunar Planet. Sci. XL, 2441 (abstract).

Becker, K.J., Anderson, J.A., Sides, S.C., Miller, E.A., Eliason, E.M., Keszthelyi, L.P., 2007. Processing HiRISE images using ISIS3. Lunar Planet. Sci. XXXVIII, 1779 (abstract).

Bibring, J.-P., Langevin, Y., Mustard, J.F., Poulet, F., Arvidson, R., Gendrin, A., Gondet, B., Mangold, N., Pinet, P., Forget, F., 2006. Global mineralogical and aqueous Mars history derived from OMEGA/Mars express data. Science 312, 400–404.

Bishop, J.L., and 11 colleagues, 2008. Phyllosilicate diversity and past aqueous activity revealed at Mawrth Vallis, Mars. Science 321, 830–833.

Boles, J.R., Eichhubl, P., Garven, G., Chen, J., 2004. Evolution of a hydrocarbon migration pathway along basin-bounding faults: Evidence from fault cement. Bull. Am. Assoc. Petro. Geog. 88, 947–970.

Bourke, M.C., Edgett, K.S., Cantor, B.A., 2008. Recent aeolian dune changes on Mars. Geomorphology 94, 247–255. doi:10.1016/j.geomorph.2007.05.012.

Bowen, B.B., Martini, B.A., Chan, M.A., Parry, W.T., 2007. Reflectance spectroscopic mapping of diagenetic heterogeneities and fluid-flow pathways in the Jurassic Navajo Sandstone. Bull. Am. Assoc. Petro. Geog. 91, 173–190.

Boynton, W.V., and 24 colleagues, 2002. Distribution of hydrogen in the near surface of Mars: Evidence for subsurface ice deposits. Science 297, 81–85.

Bray, V.J., Tornabene, L.L., McEwen, A.S., Mattson, S.S., 2009. Measurement of small-scale pits in the Corinto Crater, Mars. Lunar Planet. Sci. XL, 1389 (abstract).

Bridges, J.C., and 16 colleagues, 2003. Selection of the landing site in Isidis Planitia of Mars probe Beagle 2. J. Geophys. Res. 108. doi:10.1029/2001JE001820.

Bridges, N.T., Geissler, P.E., McEwen, A.S., Thomson, B.J., Chuang, F.C., Herkenhoff, K.E., Keszthelyi, L.P., Martínez-Alonso, S., 2007. Windy Mars: A dynamic planet as seen by the HiRISE camera. Geophys. Res. Lett. 34. L23205.

Bridges, N.T., and 11 colleagues, 2009. Aeolian bedforms, yardangs, and indurated surfaces in the Tharsis Montes as seen by the HiRISE camera: Evidence for dust aggregates. Icarus 205, 165–182.

Brown, A.J., Byrne, S., Tornabene, L.L., Roush, T., 2008. Louth crater: Evolution of a layered water ice mound. Icarus 196, 433–445.

Burr, D.M., Carling, P.A., Beyer, R.A., Lancaster, N., 2004. Flood-formed dunes in Athabasca Valles, Mars: Morphology, modeling, and implications. Icarus 171, 68–83.

Byrne, S., Ingersoll, A.P., 2003a. A sublimation model for martian south polar ice features. Science 299, 1051–1053.

Byrne, S., Ingersoll, A.P., 2003b. Martian climatic events on timescales of centuries: Evidence from feature morphology in the residual south polar ice cap. Geophys. Res. Lett. 30, 29-1, CiteID 1696. doi:10.1029/2003GL017597.

Byrne, S., Herkenhoff, K.E., Russell, P., Hansen, C., McEwen, A.S.the HiRISE Team, 2007. Preliminary HiRISE polar geology results. Lunar Planet. Sci. XXXVIII, 1930 (abstract).

Byrne, S., Russell, P., Fishbaugh, K., Hansen, C., Herkenhoff, K.E., McEwen, A.S.the HiRISE Team, 2008. Explaining the persistence of the Southern Residual Cap of Mars: HiRISE data and landscape evolution models. Lunar Planet. Sci. XXXIX, 2252 (abstract).

Chan, M.A., Ormo, J., Murchie, S., Okubo, C.H., Komatsu, G., Wray, J.J., McGuire, P., McGovern, J.A., the HiRISE Team, 2009. Geomorphic knobs of Candor Chasma, Mars: New Mars reconnaissance orbiter data and comparisons to terrestrial analogs. Icarus 205, 138–153.

Chojnacki, M., Hynek, B.M., 2008. Geological context of water-altered minerals in Valles Marineris, Mars. J. Geophys. Res. 113. E12005. doi:10.1029/2007JE003070.

Christensen, P.R., and 10 colleagues, 2004. The thermal emission imaging system (THEMIS) for the Mars 2001 Odyssey Mission. Space Sci. Rev. 110, 85–130.

Christensen, P.R., Kieffer, H.H., Titus, T.N., 2005a. Infrared and visible observations of south polar spots and fans. EOS Trans. AGU 86, 52, P23c-04.

Christensen, P.R., and 11 colleagues, 2005b. Evidence for igneous diversity and magmatic evolution on Mars from infrared spectral observations. Nature 436, 882. doi:10.1038/nature04075.

Chuang, F.C., Beyer, R.A., submitted for publication. Modification of martian slope streaks by eolian processes. Icarus.

Chuang, F.C., Beyer, R.A., McEwen, A.S., Thomson, B.J., 2007. HiRISE observations of slope streaks on Mars. Geophys. Res. Lett. 34 (20). L20204.

Davatzes, A.K., Gulick, V.C., 2007. High resolution imaging of the outflow channels on Mars. AGU (fall Meeting) P34A-06 (abstract).

Delamere, W.A., and 13 colleagues, 2009. Color imaging of Mars by the High Resolution Imaging Science Experiment (HiRISE). Icarus 205, 38–52.

Dickson, J.L., Head, J.W., Marchant, D.R., 2008. Late Amazonian glaciation at the dichotomy boundary on Mars: Evidence for glacial thickness maxima and multiple glacial phases. Geology 36 (5), 411–414.

Dundas, C.M., McEwen, A.S., 2009. An assessment of evidence for pingos on Mars using HiRISE. Icarus 205, 244–258.

Dundas, C.M., Mellon, M.T., McEwen, A.S., Lefort, A.N., Keszthelyi, L.P., Thomas, N., 2008. HiRISE observations of fractured mounds: Possible martian pingos. Geophys. Res. Lett. 35. L04201. doi:10.1029/2007GL031798.

Edwards, C.S., Christensen, P.R., Hamilton, V.E., 2008. Evidence for extensive olivine-rich basalt bedrock outcrops in Ganges and Eos chasmata, Mars. J. Geophys. Res. 113. E11003. doi:10.1029/2008JE003091.

Ehlmann, B.L., Mustard, J.F., Fasset, C.I., Schon, S.C., Head, J.W., des Marais, D.J., Grant, J.A., Murchie, S.L., 2008a. Clay minerals in delta deposits and organic preservation potential on Mars. Nat. Geosci. 1, 355–358.

Ehlmann, B.L., and 13 colleagues, 2008b. Orbital identification of carbonate-bearing rocks on Mars. Science 322, 1828–1832.

Feldman, W.C., and 14 colleagues, 2004. The global distribution of near-surface hydrogen on Mars. J. Geophys. Res. 109, E09006.

Feldman, W.C., Bandfield, J.L., Diez, B., Elphic, R.C., Maurice, S., Nelli, S.M., 2008a. North to south asymmetries in the water-equivalent hydrogen distribution at high latitudes on Mars. J. Geophys. Res. 113. E08006.

Feldman, W.C., Bourke, M.C., Elphic, R.C., Maurice, S., Bandfield, J., Prettyman, T.H., Diez, B., Lawrence, D.J., 2008b. Hydrogen content of sand dunes within Olympia Undae. Icarus 196, 422–432.

Fergason, R.L., Christensen, P.R., 2008. Formation and erosion of layered materials: Geologic and dust cycle history of eastern Arabia Terra, Mars. J. Geophys. Res. 113. E12001. doi:10.1029/2007JE002973.

Fishbaugh, K.E., Byrne, S., Herkenhoff, K.E., Kirk, R.L., Fortezzo, C., Russell, P., McEwen, A., submitted for publication. Redefining the meaning of "layer" in the martian North Polar Layered Deposits and the impact on the climate connection. Icarus.

Fueten, F., Stesky, R., MacKinnon, P., Hauber, E., Zegers, T., Gwinner, K., Scholten, F., Neukum, G., 2008. Stratigraphy and structure of interior layered deposits in west Candor Chasma, Mars, from High Resolution Stereo Camera (HRSC) stereo imagery and derived elevations. J. Geophys. Res. 113. E10008. doi:10.1029/2007JE003053.

Garbeil, H., Mouginis-Mark, P.J., Boyce, J.M., 2007. New insights on ejecta emplacement at martian impact craters from HiRISE images. AGU (fall Meeting), P23D-07 (abstract).

Geissler, P.E., and 12 colleagues, 2008. First in situ investigation of a dark wind streak on Mars. J. Geophys. Res. 113, E12S31. doi:10.1029/2008JE003102.

Golombek, M.P., and 18 colleagues, 2008. Size-frequency distributions of rocks on the northern plains of Mars with special reference to Phoenix landing surfaces. J. Geophys. Res. 113, E00A09. doi:10.1029/2007JE003065.

Grant, J.A., Irwin III, R.P., Grotzinger, J.P., Milliken, R.E., Tornabene, L.L., McEwen, A.S., Weitz, C.M., Squyres, S.W., Glotch, T.D., Thomson, B.J., 2008a. HiRISE imaging of impact megabreccia and sub-meter aqueous strata in Holden crater, Mars. Geology 36, 195–198.

Grant, J.A., Wilson, S.A., Cohen, B.A., Golombek, M.P., Geissler, P.E., Sullivan, R.J., Kirk, R.L., Parker, T.J., 2008b. Degradation of Victoria crater, Mars. J. Geophys. Res. 113. E11010. doi:10.1029/2008JE003155.

Grant, J.A., Wilson, S.A., Noe Dobrea, E., Fergason, R.L., Griffes, J.L., Moore, J.M., Howard, A.D., 2009. HiRISE views of an enigmatic deposit in the Electris region of Mars. Icarus 205, 53–63.

Greeley, R., and 17 colleagues, 2008. Columbia Hills, Mars: Aeolian features seen from the ground and orbit. J. Geophys. Res. 113, E06S06. doi:10.1029/2007JE002971.

Griffes, J.L., Grant, J.A., Golombek, M., Vasavada, A., McEwen, A.S.the HiRISE Team, 2008. HiRISE observations of potential Mars science landing sites. Lunar Planet. Sci. XXXIX, 1886 (abstract).

Gulick, V.C.the HiRISE Team, 2008. A closer look at valley, channel and gully formation on Mars with HiRISE. Lunar Planet. Sci. Conf. XXXIX, 2411 (abstract).

Hansen, C.J., Thomas, N., Portyankina, G., McEwen, A.S., Becker, K., Byrne, S., Herkenhoff, K., Kieffer, H.K., Mellon, M., submitted for publication. HiRISE observations of gas sublimation-driven activity in Mars' southern polar regions: I. Erosional features on the surface. Icarus.

Hart, S.D., Gulick, V.C., Parsons, R.A., Barnhart, C.J., 2009. Gully slopes and discharges on Lyot Crater's Central Peak. Lunar Planet. Sci. XL, 2349 (abstract).

Hauber, E., Charalambakis, E., Gwinner, K., Grott, M., Knapmeyer, M., Matz, K.D., Wahlisch, M., 2007. Displacement-length relationships of normal faults on Mars: New observations with MOLA and HSRC. Lunar Planet. Sci. XXXVIII, 1760 (abstract).

Hauber, E., Gwinner, K., Kleinhans, M., Reiss, D., Di Achille, G., Ori, G.-G., Scholten, F., Marinangeli, L., Jaumann, R., Neukum, G., 2008. Sedimentary deposits in Xanthe

Terra: Implications for the ancient climate on Mars. Planet. Space Sci.. doi:10.1016/j.pss.2008.06.00.
Hayward, R.K., Mullins, K.F., Fenton, L.K., Hare, T.M., Titus, T.N., Bourke, M.C., Colaprete, A., Christensen, P.R., 2007. Mars global digital dune database and initial science results. J. Geophys. Res. 112. E1107. doi:10.1029/2007JE002943.
Head, J.W., Marchant, D.R., Kreslavsky, M.A., 2008. Formation of gullies on Mars: Link to recent climate history and insolation microenvironments implicate surface water flow origin. Proc. Natl. Acad. Sci. USA 105, 13258–13263.
Herkenhoff, K.E., Byrne, S., Russell, P.S., Fishbaugh, K.E., McEwen, A.S., 2007. Meter-scale morphology of the North Polar Region of Mars. Science 317, 1711–1715.
Herkenhoff, K.E., Byrne, S., Fishbaugh, K., Hansen, C., Russell, P.and the HiRISE Team, 2008. HiRISE observations of the south polar region of Mars. Lunar Planet. Sci. XXXIX, 2361 (abstract).
Holt. J.W., and 11 colleagues, 2008. Radar sounding evidence for buried glaciers in the southern mid-latitudes of Mars. Science 322, 1235–1238.
Howard, P.G., Vitter, J.S., 1993. Fast and efficient lossless image compression. Proc. Data Compression Conf., 351–360.
Howard, A.D., Moore, J.M., Dietrich, W.E., Perron, J.T., 2008. Martian gullies: Morphometric properties and flow characteristics. Lunar Planet. Sci. XXXIX, 1629 (abstract).
Hugenholtz, C.H., 2008. Frosted granular flow: A new hypothesis for mass wasting in martian gullies. Icarus 197, 65–72.
Ivanov, B.A., McEwen, A.S.the HiRISE Team, 2009. Small impact crater clusters in high resolution HiRISE images. Lunar Planet. Sci. XXXIX, 1221 (abstract).
Jaeger, W.L., Keszthelyi, L.P., McEwen, A.S., Dundas, C.M., Russell, P.S., 2007. Athabasca Valles, Mars: A Lava-draped channel system. Science 317, 1709–1711.
Jaeger, W.L., Keszthelyi, L.P., Milazzo, M.P., Titus, T.N., Rosiek, M.R., Galuszka, D.M., Howington-Kruase, A., Kirk, R.L., McEwen, A.S., submitted for publication. Emplacement of the youngest flood lava on Mars: A short, turbulent story. Icarus.
Jakosky, B.M., Haberle, R.M., 1990. Year-to-year instability of the Mars south polar cap. J. Geophys. Res. 95, 1359–1365.
Kadish, S.J., Head, J.W., Barlow, N.G., Marchant, D.R., 2008. Martian pedestal craters: Marginal sublimation pits implicate a climate-related formation mechanism. Geophys. Res. Lett. 35. L16104. doi:10.1029/2008GL034990.
Kargel, J.S., Strom, R.G., 1992. Ancient glaciation on Mars. Geology 20, 3–7.
Kereszturi, A., Mohlmannm, D., Berczi, Sz., Ganti, T., Kuti, A., Sik, A., Horvath, A., 2009. Recent rheologic processes on dark polar dunes of Mars: Driven by interfacial water? Icarus 201, 492–503.
Keszthelyi, L., Jaeger, W., Dundas, C., Martinez-Alonso, S., McEwen, A., Milazzo, M., submitted for publication. Early HiRISE observations of hydrovolcanic interactions on Mars. Icarus.
Keszthelyi, L., Jaeger, W., McEwen, A., Tornabene, L., Beyer, R.A., Dundas, C., Milazzo, M., 2008. High Resolution Imaging Science Experiment (HiRISE) images of volcanic terrains from the first 6 months of the Mars Reconnaissance Orbiter Primary Science Phase. J. Geophy. Res. 113. E04005. doi:10.1029/2007JE002968.
Kieffer, H.H., 2000. Annual punctuated CO_2 slab-ice and jets on Mars. Lunar Planet. Sci. XXXI, 1057 (abstract).
Kieffer, H.H., 2007. Cold jets in the martian polar caps. J. Geophys. Res. 112. E08005.
Kieffer, H.H., Christensen, P.R., Titus, T.N., 2006. CO_2 jets formed by sublimation beneath translucent slab ice in Mars' seasonal south polar ice cap. Nature 442, 793–796.
Kirk, R.L., and 18 colleagues, 2008. Ultrahigh resolution topographic mapping of Mars with MRO HiRISE stereo images: Meter-scale slopes of candidate Phoenix landing sites. J. Geophys. Res., 113, E00A24. doi:10.1029/2007JE003000.
Kolb, K.J., Okubo, C.H., Coregistration of Mars Orbiter Laser Altimeter (MOLA) topography with high-resolution Mars images. Comput. Geosci., in press.
Kolb, K.J., McEwen, A.S., Pelletier, J.D., HiRISE Science Team, 2009. Measuring slopes of gully fan apices using digital elevation models. In: 40th Lunar and Planetary Science Conference, 2268 (abstract).
Kolb, K.J., Pelletier, J.D., McEwen, A.S., submitted for publication. Modeling the Formation of Bright Slope Deposits Associated with Gullies in Hale crater, Mars: Implications for Recent Liquid Water. Icarus.
Kreslavsky, M., 2008. Young populations of small impact craters on Mars as observed in HiRISE images. AGU (fall meeting), 8472 (abstract).
Kreslavsky, M.A., Head, J.W., 2000. Kilometer-scale roughness of Mars: Results from MOLA data analysis. J. Geophys. Res. 105, 26695–26711.
Kreslavsky, M.A., Head, J.W., 2002. Mars: Nature and evolution of young latitude-dependent water-ice rich mantle. Geophys. Res. Lett. 29, pp. 14-1, CiteID 1719. doi:10.1029/2002GL015392.
Lachenbruch, A.H., 1962. Mechanics of thermal contraction cracks and ice-wedge polygons in permafrost. Geol. Soc. Am. Spec. Paper 70, 69 pp.
Lanza, N.L., Meyer, G., Okubo, C., Newsom, H.E., Wiens, R.C., 2009. Evidence for debris flow and shallow subsurface flow on Mars. Icarus 205, 103–112.
Lanz, J.K., Saric, M.B., 2009. Cone fields in SW Elysium Planitia: Hydrothermal venting on Mars? J. Geophys. Res. 114. E02008. doi:10.1029/2008JE003209.
Laskar, J., Correia, A.C., Gastineau, M., Joutel, F., Levard, B., Robutel, P., 2004. Long term evolution and chaotic diffusion of the insolation quantities on Mars. Icarus 170, 343–364.
Lee, S.W., Skulsky, E.D., Chapel, J., Cwynar, D., Gehling, R., Delamere, W.A., 2001. Mars Reconnaissance Orbiter Design Approach for High-Resolution Surface Imaging. In: 26 Annual AAS, Guidance and Control Conference, Breckenridge, CO, February, 03-065 (abstract).
Lefort, A., Russell, P.S., Thomas, N., McEwen, A.S., Dundas, C.M., Kirk. R.L., 2009a. Observations of periglacial landforms in Utopia Planitia with the High Resolution Imaging Science Experiment (HiRISE). J. Geophys. Res., doi:10.1029/2008JE003264.
Lefort, A., Russell, P.S., Thomas, N., 2009b. Scalloped terrain in the Peneus and Amphitrites Paterae region of Mars as observed by HiRISE. Icarus 205, 259–268.
Levrard, B., Forget, F., Montmessin, F., Laskar, J., 2007. Recent formation and evolution of northern martian polar layered deposits as inferred from a Global Climate Model. J. Geophys. Res. 112. E06012.
Levy, J.S., Head, J.W., Marchant, D.R., Kowalewski, D.E., 2008. Identification of sublimation-type thermal contraction crack polygons at the proposed NASA Phoenix landing site: Implications for substrate properties and climate-driven morphological evolution. Geophys. Res. Lett. 35. L04202. doi:10.1029/2007GL032813.
Levy, J., Head, J., Marchant, D., 2009. Thermal contraction crack polygons on Mars: Classification, distribution, and climate implications from HiRISE observations. J. Geophys. Res. 114. E01007. doi:10.1029/2008JE003273.
Lewis, K.W., Aharonson, O., Grotzinger, J.P., Kirk, R.L., McEwen, A.S., Suer, T.-A., 2008. Quasi-periodic bedding in the sedimentary rock record of Mars. Science 322, 1532–1535.
Loizeau, D., and 10 colleagues, 2007. Phyllosilicates in the Mawrth Vallis region of Mars. J. Geophys. Res. Planets 112, 8.
Malin, M.C., Edgett, K.S., 2001. Mars Global Surveyor Mars Observer Camera: Interplanetary cruise through primary mission. J. Geophys. Res. 106 (E6), 23429–23571.
Malin, M.C., Calvin, W., Clancy, R.T., Haberle, R.M., James, P.B., Lee, S.W., Thomas, P.C., Caplinger, M.A., 2001a. The Mars Color Imager (MARCI) on the Mars Climate Orbiter. J. Geophys. Res. 106, 17651–17672.
Malin, M.C., Caplinger, M.A., Davis, S.D., 2001b. Observational evidence for an active surface reservoir of solid carbon dioxide on Mars. Science 294, 2146–2148.
Malin, M.C., Edgett, K.S., Posiolova, L.V., McColley, S.M., Noe Dobrea, E.Z., 2006. Present-day impact cratering and contemporary gully activity on Mars. Science 314, 1573–1577.
Malin, M.C., and 13 colleagues, 2007. Context Camera Investigation on board the Mars Reconnaissance Orbiter. J. Geophys. Res. 112, E05S04.
Mangold, N., 2005. High latitude patterned ground on Mars: Classification, distribution and climate control. Icarus 174, 336–359.
Mangold, N., Baratoux, D., Costard, F., Forget, F., 2008. Current Gullies Activity: Dry Avalanches Observed Over Seasonal Frost as Seen on HiRISE Images. Workshop on Martian Gullies. vol. 1301, LPI Contribution, February 4–5, Houston, Texas, pp. 68–69.
Martinez-Alonso, S., Mellon, M.T., Banks, M.E., Keszthelyi, L.P., McEwen, A.S., the HiRISE Team, submitted for publication. Evidence of volcanic and glacial activity in Chryse/Acidalia Planitiae, Mars. Icarus.
McCleese, D.J., Schofield, J.T., Taylor, F.W., Calcutt, S.B., Foote, M.C., Kass, D.M., Leovy, C.B., Paige, D.A., Read, P.L., Zurek, R.W., 2007. Mars Climate Sounder: An investigation of thermal and water vapor structure, dust and condensate distributions in the atmosphere, and energy balance of the polar regions, J. Geophys. Res. 112. doi:10.1029/2006JE002790.
McCoy, T.J., and 18 colleagues, 2008. Structure, stratigraphy, and origin of Husband Hill, Columbia Hills, Gusev crater, Mars. J. Geophys. Res., 113, E06S03. doi:10.1029/2007JE003041.
McEwen, A.S., Bierhaus, E.B., 2006. The importance of secondary cratering to age constraints on planetary surfaces. In: Jeanloz, R., Albee, A.L., Burke, K.C., Freeman, K.H. (Eds.), Ann. Rev. Earth Plant. Sci. 34, pp. 535–568.
McEwen, A.S., 14 colleagues, 2007a. Mars Reconnaissance Orbiter's High Resolution Imaging Science Experiment (HiRISE). J. Geophys. Res. 112, E05S02. doi:10.1029/2005JE002605.
McEwen, A.S., and 32 colleagues, 2007b. A closer look at water-related geologic activity on Mars. Science 317, 1706–1709.
McEwen, A.S., Tornabene, L., Grant, J., Wray, J., Mustard, J., 2008. Noachian megabreccia on Mars. AGU (fall) P43D-04 (abstract).
Mellon, M.T., Jakosky, B.M., 1993. Geographic variations in the thermal and diffusive stability of ground ice on Mars. J. Geophys. Res. 98 (2), 3345–3364.
Mellon, M.T., Jakosky, B.M., 1995. The distribution and behavior of martian ground ice during past and present epochs. J. Geophys. Res. 100, 11781–11799.
Mellon, M.T., Phillips, R.J., 2001. Recent gullies on Mars and the source of liquid water. J. Geophys. Res. 106, 23165–23180.
Mellon, M., Feldman, W., Prettyman, T., 2004. The presence and stability of ground ice in the southern hemisphere of Mars. Icarus 169 (2), 324–340.
Mellon, M.T., Arvidson, R.E., Marlow, J.J., Phillips, R.J., Asphaug, E., 2008. Periglacial landforms at the Phoenix landing site and the northern plains of Mars. J. Geophys. Res. 113. E00A23. doi:10.1029/2007JE003039.
Metz, J.M., Grotzinger, J.P., Milliken, R., Mohrig, D., McEwen, A.S., Weitz, C.M., 2008. Sublacustrine depositional fans in Melas Chasma. AGU (fall meeting), P32B-02 (abstract).
Milazzo, M.P., Keszthelyi, L.P., Jaeger, W.L., Rosiek, M., Mattson, S., Verba, C., Beyer, R.A., Geissler, P.E., McEwen, A.S.the HiRISE Team, 2009. Discovery of columnar jointing on Mars. Geology 37, 171–174.
Milkovich, S., Plaut, J., 2008. Martian South Polar Layered Deposit stratigraphy and implications for accumulation history. J. Geophys. Res. 113. E06007.
Milliken, R.E., and 11 colleagues, 2008. Opaline silica in young deposits on Mars. Geology 36, 847–850.
Milliken, R.E., Edgett, K.S., Swayze, G., Clark, R.N., Thomson, B.J., Anderson, R., Bell, J.F., 2009. Clay and Sulfate-bearing rocks in a stratigraphic sequence in Gale Crater. In: 40th Lunar and Planetary Science Conference, 1479 (abstract).
Mouginis-Mark, P.J., Rowland, S.K., 2008. Lava flows at Arsia Mons: Insights from a graben imaged by HiRISE. Icarus 198, 27–36.

Murchie, S., and 49 colleagues, 2007. Compact Reconnaissance Imaging Spectrometer for Mars (CRISM) on Mars Reconnaissance Orbiter (MRO). J. Geophys. Res. 112, E05S03. doi:10.1029/2006JE002682.
Murchie, S., Choo, T., Humm, D., Rivkin, A.S., Bibring, J.-P., Langevin, Y., Gondet, B., Roush, T.L., Duxbury, T.the CRISM Team, 2008. MRO/CRISM observations of Phobos and Deimos. Lunar Planet. Sci. XXXIX, 1434 (abstract).
Murchie, S.L., and 15 colleagues, 2009. A synthesis of martian aqueous mineralogy after one Mars year of observations from the Mars Reconnaissance Orbiter. J. Geophys. Res., submitted for publication.
Murray, B.C., Pais, D., Pathare, A., Byrne, S., 2005. The peculiar stratigraphy of offset troughs within the martian north polar layered deposits: Evidence for deformation? AGU (fall meeting) P23C-07 (abstract).
Mustard, J.F., Cooper, C.D., Rifkin, M.K., 2001. Evidence for recent climate change on Mars from the identification of youthful near-surface ground ice. Nature 412, 411–414.
Mustard, J.F., and 35 colleagues, 2008. Hydrated silicate minerals on Mars observed by the Mars Reconnaissance Orbiter CRISM instrument. Nature 454, 305–309.
Neukum, G., Jaumann, R., the HRSC Co-Investigator and Experiment Team 2004. The High Resolution Stereo Camera of Mars Express. In: Wilson, A., Chicarro, A. (Eds.), Mars Express: the scientific payload. ESA SP-1240, Noordwijk, The Netherlands, pp. 17–35.
Newsom, H., Lanza, N., Ollila, A., Wiseman, S., Roush, T.L., Marzo, G.A., Tornabene, L., Okubo, C., Osterloo, M., Hamilton, V., Crumpler, L., submitted for publication. Evidence for inverted channel formation on the floor of Miyamoto crater, Mars. Icarus.
Noe Dobrea, E.Z., and 18 colleagues, 2009. Mineralogy and stratigraphy of phyllosilicate-bearing and dark mantling units in the greater Mawrth Vallis area: Constraints on geological origin, J.Geophys. Res., submitted for publication.
Okubo, C.H., McEwen, A.S., 2007. Fracture controlled paleo-fluid flow in Candor Chasma, Mars. Science 315, 983–985.
Okubo, C.H., Schultz, R.A., Polit, A.T., McEwen, A.S.the HiRISE Team, 2007. Displacement-length scaling of joints in layered deposits, Southwest Candor Chasma. Lunar Planet. Sci. XXXVIII (1338), 1225.
Okubo, C.H., Schultz, R.A., Chan, M.A., Komatsu, G.the HiRISE Team, 2008a. Deformation band clusters on Mars and implications for subsurface fluid flow. Bull. Geol. Soc. Am. 121, 474–482.
Okubo, C.H., Lewis, K.W., McEwen, A.S., Kirk, R.L., 2008b. Relative age of interior layered deposits in southwest Candor Chasma based on high-resolution structural mapping. J. Geophys. Res. 113. E12002. doi:10.1029/2008JE003181.
Orosei, M., and 14 colleagues, 2008. Radar subsurface sounding over the putative frozen sea in Cerberus Palus, Mars. Lunar Planet. Sci. XXXIX, 1866 (abstract).
Osterloo, M.M., Hamilton, V.E., Bandfield, J.L., Glotch, T.D., Baldridge, A.M., Christensen, P.R., Tornabene, L.L., Anderson, F.S., 2008. Chloride-bearing materials in the southern highlands of Mars. Science 319, 1651–1654.
Pang, K.D., Pollack, J.B., Veverka, J., Lane, A.L., Ajello, J.M., 1978. The composition of PHOBOS – Evidence for carbonaceous chondrite surface from spectral analysis. Science 199, 64–66.
Parker, T.J., McEwen, A.S., Kirk, R.L., Bridges, N.T., 2007. HiRISE captures the Viking and Mars Pathfinder landing sites. Lunar Planet. Sci. XXXVIII, 2368 (abstract).
Parsons, R.A., Kreslavsky, M., Nimmo, F., 2008. Martian gully slope measurements made using HiRISE stereo pairs. Lunar Planet. Sci. XXXIX, 2328 (abstract).
Pelletier, J.D., Kolb, K.J., McEwen, A.S., 2008. Recent bright gully deposits on Mars: Wet or dry flow? Geology 36, 211–214.
Philippoff, A.J., Tornabene, L.L., McEwen, A.S., Baker, V.R., Melosh, H.J., Berman, D.C.the HiRISE Science Team, 2009. Geomorphic Mapping of Hale Crater, Mars. Lunar Planet. Sci. XL, 1737 (abstract).
Phillips, C.B., Burr, D.M., Beyer, R.A., 2007. Mass movement within a slope streak on Mars. Geophys. Res. Lett. 34. L21202.
Piqueux, S., Christensen, P., 2008. North and south sub-ice gas flow and venting of the seasonal caps of Mars: A major geomorphological agent. J. Geophys. Res. 113. E06005. doi:10.1029/2007JE003009.
Piqueux, S., Byrne, S., Richardson, M., 2003. The sublimation of Mars' southern seasonal CO_2 ice cap and the formation of spiders. J. Geophys. Res. 108 (E8), 508.
Portyankina, G., Markiewicz, W.J., Hansen, C.J., Thomas, N., submitted for publication. HiRISE observations of gas sublimation-driven activity in Mars' southern polar regions: III. Models of processes involving translucent ice. Icarus.
Poulet, F., Bibring, J.-P., Mustard, J.F., Gendrin, A., Mangold, N., Langevin, Y., Arvidson, R.E., Gondet, B., Gomez, C., 2005. Phyllosilicates on Mars and implications for early martian climate. Nature 438, 623–627.
Preblich, B., McEwen, A., Studer, D., 2006. Mapping rays and secondary craters from Zunil, Mars. J. Geophys. Res. 112. E05006.
Putzig, N.E., Mellon, M.T., Kretke, K.A., Arvidson, R.E., 2005. Global thermal inertia and surface properties of Mars from the MGS mapping mission. Icarus 173, 325–341.
Rover Team, 2006. The ExoMars rover and Pasteur payload Phase A study: an approach to experimental astrobiology. Int. J. Astrobiol. 5, 221–241.
Russell, P.S., Head, J.W., Hecht, M.H., 2004. Evolution of ice deposits in the local environment of martian circum-polar craters and implications for polar cap history. Lunar Planet. Sci. XXXV, 2004 (abstract).
Russell, P.S., Byrne, S., Herkenhoff, K., Fishbaugh, K., Thomas, N., McEwen, A.the HiRISE Team, 2008a. Active mass-wasting processes on Mars' north polar scarps discovered by HiRISE. Lunar Planet. Sci. XXXIX, 2313 (abstract).
Russell, P.S., Thomas, N., Byrne, S., Herkenhoff, K., Fishbaugh, K., Okubo, C., Milazzo, M., Daubar, I., Hansen, C., McEwen, A., 2008b. Seasonally-active frost-dust avalanches on a north polar scarp of Mars captured by HiRISE. Geophys. Res. Lett. 35. L23204. doi:10.1029/2008GL035790.
Schaller, C.J., 2006. Automated HiRISE data processing: Conductor in action. Lunar Planet. Sci. XXXVII, 2134 (abstract).
Schon, S.C., Head, J.W., Fassett, C.I., 2009. Unique chronostratigraphic marker in depositional fan stratigraphy on Mars: Evidence for ca. 1.25 Ma gully activity and surficial meltwater origin. Geology 2009 (37), 207–210.
Schultz, R.A., Lin, J., 2001. Three-dimensional normal faulting models of Valles Marineris, Mars, and geodynamic implications. J. Geophys. Res. 106, 16549–16566.
Searls, M.L., Mellon, M.T., Martinez-Alonso, S.and the HiRISE Team, 2008. Slope analysis and ice stability of the mid latitude dissected terrain on Mars. Lunar Planet. Sci. XXXIX, 2376 (abstract).
Seelos, K.D., and 12 colleagues, 2008. Geomorphologic and mineralogic characterization of the northern plains of Mars at the Phoenix Mission candidate landing sites. J. Geophys. Res. 113, E00A13. doi:10.1029/2008JE003088.
Seu, R., and 26 colleagues, 2007. SHARAD sounding radar on the Mars Reconnaissance Orbiter. J. Geophys. Res. 112, doi:10.1029/2006JE002745.
Sharp, R.P., 1982. Landscape evolution (a review). Proc. Natl. Acad. Sci. – Phys. Sci. 79 (14), 4477–4486.
Shipton, Z.K., Evans, J.P., Kirschner, D., Kolesar, P.T., Williams A.P., Heath, J., 2004. Analysis of CO_2 leakage through "low-permeability" faults from natural reservoirs in the Colorado Plateau, east-central Utah. In: Baines, S.J., Worden, R.H. (Eds.), Geological storage of Carbon Dioxide, vol. 233. Geological Society of London Special Publication. pp. 43–58.
Shipton, Z.K., Evans, J.P., Dockrill, B., Heath, J., Kirchner, D., Kolesar, P.T., 2005. Natural leaking CO_2-charged systems as analogs for failed geologic storage reservoirs. In: Thomas, D.C., Benson, S.M. (Eds.), Carbon Dioxide Capture for Storage in Deep Geologic Formations – Results from the CO_2 Capture Project. Elsevier, London, pp. 699–712.
Shreve, R.L., 1985. Esker characteristics in terms of glacier physics, Katahdin esker system, Maine. Geol. Soc. Am. Bull. 96, 639–646.
Sizemore, H.G., Mellon, M.T., Golombek, M.P., 2009. Ice table depth variability near small rocks at the Phoenix landing site, Mars: A pre-landing assessment. Icarus 199, 303–309.
Smith, D.E., and 23 colleagues, 2001. Mars Orbiter Laser Altimeter: Experiment summary after the first year of global mapping of Mars. J. Geophys. Res. 106 (10), 23689–23722.
Smith, M.R., Gillespie, A.R., Montgomery, D.R., 2008a. Effect of obliteration on crater-count chronologies for Martian surfaces. Geophys. Res. Lett. 35. L10202.
Smith, P.H., and 38 colleagues, 2008b. Introduction to special section on the Phoenix Mission: Landing Site Characterization Experiments, Mission Overviews, and Expected Science. J. Geophys. Res., 113, E00A18, doi:10.1029/2008JE003083.
Souza-Egipsy, V., Ormö, J., Bowen, B.B., Chan, M.A., Komatsu, G., 2006. Ultrastructural study of iron oxide precipitates: Implications for the search for biosignatures in the Meridiani hematite concretions, Mars. Astrobiology 6, 527–545.
Squyres, S.W., and 17 colleagues, 2008. Detection of silica-rich deposits on Mars. Science 320, 1063–1067.
Sullivan, R., and 10 colleagues, 2008. Wind-driven particle mobility on Mars: Insights from Mars Exploration Rover observations at "El Dorado" and surroundings at Gusev crater. J. Geophys. Res. 113, E06S07. doi:10.1029/2008JE003101.
Sullivan, R., Thomas, P., Veverka, J., Malin, M., Edgett, K.S., 2001. Mass movement slope streaks imaged by the Mars Orbiter Camera. J. Geophys. Res. 106 (10), 23607–23633.
Supulver, K.D., Edgett, K.S., Malin, M.C., 2001. Seasonal changes in frost cover in the martian south polar region: Mars Global Surveyor MOC and TES monitoring of the Richardson crater dune field. Lunar Planet. Sci. XXXII, 1966 (abstract).
Swayze, G.A., and 13 colleagues, 2008. Discovery of the acid-sulfate mineral Alunite in Terra Sirenum, Mars, using MRO CRISM: Possible evidence for acid saline lacustrine deposits? AGU Fall Meeting, #P44A-04 (abstract).
Tanaka, K., Rodriguez, J., Skinner, J., Bourke, M., Fortezzo, C., Herkenhoff, K., Kolb, E., Okubo, C., 2008. North polar region of Mars: Advances in stratigraphy, structure, and erosional modification. Icarus 196, 318–358.
Thomas, P., Squyres, S., Herkenhoff, K., Howard, A., Murray, B., 1992. Polar Deposits on Mars. In: Kieffer, H.H., Jakosky, B.M., Snyder, C.W., Mathews, M.S. (Eds.), Mars. University of Arizona Press, Tucson, pp. 767–795.
Thomas, P.C., Malin, M.C., Edgett, K.S., Carr, M.H., Hartmann, W.K., Ingersoll, A.P., James, P.B., Soderblom, L.A., Veverka, J., Sullivan, R., 2000. North–south geological differences between the residual polar caps on Mars. Nature 404, 161–164.
Thomas, P.C., Malin, M.C., James, P.B., Cantor, B.A., Williams, R.M.E., Gierasch, P., 2005. South polar residual cap of Mars: Features, stratigraphy, and changes. Icarus 174 (2), 535–559.
Thomas, N., Hansen, C.J., Portyankina, G., Russell, P.S., 2009a. HiRISE observations of gas sublimation-driven activity in Mars' southern polar regions: II. Surficial deposits and their origins. Icarus 205, 296–310.
Thomas, P., James, P.B., Calvin, W.M., Haberle, R., Malin, M.C., 2009b. Residual South Polar Cap of Mars: Stratigraphy, history, and implications of recent changes. Icarus, in press. doi:10.1016/j.carus.2009.05.014.
Thomson, B.J., Bridges, N.T., Greeley, R., 2008a. Rock abrasion features in the Columbia Hills, Mars. J. Geophys. Res. 113. E08010. doi:10.1029/2007JE003018.
Thomson, B.J., Bridges, N.T., Milliken, R.E., Bell, J.F., Calvin, W.M., Weitz, C.M., 2008b. New constraints on the origin and evolution of the layered deposits in Gale Crater, Mars. Lunar Planet. Sci. XXXIX, 1456 (abstract).
Tornabene, L.L., McEwen, A.S.the HiRISE Team, 2008. Recent channel systems emanating from Hale crater ejecta: Implications for the Noachian landscape evolution of Mars. Lunar Planet. Sci. XXXIX, 2180 (abstract).

Tornabene, L.L., Moersch, J.E., McSween, H.Y., McEwen, A.S., Piatek, J.L., Milam, K.A., Christensen, P.R., 2006. Identification of large (2–10 km) rayed craters on Mars in THEMIS thermal infrared images: implications for possible martian meteorite source regions. J. Geophys. Res. 111. E10006.

Tornabene, L.L., McEwen, A.S., Osinski, G.R., Mouginis-Mark, P.J., Williams, R.M.E., Wray, J.J., Grant, J.A., the HiRISE Team, 2007. Impact melting and the role of sub-surface volatiles: Implications for the formation of valley networks and phyllosilicate-rich lithologies on early Mars. In: Seventh International Conference Mars, vol. 1353. LPI Contrib., pp. 3288–3291 (abstract).

Weitz, C.M., Milliken, R.E., Grant, J.A., McEwen, A.S., Williams, R.M.E., Bishop, J.L., 2008. Light-toned strata and inverted channels adjacent to Juventae and Ganges Chasmata, Mars. Geophys. Res. Lett. 35. L19202.

Weitz, C.M., Milliken, R.E., Grant, J.A., McEwen, A.S., Williams, R.E., Bishop, J.L., Thomson, B.J., 2009. Mars Reconnaissance Orbiter observations of light-toned layered deposits and associated fluvial landforms along the plains adjacent to Valles Marineris. Icarus 205, 73–102.

Wells, E.N., Veverka, J., Thomas, P., 1984. Mars – Experimental study of albedo changes caused by dust fallout. Icarus 58, 331–338.

Welty, C.B., Crown, D.A., Balme, M.R., 2008. Small-scale morphologic properties of martian gullies: Insights from analysis of HiRISE images. Lunar Planet. Sci. XXXIX, 2295 (abstract).

Wilkins, S.J., Schultz, R.A., Anderson, R.C., Dohm, J.M., Dawers, N.H., 2002. Deformation rates from faulting at the Tempe Terra extensional province, Mars. Geophys. Res. Lett. 29 (18), 1884.

Williams, R.M.E., Malin, M.C., 2008. Sub-kilometer fans in Mojave crater, Mars. Icarus 198, 365–383.

Wray, J.J., Ehlmann, B.L., Squyres, S.W., Mustard, J.F., Kirk, R.L., 2008. Compositional stratigraphy of clay-bearing layered deposits at Mawrth Vallis, Mars. Geophys. Res. Lett. 35, 12202.

Wray, J.J., Milliken, R.E., Swayze, G.A., Dundas, C., Bishop, J.L., Murchie, S.L., Seelos, F.P., Squyres, S.W., 2009. Columbus crater and other possible Paleolakes in Terra Sirenum, Mars. Lunar Planet. Sci. XL, 1896 (abstract).

Wright, S.P., Ramsey, M.S., 2006. Thermal infrared data analysis of Meteor crater, Arizona: Implications of Mars spaceborne data from the Thermal Emission Imaging System. J. Geophys. Res. 111. E02004.

Zurek, R.W., Smrekar, S.E., 2007. An overview of the Mars Reconnaissance Orbiter (MRO) science mission. J. Geophys. Res. 112. E05S01.